Investigating the therapeutic potential of the novel CXCL12 neutralizing ligand-LIT927 as a treatment for asthma

Bushra Shammout

Doctor of Philosophy

ASTON UNIVERSITY

September 2023

Abstract

Background: Chronic allergic airway disease is primarily characterized by airway remodeling, which severely compromises lung function. This remodeling process involves the thickening of airway smooth muscles, alterations in the vasculature, and a significant influx of inflammatory cells. Unfortunately, current therapeutic approaches often fall short in effectively addressing these structural changes. The core objective of this thesis is to investigate the therapeutic potential of LIT-927, a novel CXCL12-neutralizing ligand. This research will specifically focus on its influence on vascular and bronchial remodeling and its interactions with pericytes.

Methods: In this study, mice were exposed to a protocol of chronic airway inflammation induced by the common environmental aeroallergen, house dust mite (HDM). Phenotypic alterations in the lungs, in the presence of LIT-927, were assessed through flow cytometry and immunostaining. Additionally, the functional capabilities of pericytes were evaluated using in vitro migration assays.

Results: The administration of LIT-927 mitigated HDM-induced bronchial and vascular remodeling. In the context of chronic allergic inflammation, pericytes exhibited heightened expression of CXCR4, indicating an enhanced chemotactic response to CXCL12. Pericytes displayed increased CXCR4 expression in response to chronic allergic inflammation and demonstrated increased migration towards its cognate chemokine, CXCL12. This augmented migratory capacity was accompanied by the accumulation of pericytes in the airway wall, increased smooth muscle thickness, and respiratory distress symptoms. Notably, the uncoupling of pericytes from pulmonary vessels and their subsequent migration to the airway wall were effectively inhibited following topical treatment with the CXCL12 neutralizing ligand LIT-927

Conclusion: This study highlights the pivotal role of the CXCL12/CXCR4 axis in promoting pulmonary pericyte accumulation and airway remodeling. Our findings position LIT-927 as a promising therapeutic agent for addressing tissue remodeling associated with chronic inflammation.

Acknowledgements

Completing this PhD has been a journey of immense learning, growth, and perseverance. I would like to extend my heartfelt gratitude to everyone who has supported me along the way.

Primarily, I am deeply grateful to my parents and siblings whose unwavering love, encouragement, and belief in me have been the cornerstone of my achievements. Your sacrifices and support have been a constant source of strength and inspiration throughout my academic journey.

I owe a profound debt of gratitude to my supervisor, Dr. Jill Johnson. Your guidance, patience, and insightful feedback have been invaluable. Your support through some of the most challenging times of my life has been a beacon of light, helping me to navigate through the complexities of my research with confidence and resilience. I am truly fortunate to have had you as my mentor.

To my friends and colleagues, thank you for your camaraderie, for listening, and for providing the much-needed breaks and moments of levity. Your support has made this journey not only bearable but also enjoyable.

Lastly, I would like to thank all the faculty members and administrative staff who have assisted me in many ways throughout my PhD journey. Your contributions, though often behind the scenes, have been essential to my success.

Thank you all for being a part of this incredible journey.

Publications

Bignold, R., Shammout, B., Rowley, J.E., Repici, M., Simms, J., Johnson, J.R., 2022. Chemokine CXCL12 drives pericyte accumulation and airway remodeling in allergic airway disease. Respir. Res. 23, 183. https://doi.org/10.1186/s12931-022-02108-4

Shammout, B., Johnson, J.R., 2019. Pericytes in Chronic Lung Disease. Adv. Exp. Med. Biol. 1147, 299–317. https://doi.org/10.1007/978-3-030-16908-4_14

Shammout, B, Johnson, J.R "Inflammation-Induced Pericyte Dysfunction Is Abrogated by Interfering with the CXCL12/CXCR4 Signaling Pathway." *American Thoracic Society 2021 International Conference*, May 14-19, 2021, San Diego, CA. DOI:10.1164/ajrccm conference.2021.203.1_MeetingAbstracts.A4490.

Shammout, B., Johnson, J.R. "Modelling Fibrosis via Three Dimensional Pericyte-Endothelial Cell Coculture Using Biocompatible Nanoparticle Assembly and Spheroid Bioprinting Identifies Novel Therapeutic Targets." *American Thoracic Society 2020 International Conference*, May 15-20, 2020, Philadelphia, PA. DOI:10.1164/ajrccm-conference.2020.201.1_MeetingAbstracts.A4061.

Contents

1. Introduction

1.1 Lung Anatomy, Vasculature and Physiology

The lungs are essential respiratory organs involved in the vital processes of gas exchange. The lungs begin with the trachea, which bifurcates into abranching system of bronchi and bronchioles, ending in the alveolar sacs. This airway system is crucial for directing airflow in and out of the lungs. Each lung is divided into sections; the right lung comprises three lobes — superior, middle, and inferior, while the left lung has two, superior and inferior. (Haddad & Sharma, 2024).These are further divided into bronchopulmonary segments that enhance the lung's efficiency in gas exchange and disease containment (Haddad & Sharma, 2024). At a microscopic level, the alveoli are the primary gas-exchange units of the lungs. The interface between alveolar air and the capillary blood allows for the exchange of oxygen and carbon dioxide through diffusion. The alveolar walls house various cell types, including type I and type II alveolar cells, responsible for facilitating gas exchange and producing surfactant, which reduces surface tension in the alveoli (Han & Mallampalli, 2015)

The mechanics of breathing involve the expansion and recoil of the lung tissue, driven by the diaphragm and intercostal muscles (Aliverti, 2016) During inhalation and exhalation, pleural pressure dynamics play a critical role in air movement (Lekeux et al., 2014). The exchange of gases, primarily oxygen uptake and carbon dioxide removal, occurs at the alveolar level. Hemoglobin within the blood binds these gases and transports them between the lungs and body tissues (Aliverti, 2016).

Breathing is regulated both neurally and chemically. The medulla oblongata and peripheral chemoreceptors adjust the breathing rate and depth based on the body's needs. (De Troyer & Boriek, 2011). Additionally, fluctuations in carbon dioxide levels, oxygen levels, and blood pH prompt adjustments in respiratory rate and depth, ensuring homeostasis is maintained (De Troyer & Boriek, 2011).

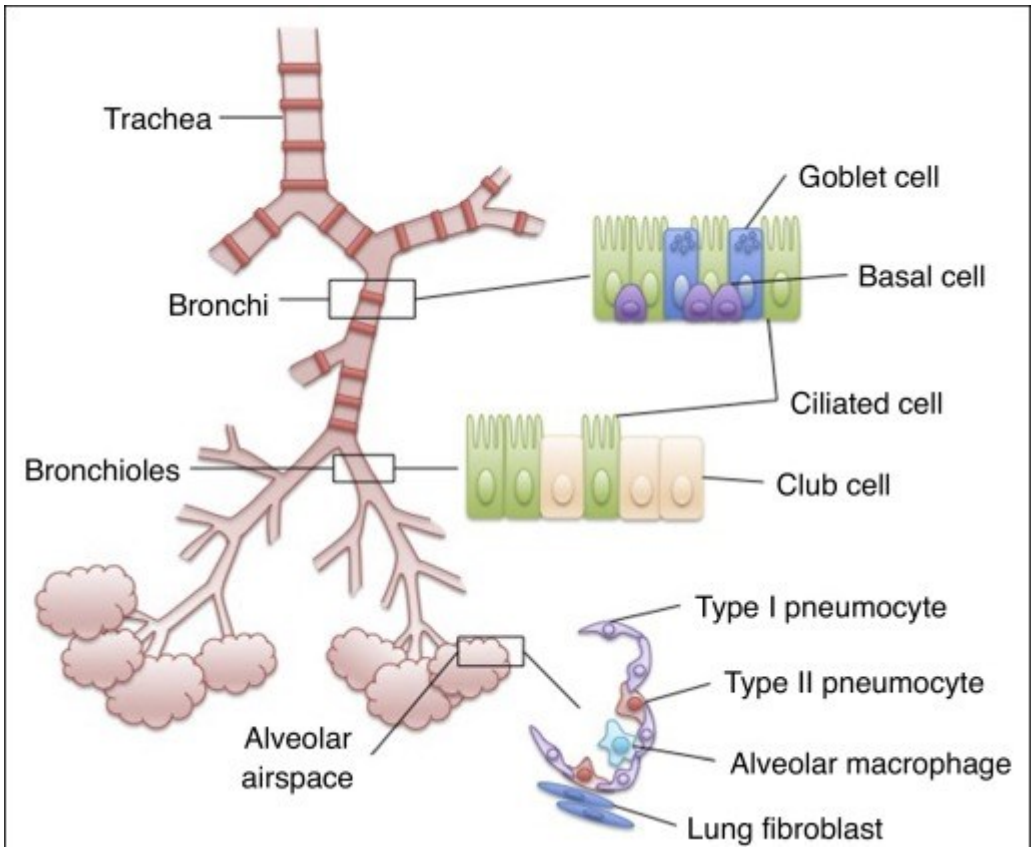

Figure 1.1 illustrates the anatomical composition of the lung, delineating its hierarchical branching structure from the central trachea to the bronchioles. The upper airways are characterized by cartilaginous rings and are lined with various cell types including basal cells, ciliated cells, and mucus-producing goblet cells. In contrast, the lower airways lack cartilage and are primarily composed of ciliated epithelial cells along with non-ciliated epithelial cells (Club cells), occasionally interspersed with goblet cells. Terminal bronchioles further divide into alveolar ducts and ultimately alveoli. Alveoli comprise Type I and II pneumocytes (epithelial cells), an extracellular matrix encircled by capillaries, lung fibroblasts, and alveolar macrophages responsible for surveilling the airways for any signs of damage or pathogens. (Ince et al., 2018)

The lungs, being highly vascularized organs, have a large surface area of about 90 square meters dedicated to efficient gas exchange (Donoghue et al., 2006). Like other parts of the body, the entire pulmonary vascular system is lined with a continuous layer of endothelial cells, which are separated from the underlying tissue by a thin basement membrane (Krüger-Genge et al., 2019). This basement membrane comprises proteins such as laminins, collagens, and proteoglycans within which pericytes are embedded and directly associated with endothelial cells (Thomsen et al., 2017) . The lung's extensive vascular network is intricately linked with the alveoli to facilitate gas exchange(Haddad & Sharma, 2024). Additionally, the lung has a unique dual blood supply; the systemic bronchial arteries provide oxygen to the trachea and bronchi, including the bronchial lamina propria and epithelium, while the pulmonary circulation from the right ventricle supplies the majority of the lung parenchyma (Suresh & Shimoda, 2016). The pulmonary vasculature is a critical component of the respiratory system, playing a central role in gas exchange and acting as a filter for blood from the right heart to the left (Suresh & Shimoda, 2016). The lung vasculature is uniquely designed to facilitate the efficient transfer of oxygen into the blood and the removal of carbon dioxide from it (Suresh & Shimoda, 2016). The pulmonary arteries carry deoxygenated blood from the right ventricle of the heart to the lungs, where it branches extensively into smaller arterioles and ultimately capillaries that envelop the alveoli (Suresh & Shimoda, 2016). This extensive capillary network is where gas exchange occurs, and it is finely tuned to optimize the diffusion of gases between the air spaces and blood (Suresh & Shimoda, 2016).

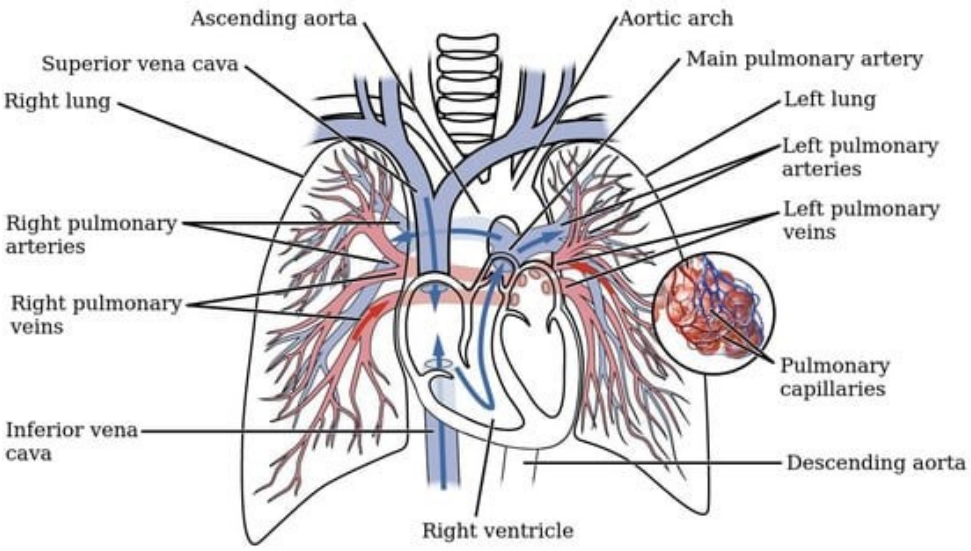

Figure 1.2: Schematic of the pulmonary circuit pulmonary circulation begins at the pulmonary artery, which bifurcates into left and right branches entering the respective lungs. Within the lungs, these arteries follow the bronchial tree and branch into arterioles and capillaries at the alveolar level. Pulmonary veins then collect the oxygenated blood from the capillaries and return it to the left atrium of the heart. This low-pressure, high-flow circuit is essential for maintaining the blood's oxygenation and minimizing the workload on the heart (Capuano et al., 2019)

The primary function of the pulmonary vasculature is to facilitate the exchange of gases (Capuano et al., 2019). The capillaries, the thinnest and most numerous of the blood vessels, are ideally situated and structured for this purpose. The unique arrangement allows for maximum exposure of blood to alveolar air, enabling efficient gas diffusion (Gillich et al., 2020).Furthermore, the pulmonary endothelium plays a vital role in regulating vascular tone and blood flow, adapting to varying oxygen levels to optimize gas exchange (Sandoo et al., 2010).

Lung angiogenesis, the formation of new blood vessels within the lung tissue, plays a crucial role in both physiological and pathological processes. Angiogenesis in the lungs involves a complex interplay of cellular and molecular signals. The primary cells involved include endothelial cells, which form the lining of new blood vessels, and pericytes, which stabilize the newly formed vessels (Eldridge & Wagner, 2019).

The regulation of lung angiogenesis is tightly controlled by cytokines, growth factors, and extracellular matrix components (Mongiat et al., 2016). Hypoxia, a common condition in various lung diseases, is a potent stimulator of angiogenesis (Krock et al., 2011). HIFs are critical mediators that upregulate angiogenic factors like VEGF (Muz et al., 2015). Inflammatory cytokines, such as tumor necrosis factor-alpha (TNF-α) and interleukins (ILs), also play significant roles in modulating angiogenesis by either promoting or inhibiting endothelial cell function and vascular growth (Gardiner et al., 2005)

The lung is subject to constant mechanical forces due to breathing. These forces can influence angiogenesis by affecting endothelial cell behavior and the expression of angiogenic factors (Gordon et al., 2020). For example, cyclic stretch has been shown to enhance VEGF expression and promote angiogenesis (Yan et al., 2020). During lung development, angiogenesis is crucial for alveolarization, the process by which alveoli, the small air sacs where gas exchange occurs, are formed (Schittny, 2017).

Aberrant angiogenesis is implicated in various lung diseases, including chronic obstructive pulmonary disease (COPD), pulmonary hypertension (PH), and lung cancer (Voelkel et al., 2007) . In COPD, chronic inflammation, and oxidative stress lead to structural changes in the lung, including abnormal angiogenesis (Siafakas et al., 2007). Studies have shown increased VEGF levels in COPD patients, correlating with disease severity (Siafakas et al., 2007). PH is characterized by increased pulmonary arterial pressure and vascular remodeling (Karnati et al., 2021). Excessive angiogenesis contributes to the thickening of the vascular walls and increased resistance. Targeting angiogenic pathways, particularly the VEGF pathway, has been explored as a therapeutic approach in PH (Tobal et al., 2021)

Angiogenesis is a hallmark of cancer, including lung cancer (Nishida et al., 2006). Tumor growth and metastasis depend on the development of new blood vessels to supply nutrients and oxygen(Nishida et al., 2006). Anti-angiogenic therapies, such as bevacizumab, which targets VEGF , have been used in the treatment of lung cancer, highlighting the importance of angiogenesis in tumor progression (Ngaha et al., 2023)

1.2 Asthma

Asthma epidemiology

Asthma is a chronic respiratory disease that ` characterized by recurrent episodes of wheezing, shortness of breath, chest tightness, and coughing, which result from inflammation and narrowing of the airways (Bergeron et al., 2010) Asthma, affects approximately 300 million people globally and is a leading chronic disease worldwide and a major contributor to global morbidity and (Z. Wang et al., 2023). Prevalence rates vary extensively by country, age, sex, and socioeconomic status, with developed countries like the United States, United Kingdom, and Australia reporting some of the highest rates (To et al., 2012)

Asthma can begin at any age but most often starts in childhood, making it the most common non-communicable disease among children (Dharmage et al., 2019). Interestingly, while more boys are diagnosed with asthma in childhood, the trend reverses in adulthood, with higher prevalence in women (Naeem & Silveyra, 2019). This shift may be influenced by hormonal and genetic factors (Postma, 2007). Ethnic minorities and economically disadvantaged groups, particularly African Americans and Hispanics in the United States, exhibit higher asthma prevalence and morbidity than Caucasian populations (Forno & Celedón, 2009) . Factors contributing to these disparities include differences in access to healthcare, environmental exposures, and educational levels (Grant et al., 2022)

The role of environmental factors such as air pollution, allergens, tobacco smoke, and occupational hazards is critical in the exacerbation of asthma (Strachan, 2000). Urbanization correlates with increased asthma prevalence, possibly supporting the hygiene hypothesis, which posits that reduced early-life exposure to infectious agents might heighten susceptibility to allergic diseases (Rodriguez et al., 2019). Genetic predispositions also play a significant role, with research identifying specific genes that contribute to airway hyperreactivity and inflammation (Ranjbar et al., 2022)

Asthma Pathophysiology

The pathophysiology of asthma involves a complex interplay of cellular and molecular events that occur in response to various environmental triggers (Bush, 2019). The onset of an allergic response, as seen in conditions such as asthma, typically begins with allergen sensitization and epithelial damage (Kudo et al., 2013). Allergens can be numerous and varied, including substances like pollen, dust mites and pet dander (Lloyd & Robinson, 2007). Upon initial exposure to an allergen, antigen-presenting cells (APCs) within the airway mucosa capture, process, and present the allergenic proteins to naïve T helper cells (Humeniuk et al., 2017). This interaction, under certain conditions, promotes the differentiation of these cells into T helper 2 (Th2) cells (Harker & Lloyd, 2023). Th2 cells then produce interleukins such as IL-4, IL-5, and IL-13, which have various roles in promoting an allergic response. IL-4, for example, stimulates B cells to produce Immunoglobulin E (IgE) antibodies specific to the allergen (Gevaert et al., 2022)

Simultaneously, environmental pollutants, viruses, or bacteria may cause epithelial damage, disrupting the protective barrier of the airway and allowing deeper penetration of allergens (Strachan, 2000). The damaged epithelial cells also release cytokines such as TSLP, IL-25, and IL-33, which further promote the Th2 response. IgE antibodies produced during this sensitization process bind to mast cells (Whetstone et al., 2022). Upon subsequent exposure to the same allergen, the allergen cross-links the IgE on the mast cells, triggering them to release pro-inflammatory mediators like histamine, leukotrienes, and prostaglandins (Quirt et al., 2018) Overall, this multifaceted immune response results in the hallmark symptoms of asthma, such as bronchoconstriction, vascular remodeling, mucus production, and airway inflammation and hyperresponsiveness (Bergeron et al., 2010)

Asthma Phenotypes and Endotypes

Phenotypes in asthma refer to the observable characteristics of the disease, such as the severity of symptoms, age of onset, and response to treatment (Gonzalez-Uribe et al., 2023). Endotypes are defined by the specific biological mechanisms that underlie these observable traits. Distinguishing between phenotypes is crucial for targeted therapies (Pembrey et al., 2018).

Allergic asthma, the most common asthma phenotype, is typically triggered by environmental allergens such as pollen, pet dander, dust mites, and mold (Wenzel, 2012). It often begins in childhood and is associated with other atopic disorders such as allergic rhinitis and eczema (Spergel, 2010). The underlying endotype of allergic asthma involves a Type 2 (Th2) immune response. This response is characterized by elevated levels of IgE antibodies, eosinophilia, and the release of cytokines such as IL-4, IL-5, and IL-13. These cytokines promote inflammation and hyperresponsiveness of the airways (Fahy, 2015). Patients with allergic asthma may experience symptoms seasonally or year-round, depending on their specific allergen sensitivities (Foong et al., 2017). Treatment typically includes inhaled corticosteroids (ICS) to reduce inflammation and immunotherapy to decrease sensitivity to allergens (Baxi & Phipatanakul, 2010)

Non-allergic asthma, in contrast, does not involve allergic reactions and is not triggered by environmental allergens (Pembrey et al., 2018). It often appears later in life and does not typically coincide with other allergic conditions (Klain et al., 2022)

The inflammatory Pathway in non-allergic asthma is less dependent on the Th2 immune response (Sze et al., 2020). Instead it involves neutrophils and might be associated with a Th1 and Th17 inflammatory response with elevated levels of IL-8, TNF-alpha and IL-17(Baos et al., 2018). These cytokines contribute to airway inflammation that is less responsive to steroids (Wadhwa et al., 2019) . Non-allergic asthma is often more resistant to conventional asthma treatments such as corticosteroids (Boyman et al., 2015). Patients may require alternative strategies such as increased doses of inhaled steroids, use of systemic steroids, or newer biologic medications that target specific inflammatory pathways (Radonjic-Hoesli et al., 2015)

Understanding whether asthma is allergic or non-allergic is critical for effective management (Gonzalez-Uribe et al., 2023).Allergic asthma may benefit from strategies that reduce allergen exposure and use targeted biologic treatments aimed at reducing IgE levels or blocking specific cytokines involved in the Th2 pathway (León & Ballesteros-Tato, 2021). Non-allergic asthma, on the other hand, might respond better to treatments that target neutrophilic inflammation or newer approaches like bronchial thermoplasty (Colas et al., 2020)

Fibrosis and Bronchial Remodeling in Asthma

In asthma, the airways of the lungs undergo characteristic changes, with the bronchi and bronchioles being the primary sites of pathophysiological changes (Samitas et al., 2018) . These large and medium-sized airways possess smooth muscle layers that, in the context of asthma, exhibit hyperresponsiveness, leading to their constriction in response to various stimuli (Xiong et al., 2022). This bronchoconstriction, induced by the release of mediators like histamine and leukotrienes, is a key component of the airflow obstruction observed in asthmatic individuals (Doeing & Solway, 2013). In addition to bronchoconstriction, the bronchi and bronchioles also undergo structural changes known as airway remodelling. This includes thickening of the airway wall due to fibrosis, increased smooth muscle mass, glandular hypertrophy, and neovascularization (J. W. Wilson & Kotsimbos, 2003) These changes, along with the infiltration of inflammatory cells such as eosinophils and lymphocytes into the airway wall, contribute to the chronic and progressive nature of asthma as highlighted in Figure 1.3

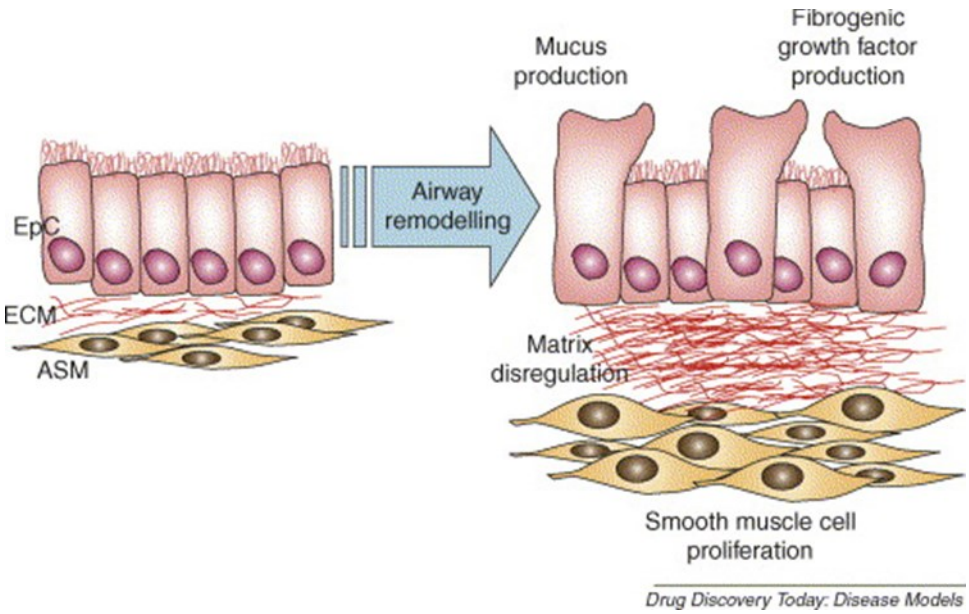

Figure 1.3 This diagram illustrates the process of bronchial remodeling in asthma. In the non-asthmatic bronchus (left), the airway wall has a smooth, thin lining, with intact epithelial cells and minimal connective tissue. There is also a thin layer of smooth muscle cells in the bronchial wall. In the asthmatic bronchus (right), several changes are evident due to bronchial remodeling. The epithelial layer becomes damaged, with increased epithelial shedding. The underlying connective tissue thickens, and the deposition of extracellular matrix components such as collagen increases. There is hypertrophy and hyperplasia of the bronchial smooth muscle cells, leading to airway narrowing and increased airway resistance. Additionally, the presence of inflammatory cells, such as eosinophils and mast cells, is increased in the airway wall, contributing to inflammation and bronchoconstriction (Doeing & Solway, 2013).

The process of fibrosis involves the excessive accumulation of extracellular matrix (ECM) proteins, which contributes to the development of various fibrotic conditions in different organs (Antar et al., 2023) In the context of lung fibrosis, the abnormal deposition of ECM proteins, such as collagen and fibronectin, is a hallmark feature of the disease (X. Zhao et al., 2022). This accumulation of ECM proteins is associated with sub-epithelial fibrosis, which is a major complication of chronic asthma and reflects the severity of airway remodeling (Lloyd & Robinson, 2007)

Furthermore, in idiopathic pulmonary fibrosis (IPF), the accumulation of ECM proteins in the lungs is a defining characteristic of the disease (M. S. Wilson & Wynn, 2009). The dysregulation of ECM assembly, leading to the accumulation of disorganized ECM proteins and insoluble matrix fibrils, is a key factor in the development of fibrosis (Kulkarni et al., 2016). The involvement of ECM proteins in fibrosis is not limited to the lungs, as evidenced by their role in renal fibrosis, myocardial fibrosis, liver fibrosis, and other fibrotic conditions (Herrera et al., 2018) . For example In chronic liver damage, the pathological accumulation of ECM proteins contributes to the progression of liver fibrosis (Mederacke et al., 2013). Similarly, in myocardial fibrosis, the contribution of the basement membrane, proteoglycans, and glycoproteins to the expansion of the ECM and the accumulation of ECM proteins is well recognized (Chute et al., 2019). Additionally, in kidney fibrosis, ECM proteins play a direct role in rare renal diseases and indirectly contribute to the progression of chronic kidney disease (Bülow & Boor, 2019)

The molecular mechanisms underlying the accumulation of ECM proteins in fibrosis involve various signaling pathways and cellular processes. For example, the transforming growth factor beta (TGF-β) pathway is implicated in promoting the production and deposition of ECM proteins in fibrotic conditions (X. Shi et al., 2020).

Moreover, the abnormal deposition of ECM proteins is associated with the activation of normal fibroblasts through a positive feedback loop, contributing to the self-sustaining nature of fibrosis once it is established (K. Wang et al., 2023)

Asthma Therapeutic Options

Over the years, various treatment modalities have been developed and refined, ranging from pharmacological interventions to innovative non-pharmacological approaches (Papi et al., 2020). Inhaled corticosteroids are the cornerstone of asthma management (Ponieman et al., 2009). They work by reducing airway inflammation, thereby decreasing the frequency and severity of asthma symptoms and exacerbations (Bårnes & Ulrik, 2015). Studies have consistently shown that ICS improves lung function and quality of life for asthma patients (Reddel et al., 2015). The efficacy of ICS in reducing airway hyperresponsiveness and inflammation has made them the first-line treatment for persistent asthma (Du et al., 2017).

LABAs, such as salmeterol and formoterol, are often used in combination with ICS for better control of asthma symptoms (Jacobson et al., 2018). These medications help relax the bronchial muscles, leading to prolonged bronchodilation (Tashkin & Fabbri, 2010). Research indicates that the combination of ICS and LABA provides superior asthma control compared to ICS (Morales, 2013). However, the use of LABAs as monotherapy is not recommended due to the increased risk of asthma-related death (Wijesinghe et al., 2008). LTRAs, such as montelukast, offer an alternative to ICS for mild asthma and as an add-on therapy for more severe cases. They work by blocking

the action of leukotrienes, inflammatory mediators that contribute to asthma symptoms (Paggiaro & Bacci, 2011). Studies have shown that LTRAs improve asthma control and reduce the need for rescue medication (Miligkos et al., 2015) However, they are generally less effective than ICS in controlling inflammation.

Biologic therapies target specific molecules involved in the inflammatory pathway of asthma. Omalizumab, an anti-IgE antibody, is effective for patients with severe allergic asthma (Bousquet et al., 2007). Mepolizumab and reslizumab, both anti-IL-5 antibodies, have shown efficacy in reducing exacerbations in patients with eosinophilic asthma (Ortega et al., 2014) These biologics represent a significant advancement in personalized asthma treatment. (Delgado-Martín et al., 2011)

Allergen immunotherapy involves the gradual introduction of allergens to desensitize the immune system. This treatment is particularly beneficial for patients with allergic asthma triggered by specific allergens (Cappella & Durham, 2012). Meta-analyses have demonstrated that allergen immunotherapy reduces asthma symptoms and medication use (W. Zhang et al., 2018). Therefore acting as a potential long-term treatment strategy that can modify the natural course of allergic diseases (W. Zhang et al., 2018)

Bronchial thermoplasty is a novel procedure that uses thermal energy to reduce the smooth muscle mass in the airways, thereby decreasing airway hyperresponsiveness (Nasim & Iyer, 2018). Clinical trials have shown that bronchial thermoplasty improves

asthma control and quality of life in patients with severe asthma who do not respond adequately to conventional treatments (Nasim & Iyer, 2018).

Lifestyle changes, such as regular physical activity, weight management, and smoking cessation, are important components of asthma management . Additionally, reducing exposure to asthma triggers, such as allergens and pollutants, can significantly improve asthma control (Stoodley et al., 2019) Evidence suggests that a comprehensive approach, incorporating pharmacological treatment with lifestyle modifications, leads to better asthma outcomes (Takala et al., 2024)

Emerging biologic therapies targeting thymic stromal lymphopoietin (TSLP) and interleukin-33 (IL-33) show promise in early clinical trials. Tezepelumab, an anti-TSLP antibody, has demonstrated significant reductions in asthma exacerbations across a broad population of asthma patients (Menzies-Gow et al., 2021) These therapies represent the next frontier in asthma treatment, offering hope for patients with severe, uncontrolled asthma (Menzies-Gow et al., 2021) .

Advances in genomics and precision medicine hold potential for the future of asthma treatment. Gene therapy aims to correct underlying genetic defects that contribute to asthma (Meyers et al., 2014). Although still in experimental stages, this approach could offer a cure for certain types of asthma (Meyers et al., 2014)

1.3 CXCL12

CXCL12 structure

CXCL12, also known as stromal cell-derived factor-1 (SDF-1), is a chemokine with significant roles in various physiological and pathological processes (Janssens et al., 2018). The CXCL12 gene, located on chromosome 10q11.21 in humans, encodes several isoforms of the protein through alternative splicing (Janssens et al., 2018). The most studied isoforms are CXCL12α and CXCL12β, differing in their C-terminal sequences. CXCL12 is characterized by its highly conserved N-terminal sequence essential for receptor binding and activity (Janssens et al., 2018)

CXCL12 is ubiquitously expressed in various tissues, including the bone marrow, heart, liver, brain, kidneys, and lungs (Guo et al., 2016). Expression levels vary significantly depending on tissue type and physiological or pathological context. For example, in the bone marrow, CXCL12 is predominantly produced by stromal cells, crucial for hematopoiesis (Guo et al., 2016)

CXCL12 Signaling

CXCL12 primarily interacts with the CXCR4 receptor and to a lesser extent with CXCR7, CXCL12 is involved in hematopoiesis, embryonic development, immune responses, and disease pathogenesis CXCR4, a G protein-coupled receptor (GPCR), is the primary receptor for CXCL12 (Guo et al., 2016). It consists of seven transmembrane helices, an extracellular N-terminus, and an intracellular C-terminus. The binding of CXCL12 to CXCR4 triggers a conformational change in the receptor, activating various downstream signaling pathways (Guo et al., 2016). CXCR4 is widely expressed across different cell types, including hematopoietic stem cells, immune cells, and endothelial cells, reflecting its broad functional roles (Shu et al., 2013)

Upon CXCL12 binding, CXCR4 activates several key signaling pathways. Activation of phosphoinositide 3-kinase (PI3K) leads to the phosphorylation and activation of Akt (also known as protein kinase B) (Delgado-Martín et al., 2011) This pathway is crucial for cell survival, growth, and proliferation. Akt activation also promotes glucose metabolism and inhibits apoptosis by phosphorylating and inactivating pro-apoptotic factors (Delgado-Martín et al., 2011). Furthermore, The mitogen-activated protein kinase (MAPK) pathway, involving extracellular signal-regulated kinases (ERK1/2),

regulates cell division, differentiation, and gene expression (Y. Shi et al., 2020). CXCR4 activation leads to the phosphorylation of ERK1/2, which then translocate to the nucleus to modulate the expression of target genes (Lu & Malemud, 2019)

The Janus kinase (JAK) and signal transducer and activator of transcription (STAT) proteins are involved in regulating immune responses and hematopoiesis (X. Hu et al., 2021) CXCR4 activation leads to the phosphorylation of JAK, which in turn phosphorylates STAT proteins (Busillo & Benovic, 2007). Phosphorylated STATs dimerize and translocate to the nucleus to influence gene expression (Pfeiffer et al., 2009). CXCR4 activation also influences the cytoskeleton dynamics through Rho GTPases, affecting cell migration and adhesion (Nayak et al., 2013). These pathways are vital for the directed migration of cells in response to CXCL12 gradients.

CXCR7 (also known as ACKR3) is another receptor for CXCL12. Unlike CXCR4, CXCR7 does not typically activate G-protein signaling (Santagata et al., 2021) Instead, it functions primarily through β-arrestin-mediated pathways and acts as a scavenger receptor to regulate the local concentration of CXCL12 and modulate CXCR4 signaling (Santagata et al., 2021). CXCR7 primarily signals through β-arrestin, a protein that regulates receptor internalization and downstream signaling (Nguyen et al., 2020). This pathway affects cell adhesion, migration, and survival, though its mechanisms are less understood compared to CXCR4 (Nguyen et al., 2020). Furthermore, by internalizing and degrading CXCL12, CXCR7 controls the availability of this

chemokine in the extracellular space, indirectly influencing CXCR4-mediated responses (Luker et al., 2012). This regulatory function is crucial in maintaining the balance of CXCL12 signaling in various physiological contexts (Luker et al., 2012)

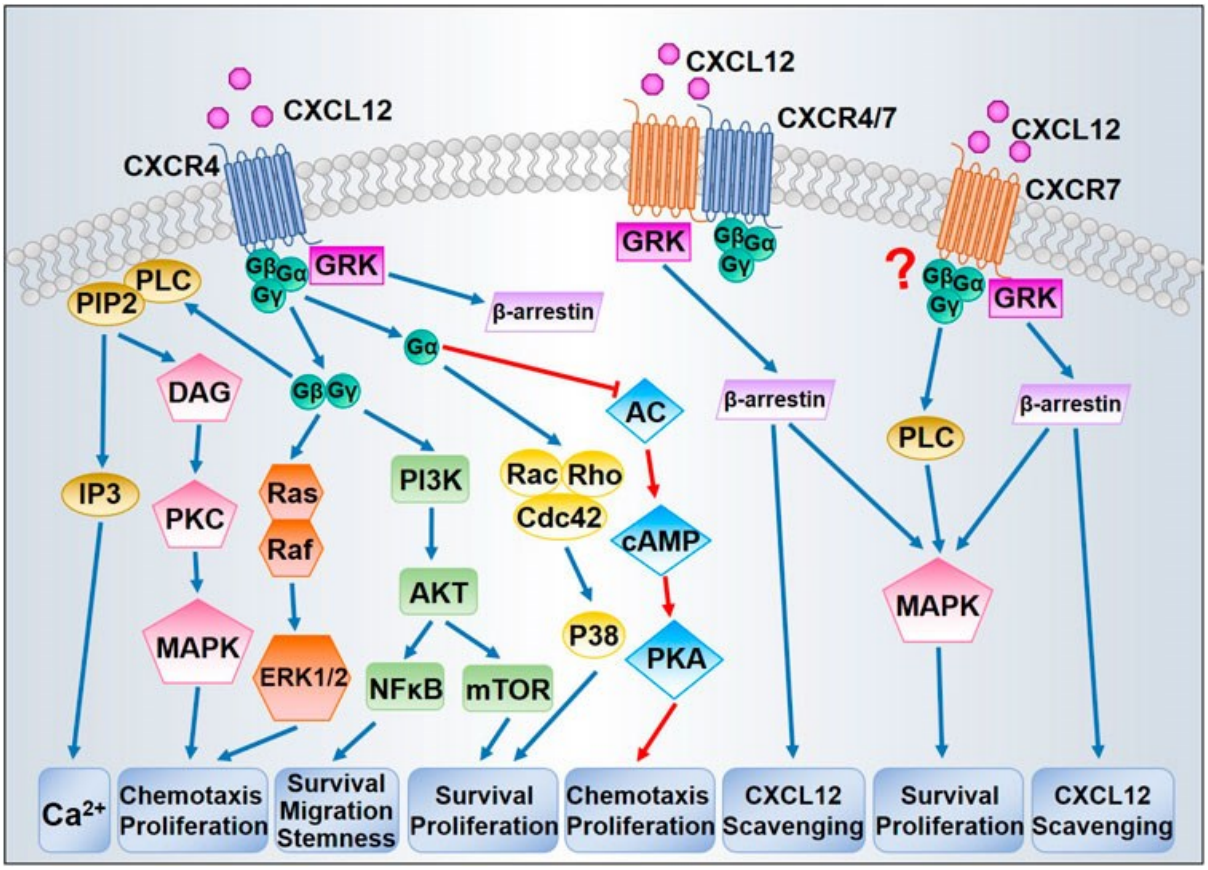

Figure 1.4 CXCL12/CXCR4/CXCR7 Signaling Pathways. When CXCL12 binds to CXCR4, it activates downstream signaling via G proteins and GRKs. The dissociation of G protein complexes subsequently activates the MAPK, ERK1/2, and AKT signaling pathways, which in turn support cell survival and proliferation. GRKs predominantly facilitate the recruitment of β-arrestin, leading to the internalization of CXCR4. CXCR7 can trigger β-arrestin either independently or through the formation of a CXCR4/CXCR7 heterodimer, resulting in MAPK activation and the scavenging of CXCL12. The question mark highlights the ongoing debate about whether CXCR7 is coupled to G proteins (Y. Shi et al., 2020).

The Multifaceted Role of CXCL12

CXCL12 signaling is vital for the retention and homing of hematopoietic stem cells (HSCs) within the bone marrow niche. CXCL12 produced by stromal cells creates a gradient that guides HSCs to their specific microenvironment, ensuring their quiescence, survival, and self-renewal (Mousavi, 2020). During embryogenesis, CXCL12 signaling guides the migration of progenitor cells to their destined locations (Mousavi, 2020). This signaling axis is critical for the development of the cardiovascular system, central nervous system, and gastrointestinal tract. For instance, CXCL12 is essential for the migration of primordial germ cells and the formation of the cerebellum (Mousavi, 2020).

CXCL12 plays a significant role in immune cell trafficking. It directs the migration of lymphocytes, dendritic cells, and other leukocytes to sites of inflammation or injury (Koch & Engele, 2020). This chemokine also contributes to the organization of lymphoid tissues and the formation of germinal centers, essential for B cell maturation and adaptive immune responses (Koch & Engele, 2020).

CXCL12 in Disease Pathologies

The CXCL12 is implicated in several aspects of cancer biology, including tumor growth, angiogenesis, metastasis, and the tumor microenvironment (Y. Shi et al., 2020). High levels of CXCL12 expression are associated with poor prognosis in cancers such as breast, lung, and colorectal cancer (Y. Shi et al., 2020). CXCL12 promotes tumor cell survival and proliferation, recruits endothelial progenitor cells to support angiogenesis, and facilitates the metastatic spread of cancer cells by enhancing their migratory and invasive capacities (Y. Shi et al., 2020).

In cardiovascular diseases, CXCL12 plays a dual role. Post-myocardial infarction, CXCL12 is upregulated, promoting the recruitment of stem cells and progenitor cells to damaged heart tissue, aiding in tissue repair and regeneration (Mousavi, 2020).. However, chronic overexpression can contribute to atherosclerosis by recruiting inflammatory cells to the arterial wall, leading to plaque formation and vascular inflammation (Gencer et al., 2021)

CXCL12 is involved in the pathogenesis of various inflammatory diseases, such as rheumatoid arthritis, multiple sclerosis, and inflammatory bowel disease (García-Cuesta et al., 2019). Elevated CXCL12 levels attract inflammatory cells to affected tissues, exacerbating the inflammatory response (Peng et al., 2020). For instance, in rheumatoid arthritis, CXCL12 in the synovial fluid recruits immune cells, contributing to joint inflammation and damage (Peng et al., 2020)

CXCR4 serves as a coreceptor for HIV entry into CD4+ T cells, making CXCL12 a crucial player in HIV/AIDS pathogenesis (Vicenzi et al., 2013). Variations in CXCL12 expression and function can influence HIV susceptibility and disease progression (Lama & Planelles, 2007). Higher CXCL12 levels can inhibit HIV replication by competing with the virus for CXCR4 binding, thereby reducing viral entry into host cells(Armani-Tourret et al., 2021)

Given its involvement in multiple diseases, targeting the CXCL12/CXCR4 axis presents a promising therapeutic strategy. For example, CXCR4 Antagonists include drugs like Plerixafor (AMD3100) are being investigated for their potential to inhibit tumor metastasis (R. Zhao et al., 2022). Continued research into the detailed mechanisms of CXCL12 signaling and its broader implications in health and disease is essential for developing novel therapeutic strategies.

1.4 Pericytes

Pericytes, identifiable via electron microscopy due to the presence of processes within the capillary basement membrane are a specific cell type that can be challenging to distinguish from other cells occupying the periendothelial compartments (Armulik et al., 2011) . Pericytes share a basement membrane with endothelial cells and play a critical role in maintaining vessel integrity (Armulik et al., 2011) .

To aid in their identification, various markers have been recognized, including CD146, CD13, PDGF receptor β (PDGFβR), neural glial antigen 2 (NG2), alkaline phosphatase, RGS5, 3G5, and contractile proteins such as desmin, vimentin, and alpha-smooth muscle actin (α-SMA) (Harrell et al., 2018). As tissue-resident mesenchymal stem cells, pericytes meet the MSC criteria outlined by the International Society for Cellular Therapy (ISCT). These criteria encompass plastic adherence, the capacity to differentiate into the classic MSC triad (osteocytes, chondrocytes, and adipocytes) , and the expression of CD105, CD73, and CD90 (Oh, 2010) Existing

evidence indicates that pericytes, upon migration away from the vessel, differentiate into myofibroblasts involved in pathological fibrotic processes in organs such as the kidney, lung, and liver (Johnson, 2015)

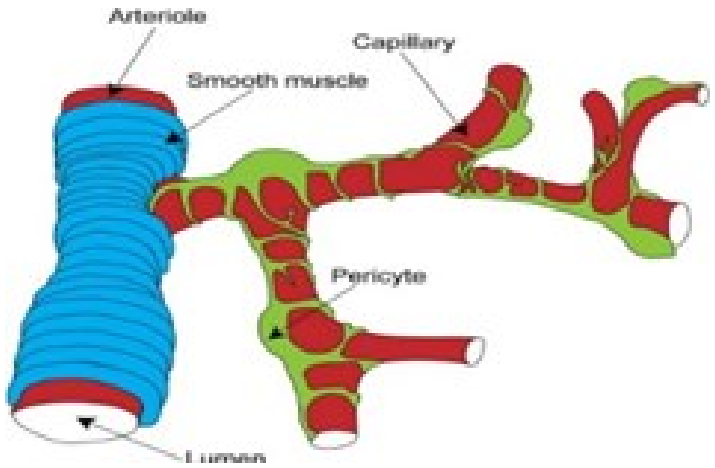

Figure 1.5: Anatomically Pericytes surround and support the microvasculature throughout the body Pericytes, identifiable via electron microscopy due to the presence of processes within the capillary basement membrane are a specific cell type that can be challenging to distinguish from other cells occupying the periendothelial compartments (Armulik et al., 2011)

Once pericytes are recruited to the vessel wall, they interact closely with endothelial cells (Bergers & Song, 2005). These two cell types share a common basement membrane and establish robust physical connections to maintain the stability and function of blood vessels (Bergers & Song, 2005). One of the key ways they achieve this is through peg and socket junctions (Daneman & Prat, 2015). Peg and socket junctions are specialized intercellular connections where the membrane of one cell (typically the pericyte) extends finger-like projections (pegs) that insert into corresponding invaginations (sockets) in the membrane of the adjacent cell (the endothelial cell) (Caporarello et al., 2019). These junctions help to anchor the cells

together, facilitating communication and structural support between pericytes and endothelial cells (Caporarello et al., 2019).

In addition to peg and socket junctions, adhesion plaques also play a crucial role. These are regions where cell adhesion molecules (such as integrins) cluster together, forming strong adhesive contacts between the cells and their shared basement membrane (Bergers & Song, 2005). This complex network of connections ensures that pericytes and endothelial cells remain tightly associated, contributing to (Birrell et al., 2010)the integrity and function of the vascular system (Bergers & Song, 2005).

Pericytes play a crucial role in vascular development, stability, and permeability. Pericytes are involved in various physiological processes, including angiogenesis, blood-brain barrier (BBB) maintenance, and immune responses (Su et al., 2019). Understanding the signaling pathways that regulate pericyte functions is essential for developing therapeutic strategies for diseases involving vascular dysfunction, such as diabetic retinopathy, stroke, and cancer (Nwadozi et al., 2020)

The PDGF pathway is one of the most critical regulators of pericyte recruitment and function. PDGF-BB, produced by endothelial cells, binds to the PDGFR-β receptor on pericytes, promoting their proliferation, migration, and survival (Xiang et al., 2019). This signaling pathway is crucial for stabilizing blood vessels during angiogenesis. Studies have shown that PDGF-BB/PDGFR-β signaling is essential for the recruitment

of pericytes to developing vessels and the maintenance of vascular integrity survival (S.-Y. Zhou et al., 2022).

The TGF-β pathway plays a significant role in maintaining vascular stability and regulating pericyte differentiation. TGF-β signaling involves the binding of TGF-β ligands to TGF-β receptors on pericytes, activating SMAD and non-SMAD pathways (Y. Zhang & Yang, 2020). This signaling promotes the differentiation of pericytes into smooth muscle-like cells and stabilizes the actin cytoskeleton. TGF-β also modulates the expression of extracellular matrix proteins, contributing to the structural integrity of blood vessels (Goumans & ten Dijke, 2018)

VEGF is a potent mediator of angiogenesis and vascular permeability. VEGF-A, produced by various cell types, including pericytes, binds to VEGF receptors (VEGFR-1 and VEGFR-2) on endothelial cells, promoting their proliferation and migration (Shibuya, 2011). Pericyte-derived VEGF-A is essential for endothelial cell survival and the formation of new blood vessels. Additionally, VEGF signaling helps maintain the BBB by regulating the expression of tight junction proteins in endothelial cells (Fu et al., 2023)

The Angiopoietin-Tie signaling pathway is critical for vascular maturation and stability. Angiopoietin-1 (Ang-1), produced by pericytes, binds to the Tie-2 receptor on endothelial cells, promoting cell survival, migration, and the stabilization of blood

vessels (Eklund et al., 2017). Ang-1/Tie-2 signaling enhances the integrity of the endothelial barrier by increasing the expression of junctional proteins such as occludin and claudin-5 (Siddiqui et al., 2015). Conversely, Angiopoietin-2 (Ang-2) can act as an antagonist or agonist of Tie-2, depending on the context, and is involved in vascular remodeling during inflammation and tumor growth(Thurston & Daly, 2012)

The Notch signalig pathway is involved in cell-cell communication and plays a vital role in vascular development and homeostasis (B. Zhou et al., 2022). Notch receptors (Notch1-4) and their ligands (Jagged1, Jagged2, Delta-like 1, and Delta-like 4) are expressed on both endothelial cells and pericytes (Tefft et al., 2022). Notch signaling regulates pericyte proliferation, differentiation, and interaction with endothelial cells. For instance, Notch3 signaling in pericytes is crucial for their maturation and the stabilization of blood vessels (Y. Wang et al., 2014)

Rho GTPases, including RhoA, Rac1, and Cdc42, are involved in cytoskeletal dynamics and cell motility (Spiering & Hodgson, 2011) .These signaling molecules play a crucial role in pericyte contraction and migration. Activation of RhoA promotes the assembly of actin stress fibers and focal adhesions, enhancing pericyte contractility (S. Wang et al., 2012). This pathway is essential for regulating blood flow in the microvasculature and maintaining vascular tone (S. Wang et al., 2012). Additionally, Rho GTPase signaling is involved in the response of pericytes to mechanical stimuli and extracellular matrix interactions (Kutcher et al., 2007). The phosphoinositide 3-kinase (PI3K)/Akt pathway is a key regulator of cell survival, growth, and metabolism (Figueiredo et al., 2020), In pericytes, PI3K/Akt signaling is activated by various growth factors, including PDGF and VEGF (Figueiredo et al.,

2020), This pathway promotes pericyte survival, proliferation, and migration (Garrison et al., 2023). Akt phosphorylation enhances the stability of the microvasculature by preventing pericyte apoptosis and supporting their role in endothelial barrier function (Figueiredo et al., 2020), Additionally, PI3K/Akt signaling is involved in the regulation of glucose metabolism in pericytes, which is particularly relevant in the context of diabetic complications (Nwadozi et al., 2020)

The mitogen-activated protein kinase (MAPK)/extracellular signal-regulated kinase (ERK) pathway is another critical signaling cascade involved in pericyte function (Takahashi et al., 2014). Activation of the MAPK/ERK pathway by growth factors such as PDGF and VEGF leads to pericyte proliferation and migration (Song et al., 2023). This pathway also plays a role in the differentiation of pericytes and the maintenance of vascular stability (Ferland-McCollough et al., 2017). Dysregulation of MAPK/ERK signaling is associated with various vascular diseases, highlighting its importance in pericyte biology (Song et al., 2023).

The CXCL12/CXCR4 signaling pathway is crucial for pericyte function, particularly in migration and angiogenesis. CXCL12, also known as stromal cell-derived factor-1 (SDF-1), binds to the CXCR4 receptor on pericytes, facilitating their recruitment to sites of vascular injury and promoting angiogenesis (Ivins et al., 2015). This signaling pathway is essential for the mobilization of pericytes during tissue repair and in pathological conditions such as cancer and fibrosis (F. Li et al., 2020). The CXCL12/CXCR4 axis also plays a significant role in the stabilization of blood vessels by promoting the interaction between pericytes and endothelial cells(Liekens et al., 2010). Inhibition of CXCL12/CXCR4 signaling has been shown to reduce pericyte

accumulation and angiogenesis, highlighting its potential as a therapeutic target (Bordenave et al., 2020)

Pericytes play a crucial role in normal angiogenesis. Angiogenesis begins with the sprouting of endothelial cells from pre-existing vessels (Payne et al., 2019)As these sprouts form, pericytes are recruited to the nascent vessels, guided by the signaling molecule Platelet Derived Growth Factor-B (PDGF-B) secreted by endothelial cells, which binds to the PDGF Receptor-beta (PDGFRβ) on pericytes (Payne et al., 2019) The close association between endothelial cells and pericytes during angiogenesis ensures several vital outcomes. Pericytes stabilize the newly formed vessels, allowing them to mature into functional capillaries (Payne et al., 2019)They inhibit excessive endothelial cell proliferation through direct and paracrine signaling, ensuring orderly vessel formation (Bergers & Song, 2005) Additionally, pericytes aid in the synthesis and deposition of vascular basement membrane components, supporting the nascent vessel (Stapor et al., 2014)

Post-angiogenesis, vascular networks undergo remodeling to optimize blood flow and meet tissue-specific needs (LeBlanc et al., 2012) During this phase, pericytes play a central role, dictating the survival or regression of vessels. Regions with low pericyte coverage often experience vessel regression (Ferland-McCollough et al., 2017) Pericytes control capillary diameter through their contractility, adjusting blood flow as

needed(Longden et al., 2023). In the brain, pericytes maintain the integrity of the blood-brain barrier (Carlsson et al., 2023). Under low oxygen conditions, they stimulate endothelial cells to initiate angiogenesis, ensuring tissue oxygenation (Carlsson et al., 2023).

Pericytes are vital for angiogenesis, helping form and stabilize new blood vessels (Chiaverina et al., 2019). Pericytes settle into nascent vessels, releasing paracrine factors such as PDGFR-β to promote vascular maturation (Payne et al., 2019). Pericytes stabilize capillary-like structures in co-cultures with endothelial cells and astrocytes (Nakagawa et al., 2007). Pericytes regulate endothelial cell migration, proliferation, and differentiation, participating in new blood vessel formation through signaling molecules like PDGFR-β, TGF-β, VEGF, Ang-1, and S1P (Gaengel et al., 2009)

Pericytes are crucial for the development and maintenance of endothelial barriers. The most robust endothelial barriers are present in the CNS and retina vasculature (P. Li & Fan, 2023). In the CNS, pericytes interact with microglia, neurons, endothelial cells (ECs), and astrocyte end-feet, forming the functional neurovascular unit (NVU) (Kisler et al., 2021). Pericyte recruitment is essential for BBB formation during embryogenesis, preceding astrocyte involvement (Daneman & Prat, 2015). Pericyte coverage also plays a critical role in controlling vascular permeability (Ferland-McCollough et al., 2017) Furthermore, Pericytes are highly sensitive to inflammatory signaling and act as immune cell precursors, driving leukocytes to inflammation sites

(Navarro et al., 2016). In vitro studies show that TNF-α-stimulated pericytes initiate immune responses, enhancing endothelial cell interactions and macrophage recruitment (Gil et al., 2022)

In various diseases, such as traumatic brain injury, stroke, multiple sclerosis, diabetic retinopathy, and Alzheimer's disease, pericytes have been found to migrate away from the vasculature, altering the endothelial cell-pericyte ratio (Bergers & Song, 2005). Pericytes, tightly associated with endothelial cells on capillaries, are crucial for the neurovascular unit and BBB (Sweeney et al., 2016). They regulate cerebral blood flow, neurovascular growth, and BBB integrity (Sweeney et al., 2016). Loss of pericyte coverage has been linked to BBB breakdown and impaired endothelial barrier function (Brown et al., 2019). Pericytes maintain BBB function by releasing Ang-1 and TGF-β1, which increase occludin expression in ECs (Cao et al., 2021)

Diabetic retinopathy (DR), a severe complication of diabetes mellitus, involves microangiopathy that can lead to blindness (Kropp et al., 2023). Loss of retinal capillary pericytes results in endothelial cell proliferation, thickened basal membranes, and retinal barrier breakdown, causing vascular lumen constriction, altered blood flow dynamics, capillary occlusion, severe hemorrhage, and retinal detachment (Z.-S. Zhang et al., 2020). Pericytes play a vital role in pathological angiogenesis regulation. Early DR changes are linked to pericyte loss due to chronic hyperglycemia, indicating

that pericyte apoptosis is a key cause of pathological angiogenesis in diabetes (P. Li & Fan, 2023)

Upon injury or stress, pericytes become activated and undergo phenotypic changes, including proliferation, migration, and differentiation into myofibroblasts (Darby et al., 2014). For example, Pericytes were found to contribute to airway remodeling by differentiating into myofibroblasts and contributing to airway smooth muscle thickening and airway hyperresponsiveness (Johnson, 2015) This transition is a critical event in the initiation and progression of fibrosis (Y. Wang et al., 2024). Pericyte activation is mediated by various signaling pathways, including TGF-β, PDGF, and Notch (Arboleda-Velasquez et al., 2014)

TGF-β, in particular, is a potent inducer of pericyte-to-myofibroblast transition (PMT), promoting ECM production and fibrosis (X. Zhao et al., 2022). Epigenetic changes, such as DNA methylation and histone modifications, also play a role in pericyte activation and fibrotic response (Duong & Hagood, 2018). Activated pericytes contribute to fibrosis by producing ECM components such as collagen, fibronectin, and proteoglycans (Wight & Potter-Perigo, 2011). They also secrete matrix metalloproteinases (MMPs) and tissue inhibitors of metalloproteinases (TIMPs), which regulate ECM turnover and remodeling (Cabral-Pacheco et al., 2020)

1.5 Aims

The CXCL12/CXCR4 axis is known to be involved in inflammatory responses and tissue remodeling, making it a potential target for therapeutic intervention in chronic allergic asthma (Janssens et al., 2018). Given the critical role of this chemokine axis in disease pathology, our research focuses on the therapeutic potential of inhibiting CXCL12 in bronchial remodelling. Despite the growing interest in the CXCL12 signalling pathway, we are the first researchers to explore the effects of inhibiting CXCL12 using a novel neutralizing ligand LIT927 on bronchial remodelling in an established mouse model of house dust mite-induced chronic allergic asthma. **The present study aims to address this knowledge gap by investigating the therapeutic potential of a novel CXCL12 neutralizing ligand, LIT-927, on bronchial and vascular remodelling via the mouse model of house dust mite-induced chronic allergic asthma.**

We hypothesize that house dust mite (HDM) exposure induces structural changes in the lung by increasing CXCL12 levels, leading increased airway smooth muscle thickening and vascular remodeling. This could be caused by pericyte uncoupling and migration, which contribute to airway smooth muscle thickening and lung dysfunction. Conversely, treatment with LIT-927, a CXCL12 neutralizing ligand, will mitigate these effects by disrupting the CXCL12 chemokine gradient, preventing pericyte migration, and thereby reducing smooth muscle thickening and vascular remodeling and improving lung function.

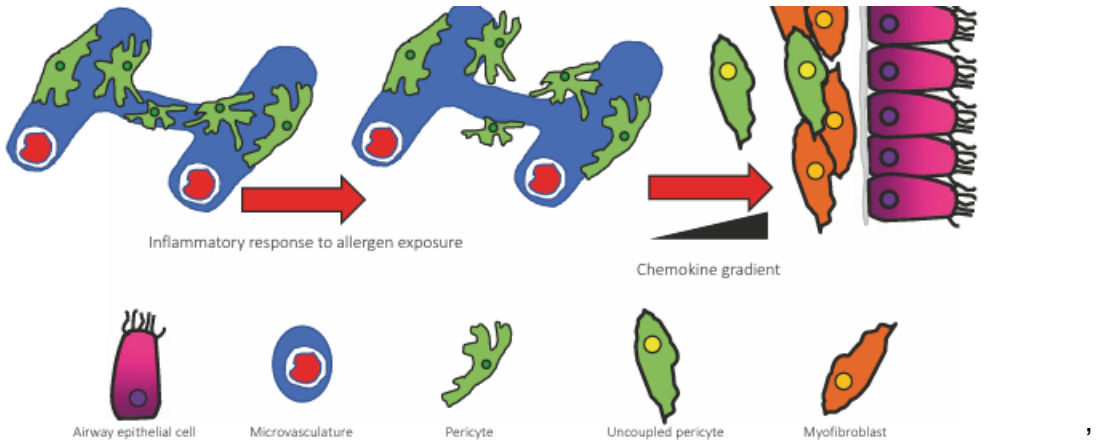

Figure 1.6 Summarizes the hypothesis that; Persistent Th2-polarized airway inflammation leads to increased CXCL12 lung expression which causes increased inflammation, alpha smooth muscle thickening, vascular remodeling and pericyte uncoupling from the pulmonary microvasculature. Subsequently, pericytes migrate into the airway smooth muscle bundles, contributing to increased airway stiffness and hyperreactivity.

Chapter 2: LIT-927 attenuates bronchial remodeling in the mouse model of house dust mite-induced chronic allergic asthma.

2.1 Introduction

Asthma is a chronic inflammatory disease characterized by airway hyperresponsiveness, bronchial remodeling, and persistent airflow obstruction (Bergeron et al., 2010). Among the various factors contributing to the pathophysiology of asthma, the CXCL12 signaling pathway has emerged as a critical player (Negrete-Garcia et al., 2009). Although the role of CXCL12 in bronchial remodeling and fibrosis is less explored compared to its well-documented effects in organs such as the liver,

kidneys, and heart, recent studies suggest that CXCL12 could be pivotal in mediating airway changes in asthma (Wu et al., 2023). Insights from these studies provide valuable context for investigating CXCL12's roles in the lungs, given the similarity in cellular mechanisms across various tissues.

The CXCL12/CXCR4 axis is known to be involved in inflammatory responses and tissue remodeling, making it a potential target for therapeutic intervention in chronic allergic asthma (Janssens et al., 2018).

CXCL12, also known as stromal cell-derived factor 1 (SDF-1), plays a significant role in the process of smooth muscle thickening, a key factor in the pathogenesis of various vascular diseases (Janssens et al., 2018). . This chemokine, through its interactions with receptors CXCR4 and CXCR7, activates downstream signaling pathways that promote the proliferation and migration of smooth muscle cells (SMCs).

The binding of CXCL12 to CXCR4 initiates a cascade involving MAPK, ERK1/2, and AKT pathways, which are critical for cell survival, proliferation, and migration (Y. Shi et al., 2020).. Additionally, CXCL12 influences the phenotypic switch of SMCs from a contractile to a synthetic state, enhancing their capacity to produce extracellular matrix components that contribute to vessel wall thickening (Koch & Engele, 2020). This process is particularly evident in conditions such as atherosclerosis and restenosis, where elevated levels of CXCL12 are associated with increased smooth muscle cell

proliferation and migration, leading to neointimal hyperplasia and vascular remodeling (Guo et al., 2016) Understanding the role of CXCL12 in these mechanisms provides insights into potential therapeutic targets for preventing or mitigating vascular diseases characterized by smooth muscle thickening (Guo et al., 2016)

Given the critical role of this chemokine axis in disease pathology, this chapter aims to assess the therapeutic potential of inhibiting CXCL12 in airway smooth muscle thickening in a well-established mouse model of house dust mite (HDM)-induced chronic allergic asthma.

We selected the mouse model of house dust mite-induced chronic allergic asthma (HDM model), as Unlike the OVA model, which centres on a single protein and often necessitates adjuvants like aluminium hydroxide for pronounced allergic responses (Aun et al., 2017), the HDM model mirrors the multifaceted nature of human asthma triggers more closely (Birrell et al., 2010) HDM extracts are composed of a complex mixture of proteins, lipids, and endotoxins, closely emulating the diversity of allergens encountered by humans (Aun et al., 2017; Birrell et al., 2010; J. Rowley et al., 2015). This complexity allows for the induction of hallmark pathological features of asthma, such as goblet cell hyperplasia, airway remodelling, and eosinophilic inflammation, often without the need for adjuvants. Furthermore, while both models permit chronic exposure studies, the chronic HDM exposure more authentically represents the progression and long-term effects of the human asthmatic condition (Aun et al., 2017;

Birrell et al., 2010; J. Rowley et al., 2015). Although the OVA model has significantly contributed to our understanding of asthma's molecular and cellular underpinnings, the HDM model, with its nuanced representation of real-world allergen exposures (Aun et al., 2017; Birrell et al., 2010; J. Rowley et al., 2015). and resultant pathophysiological processes, holds a distinctive edge for comprehensive asthma research.

The selection of LIT-927 as a neutralizing agent underscores the importance and novelty of this research. Figure 3.3 Provides an overview of the mechanism by which LIT-927 is able to bind to CXCL12.

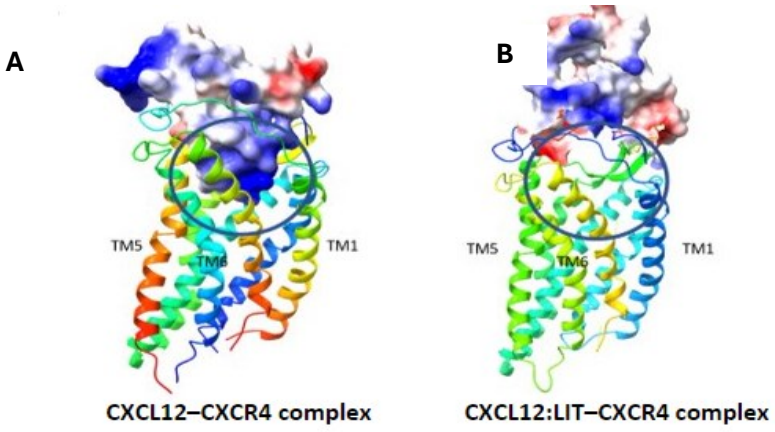

Figure 2.1: Interaction of CXCR4 with CXCL12 and its dynamics in the presence of LIT-927. **(A)** The CXCR4 receptor is depicted using a ribbon diagram with a gradient transitioning from N to C termini in a rainbow scheme. The ligand, CXCL12, is presented with a surface map and is coloured according to its charge distribution. An emphasized circle pinpoints the depth at which CXCL12 penetrates the receptor's core when not complexed with LIT-927. **(B)** A portrayal of the pre-docked

interaction of the CXCL12:LIT-927 complex with CXCR4. This emphasizes the change in dynamics in the ligand-receptor interaction due to LIT-927's presence.

A comparative analysis reveals distinct advantages of LIT-927 over traditional CXCL12 and CXCR4 inhibitors. LIT-927 offers several advantages over traditional treatments. Unlike CXCR4 inhibitors such as AMD3100, which can promote the release of CXCL12 from bone marrow, LIT-927 selectively targets CXCL12, ensuring that CXCR4 signaling remains unaffected. This selectivity reduces the likelihood of off-target effects (Daubeuf et al., 2013) In terms of administration, LIT-927's oral bioavailability provides a convenient option compared to some monoclonal antibodies (mAbs) that require intravenous or subcutaneous administration (Daubeuf et al., 2013).

Preliminary evidence indicates that LIT-927 has a promising safety profile. This stands in contrast to other strategies, such as RNA-based methods, which might introduce unforeseen off-target consequences or trigger immune responses (Daubeuf et al., 2013). The precision targeting of LIT-927 enhances its potential for use in combination with other treatments for lung diseases without increasing the risk of amplified toxicity (Daubeuf et al., 2013). Finally, LIT-927 boasts greater stability and cost-effectiveness compared to mAbs or RNA-based therapeutics (Daubeuf et al., 2013).

In conclusion this chapter aims to offer a novel and promising approach to asthma treatment. The findings from this study could pave the way for more integrated and effective therapeutic strategies, ultimately improving the management and outcomes for patients with chronic allergic asthma.

2.2. Methods

2.2.1 In vivo HDM model

Female C57BL/6 mice (n=30, aged 6–8 weeks) were acquired from Charles River and maintained either at Imperial College London's central animal facility (South Kensington campus) or at Aston University's central animal facility, ensuring specific pathogen-free conditions. These mice were subjected to a 12-hour light-dark regime and were given access to ad libitum food and water. All procedures followed the UK Home Office and Imperial College guidelines as per the Animals (Scientific Procedures) Act 1986. All experiments on animals were conducted according to United Kingdom Home Office regulations (project license P75A73BEB held by the

Principal Investigator), and animal handling was performed by qualified personnel. All studies were performed and reported according to the revised ARRIVE guidelines (du Sert et al., 2020).

The HDM extract, sourced from either Greer Laboratories, USA or Citeq, The Netherlands, was prepared in sterile phosphate-buffered saline (PBS) to attain a 2.5 mg/ml concentration. Mice were intranasally administered 10 µl of this solution. In parallel, control mice (n=15) received an intranasal dose of 10 µl sterile PBS, adhering to an identical protocol. LIT-927, procured from Axon Medchem (Groningen, The Netherlands), was diluted in a VEH of methyl-β-cyclodextrin (Sigma) at 10% w/v to achieve a concentration of 197 ng/ml. This solution (10 µl) was intranasally given to the mice right before their exposure to the allergen.

After the administration of PBS/HDM, each mouse was evaluated for respiratory distress symptoms, encompassing indications such as sneezing, nose rubbing, evident difficulty in breathing, diminished movement, and discernible wheezing. Each symptom contributed one point, leading to a possible maximum score of 5 for each mouse.

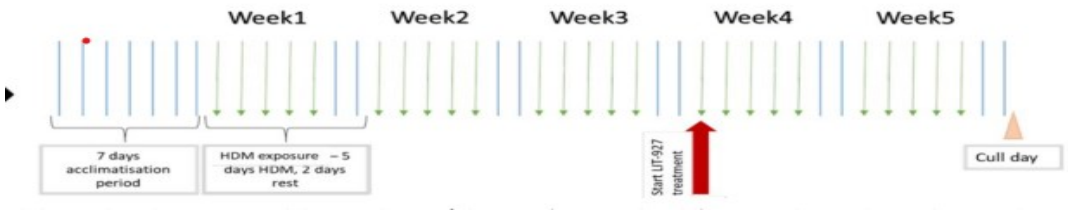

Figure 2.2: Schematic overview of the dosing strategy. C57BL/6 mice (6-8 weeks old) were exposed to either PBS (10 µL) or HDM extract (25 µg in 10 µL) for three consecutive weeks. This was followed by intranasal administration of 10 µL PBS+VEH (10% w/v methyl-β-cyclodextrin), 10 µL PBS+LIT927 at 197 ng/mL in 10% w/v methyl-β-cyclodextrin), HDM+VEH (25 µg HDM (Citeq) in 10 µL in 10% w/v methyl-β-cyclodextrin) and HDM+LIT927 (25 µg HDM in 10 µL with 197 ng/mL LIT927 in 10% w/v methyl-β-cyclodextrin) Data are derived from two independent experiments with 15 mice per group.

2.2.2 Sample collection

Mice were euthanized via an intraperitoneal injection of a pentobarbital overdose, ensuring a humane procedure. Subsequent to euthanasia, a variety of samples were collected from each mouse for distinct assessments. Bronchoalveolar lavage fluid was extracted to determine immune cell profiles. For experimental procedures, materials such as those required for lung section immunostaining, flow cytometric analysis, and cell culturing were sourced from the mice. Lungs were surgically excised and then subjected to hematoxylin and eosin staining or other specific immunostaining techniques, elaborated in the following sections.

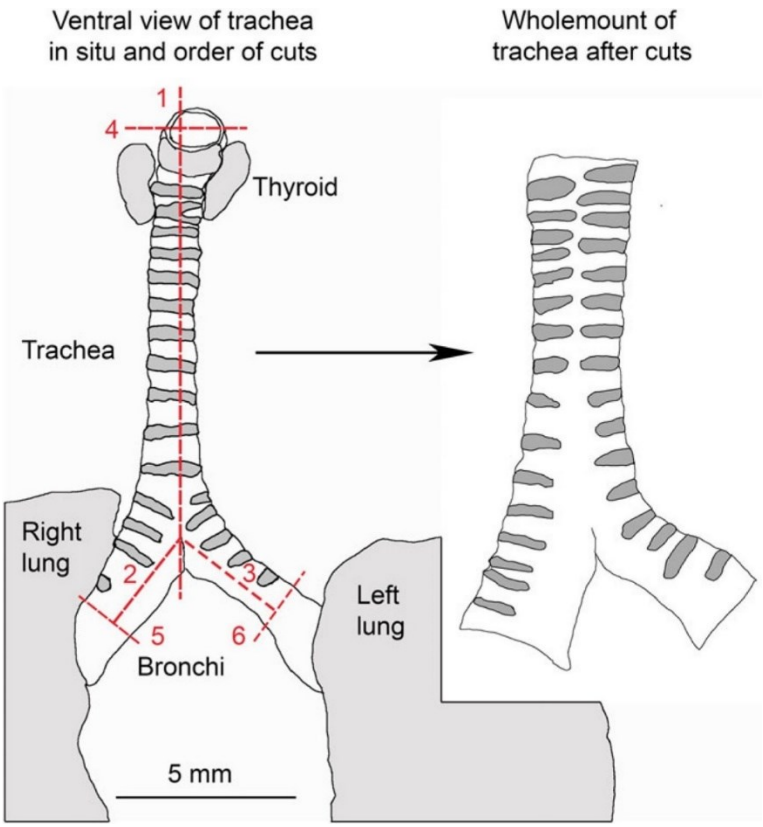

Figure 2.3 Schematic diagram of mouse trachea in situ showing the order of cuts (dashed red lines) to make a wholemount preparation. 1: longitudinal cut along ventral aspect of trachea; 2 and 3: cuts along bronchi; 4: cut across larynx; 5 and 6: cuts across bronchi. The resulting wholemount is shown on the right

2.2.3 Histological Analysis of Lung Tissues

Lung specimens were infused with 10% formalin solution and stored overnight in the same fixative. Subsequently, they were preserved in pure ethanol. Following preservation, the tissues were embedded in paraffin and sectioned to a 3 µm thickness. Standard staining procedure using hematoxylin and eosin was carried out as outlined by the Sigma-Aldrich protocol.

2.2.4 Preparation of Lung Sections and Tracheobronchial Whole Mounts

Lungs excised from mice were preserved in a sucrose solution to facilitate cryopreservation. After rinsing away the sucrose with PBS, the samples were encapsulated in TissueTek OCT (Sakura) and subsequently frozen at -80°C. Sections of 10 µm thickness were prepared using a Leica cryostat and adhered to Superfrost Plus slides (Fisher Scientific), which were then stored at -80°C. Before staining, slides were equilibrated to ambient temperature. Tissue sections were demarcated with a hydrophobic pen. A 5% NGS and 0.3% Triton-X mixture in PBS was used to block and permeabilize the sections for a minimum of 2 hours. After blocking, sections were cleansed with PBS and subjected to an overnight incubation with designated primary antibodies (as listed in Table 3). Subsequent to another PBS rinse, sections were exposed to secondary antibodies tailored to each primary antibody's origin species. To evaluate specificity, control sections were also processed without primary antibody exposure. After a 2-hour secondary antibody incubation (refer to Table 2.3 for details), sections were again rinsed and subsequently mounted with Fluoroshield inclusive of DAPI. Regarding tracheobronchial whole mounts, significant airway portions spanning from the larynx to lung sections were dissected, cleared of excess connective tissue, and secured onto Kwikgard™-coated 6-well plates (WPI). After overnight blocking with 5% NGS/0.3% Triton-X 100 in PBS, tracheal sections were longitudinally bisected and individually stained for pericytes and endothelial cells using primary and secondary antibodies. Once staining was completed, sections were triple rinsed in PBS and set using Fluoroshield. Optimal concentrations for antibodies were ascertained via titration.

Visualization of lung sections stained with hematoxylin and eosin was facilitated with the EVOS brightfield microscope (ThermoFisher). For immunostained sections, imaging was executed on a TCS SP8 FALCON Leica confocal microscope, equipped with a specific laser and objective configuration. Tracheobronchial whole mounts were examined and imaged utilizing a Zeiss LSM0-510 inverted confocal microscope, comprising a specialized set of lasers and objectives. Image processing was accomplished using LAS X software (Leica).

2.2.5 Immunofluorescence

For the immunohistochemical process, cells first underwent three washing cycles with PBS, each lasting 5 minutes. Following this, a fixation step was performed using a 3% paraformaldehyde (PFA) solution for 15 minutes at room temperature. After washing the fixative off, a blocking step was undertaken to minimize non-specific antibody bindings using a solution of 5% normal goat serum in 0.3% Triton-X-100/PBS, and this was allowed to proceed for 1 hour. The cells were then exposed to the primary antibodies (as detailed in Table 3) for a duration of 2 hours. Post-primary antibody incubation, the cells were washed and treated with the corresponding secondary antibodies for 1 hour at room temperature. To conclude the process, another series of washes was conducted, and the coverslips bearing the cells were mounted onto microscope slides. Mounting was achieved using Fluoroshield (sourced from Sigma-Aldrich), which contains the nucleic acid stain, 4',6-diamidino-2-phenylindole (DAPI), facilitating the visualization of cell nuclei.

Antigen Target	***Origin of Antibody***	***Specific Clone***	***Dilution Ratio***	***Provided by***
CD31	Hamster	2H8	1:500	Abcam
CXCR4	Rat	2B11	1:200	eBioscience
α-SMA	Mouse	1A4	1:1000	Sigma-Aldrich

Table 2.1 Antibodies used in immunostaining.

2.2.6 CXCL12 ELISA

BAL supernatants were stored at −20°C, then submitted to ELISA to determine mouse CXCL12 expression according to the manufacturer's instructions (R&D Systems, Abingdon, UK).

2.2.7 Molecular Modelling

A comprehensive model of the CXCR4 receptor was produced using MODELLER drawing from the PDB structures 3OE0 and 2N55 as reference templates. From the thousand preliminary models developed by MODELLER, refinement was undertaken using ROSETTA, with the application of the implicit membrane forcefield. The top-performing model as per ROSETTA's scoring system was selected for ensuing docking experiments. The compound LIT-927 was docked into the average NMR structure, sourced from PDB:4UAI, employing AUTODOCK with standard settings. The default charge configurations for both the ligand and receptor, as delineated in AUTODOCKTOOLS, were adopted for the series of 100 distinct docking runs. Outcomes were grouped in 2 Å intervals. The predominant cluster exhibiting the most favorable docking score for the CXCL12:LIT-297 pairing was preserved for advanced docking operations with the CXCR4. Docking was performed across the entire surface of the CXCL12.

To dock either just the CXCL12 or the pre-established CXCL12:LIT-27 complex into the comprehensive CXCR4 model, GRAMM was utilized in its low-resolution mode. For every ligand, a total of 5,000 docking runs were executed, with subsequent refinement of the resultant complexes facilitated by ROSETTA. The lowest scoring 50 structures from each docking session were clustered, adhering to a 2 Å threshold. By scrutinizing the central structure from the largest cluster in every docking session, insights were garnered regarding the influence of LIT-927 on the CXCL12's affinity for CXCR4.

2.2.8 Statistical Analysis

Data analysis was conducted using GraphPad Prism Software version 6 (GraphPad Software, San Diego, CA). For statistical evaluations, we employed the student’s t-test or one-way ANOVA followed by Tukey's post hoc test when applicable. A significance threshold was set at $P < 0.05$. Additionally, Pearson correlation analysis was utilized to determine the relationship between ASM thickening and cell counts. Results are expressed as means ± SE.

2.3. Results

2.3.1. Exposure to HDM from either Greer (Lenoir, North Carolina, USA) or Citeq (Groningen, Netherlands) Induced Clinical Symptoms of Airway Hyperresponsiveness

Symptoms were monitored daily following exposure to HDM allergens from two different manufacturers: Greer (Lenoir, North Carolina, USA) and Citeq (Groningen, Netherlands). Symptoms included sneezing, nose rubbing, hunched posture, labored breathing, and audible wheezing. In the control group of mice exposed to PBS, no symptoms of dyspnea were observed, with an average score of 0. However, by the third week of exposure to HDM from either Greer or Citeq, mice displayed symptoms of airway hyperresponsiveness such as sneezing and nose rubbing, with an average score of 1.8. These symptoms worsened over time, reaching an average score of 3.7 by the fifth week of HDM exposure. There was no significant difference in the severity or onset of symptoms between the mice exposed to Greer HDM and those exposed to Citeq HDM.

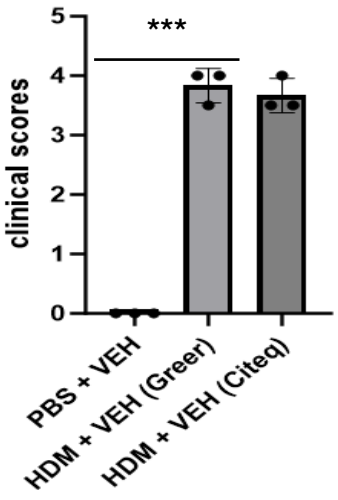

Figure 2.4 Airway Hyperresponsiveness Weekly Symptom Scores over a 5-week exposure period Following Exposure to HDM from Two Different Manufacturers-Greer (Lenoir, North Carolina, USA) or Citeq (Groningen, Netherlands). Female C57/BL6 mice (6-8 weeks old) were treated with PBS (10 µL) or HDM extract (25 µg in 10 µL) sourced from two manufacturers: Greer (Lenoir, North Carolina, USA) or Citeq (Groningen, Netherlands) for 5 days a week for 5 consecutive weeks. Sample size: n=3, from two independent experiments. Statistical Analysis was determined by one-way ANOVA for multiple groups with Tukey's post hoc test and ***$p < 0.001$.

2.3.2. Exposure to HDM from either Greer (Lenoir, North Carolina, USA) or Citeq (Groningen, Netherlands) Induced immune cell infiltration in the BAL.

Inflammation was assessed by quantifying the percentages of mononuclear cells, including lymphocytes, neutrophils, and eosinophils in bronchoalveolar lavage (BAL) fluid. Our findings demonstrated that exposure to house dust mite (HDM) from either Greer (Lenoir, North Carolina, USA) or Citeq (Groningen, Netherlands) induced increased immune infiltration in mice compared to the control group exposed to PBS. The total number of cells was significantly higher in BAL fluid from mice exposed to HDM for five weeks compared to the control group exposed to PBS ($p<0.001$). Our study also revealed that both Greer and Citeq induced an eosinophilic response, indicating a Th2-type immune reaction.

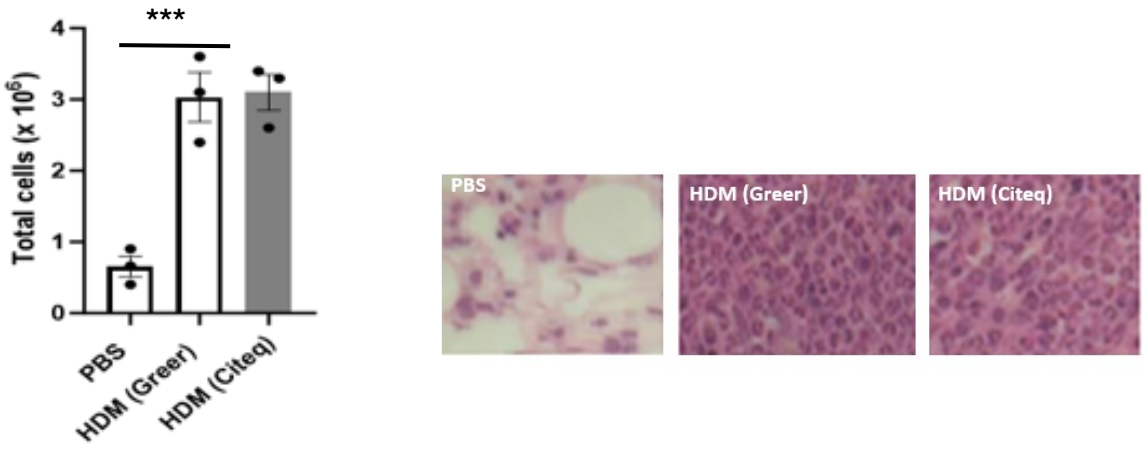

Figure 2.5: **Total Immune Cell infiltration in BAL over a 5-week exposure period Following Exposure to HDM from Two Different Manufacturers-Greer (Lenoir, North Carolina, USA) or Citeq (Groningen, Netherlands).** Female C57BL/6 mice (6-8 weeks old) were treated with PBS (10 µL) or HDM extract (25 µg in 10 µL) sourced from two manufacturers: Greer (Lenoir, North Carolina, USA) or Citeq (Groningen, Netherlands) for 5 days a week for 5 consecutive weeks. At the end of the protocol, the lungs were removed and bronchoalveolar lavage (BAL) fluid was collected Total inflammatory cell infiltrates were enumerated by Hematoxylin and eosin staining of paraffin-embedded lung sections. Data are derived from two independent experiments with n=3 mice per group. ***$p < 0.001$, determined by one-way ANOVA for multiple groups with Tukey's post hoc test. ls. n = 3.

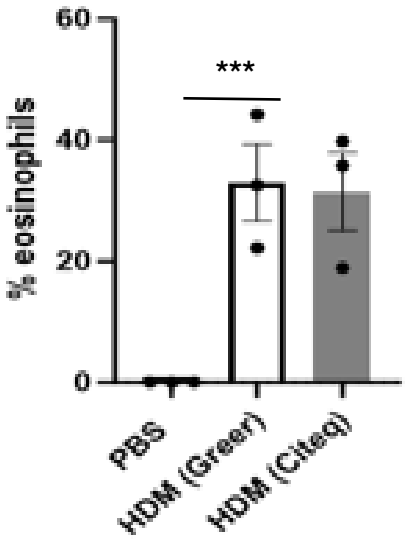

Figure 2.6 Percentage of Eosinophils in BAL over a 5-week exposure period Following Exposure to HDM from Two Different Manufacturers-Greer (Lenoir, North Carolina, USA) or Citeq (Groningen, Netherlands). Female C57BL/6 mice (6-8 weeks old) were treated with PBS (10 µL) or HDM extract (25 µg in 10 µL) sourced from two manufacturers: Greer (Lenoir, North Carolina, USA) or Citeq (Groningen, Netherlands) for 5 days a week for 5 consecutive weeks. At the end of the protocol, the lungs were removed and bronchoalveolar lavage (BAL) fluid was collected and eosinophils were enumerated Data are derived from two independent experiments with n=3 mice per group. ***$p < 0.001$, determined by one-way ANOVA for multiple groups with Tukey's post hoc test.

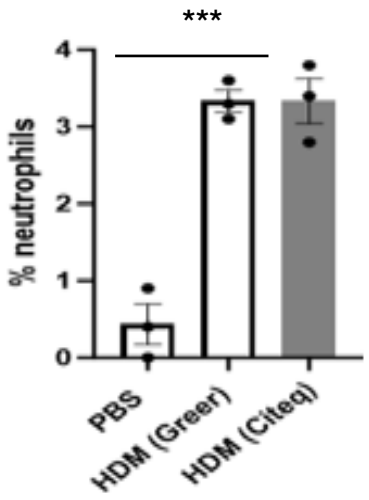

Figure 2.7: **Percentage Of Neutrophils in BAL over a 5-week exposure period Following Exposure to HDM from Two Different Manufacturers-Greer (Lenoir, North Carolina, USA) or Citeq (Groningen, Netherlands).** Female C57BL/6 mice (6-8 weeks old) were treated with PBS (10 µL) or HDM extract (25 µg in 10 µL) sourced from two manufacturers: Greer (Lenoir, North Carolina, USA) or Citeq (Groningen, Netherlands) for 5 days a week for 5 consecutive weeks. At the end of the protocol, the lungs were removed and bronchoalveolar lavage (BAL) fluid was collected and neutrophils were enumerated Data are derived from two independent experiments with n=3 mice per group. ***p < 0.001, determined by one-way ANOVA for multiple groups with Tukey's post hoc test.

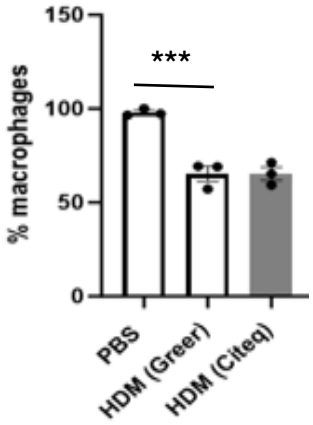

Figure 2.8: **Percentage Of Macrophages in BAL over a 5-week exposure period Following Exposure to HDM from Two Different Manufacturers-Greer (Lenoir, North Carolina, USA) or Citeq (Groningen, Netherlands).** Female C57BL/6 mice (6-8 weeks old) were treated with PBS (10 µL) or HDM extract (25 µg in 10 µL) sourced from two manufacturers: Greer (Lenoir, North Carolina, USA) or Citeq (Groningen, Netherlands) for 5 days a week for 5 consecutive weeks. At the end of the protocol, the lungs were removed and bronchoalveolar lavage (BAL) fluid was collected and macrophages were enumerated Data are derived from two independent experiments with n=3 mice per group. ***p < 0.001, determined by one-way ANOVA for multiple groups with Tukey's post hoc test.

2.3.3. Exposure to HDM from either Greer (Lenoir, North Carolina, USA) or Citeq (Groningen, Netherlands) Increased Alpha Smooth Muscle Actin Expression

To measure airway smooth muscle (ASM) thickness, we stained 10 µm-thick frozen lung sections for alpha-smooth muscle actin (α-SMA). The results demonstrated that exposure to house dust mite (HDM) allergens from two different manufacturers—Greer (Lenoir, North Carolina, USA) and Citeq (Groningen, Netherlands)—caused a significant increase in ASM thickening, with no discernible difference observed between the two sources.

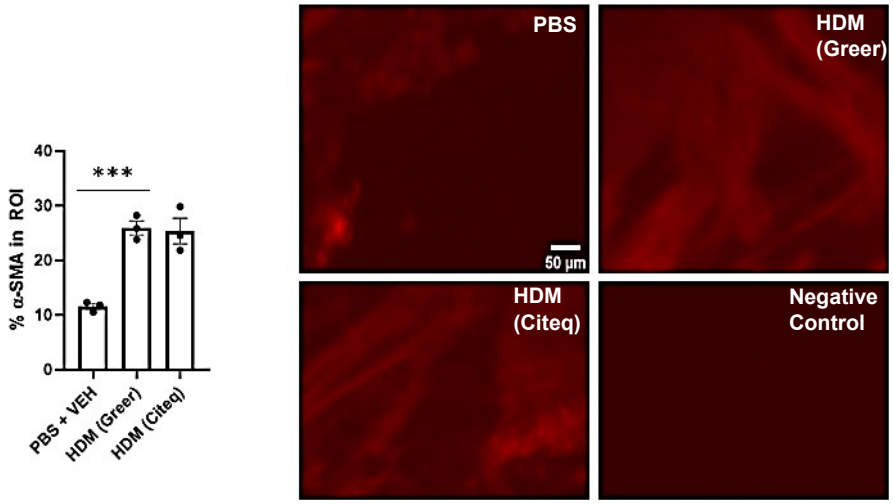

Figure 2.9 Exposure to HDM from either Greer (Lenoir, North Carolina, USA) or Citeq (Groningen, Netherlands) Induced increased alpha smooth muscle actin expression. Female C57BL/6 mice (6-8 weeks old) were exposed to either PBS (10 µL) or house dust mite (HDM) extract (25 µg in 10 µL) from Greer (Lenoir, North Carolina, USA) or Citeq (Groningen, Netherlands) for five consecutive weeks. At the end of the treatment protocol, lung sections from both PBS control and HDM-exposed mice were stained for the mesenchymal cell marker α-smooth muscle actin (α-SMA; shown in red), to assess smooth muscle thickening in the airway wall. are representative of n=3 from two independent experiments. Significant differences were determined using one-way ANOVA for multiple groups with Tukey's post hoc test (***p < 0.001). Scale bar = 50 µm.

2.3.4. Exposure to HDM increased CXCR4 and CXCL12 expression after 5 weeks

We assessed CXCR4 expression by staining 10um lung sections from control (PBS) and HDM-treated mice with the CXCR4 antibody Our research showed that HDM exposure significantly increased CXCR4 expression After 5 weeks, highlighting the potential involvement of the CXCL12-CXCR4 signalling axis in asthma. We quantified CXCL12 in the BAL fluid using an enzyme-linked immunosorbent assay (ELISA). Our study found that CXCL12 expression was significantly elevated in the BAL fluid of mice exposed to HDM for five weeks, with levels exceeding baseline after 5 weeks of exposure $p < 0.01$.

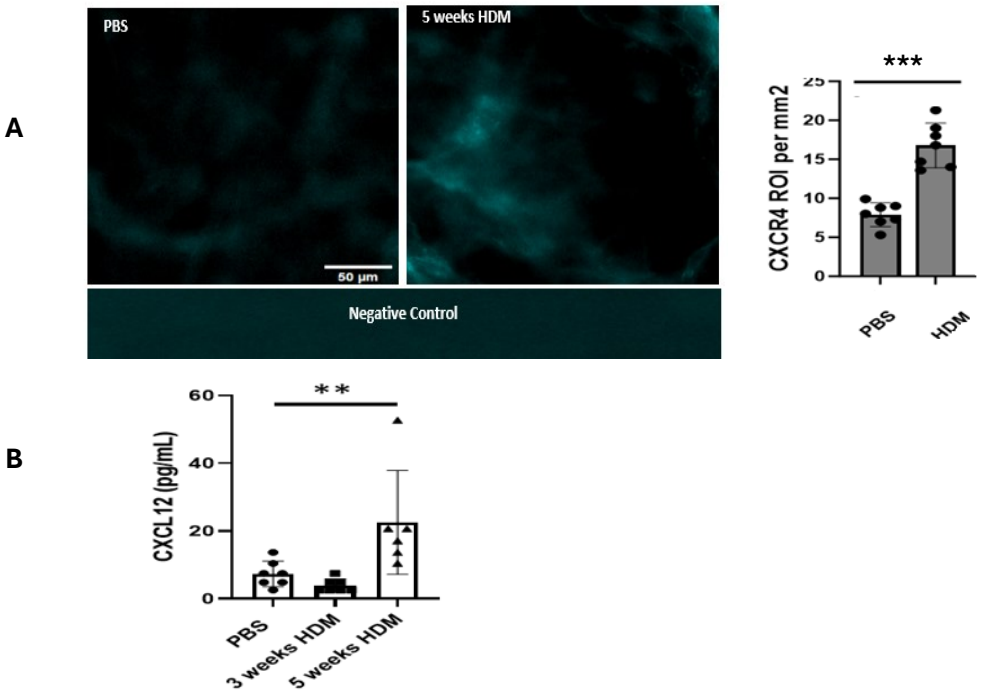

Figure 2.10: CXCR4 and CXCL12 Expression in C57BL/6 Mice Following HDM Exposure Female C57BL/6 mice (6-8 weeks old) were exposed to either PBS or HDM extract for three and five consecutive weeks. **A** At the end of the protocol, lung sections obtained from PBS control and HDM-exposed mice were stained the CXCR4 marker (cyan). Images are representative of n=7 from 2 independent experiments ***$p < 0.001$, determined by one-way ANOVA for multiple groups with Tukey's post hoc test. Scale bar = 50µm. **B** Bronchoalveolar fluid obtained from both PBS control mice and mice exposed to HDM for either 3 weeks or 5 weeks was subjected to enzyme-linked immunosorbent assay (ELISA) to assess the levels of CXCL12. Data derived from sample sizes ranging from n = 7 to n = 8 per group, representing data collected from two independent experiments, ***$p < 0.001$, determined by one-way ANOVA for multiple groups with Tukey's post hoc test.

2.3.5 LIT927 administration reversed HDM induced symptoms of dyspnea.

To monitor airway inflammation and dyspnea symptoms in mice, daily observations were conducted. The observations included behaviors such as sneezing, nose rubbing, hunched posture, labored breathing, and audible wheezing, with a maximum score of 5 points. Mice exposed to HDM extract exhibited signs of respiratory inflammation, such as sneezing and nose rubbing, by week 3 of exposure (average score of 1.8). These symptoms worsened over time, reaching an average score of 3.7 by the end of the 5-week HDM exposure. In contrast, treatment with HDM+ LIT-927 starting at week 3 caused a decrease in dyspnea scores within a week of initiation (average score of 1.5 vs. 2.8 in HDM-exposed mice given the vehicle). These scores decreased further to nearly baseline levels two weeks after the first LIT-927 dose (average score of 0.5 vs. 3.7 in HDM-exposed vehicle-treated mice; $p<0.001$).

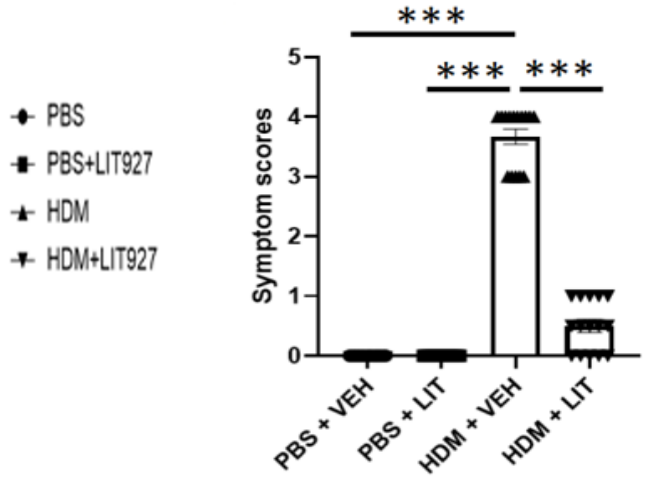

Figure 2.11: Mean Symptom Scores Across a 5-Week Treatment Regimen. Female C57BL/6 mice (6-8 weeks old) were exposed to either PBS or HDM extract for three consecutive weeks. This was followed by intranasal administration of PBS+VEH, PBS+LIT927, HDM+VEH and HDM+LIT927 Data are derived from two independent experiments with 15 mice per group. ***p < 0.001, determined by one-way ANOVA for multiple groups with Tukey's post hoc test. PBS: phosphate-buffered saline; VEH: vehicle control-10% w/v methyl-β-cyclodextrin, HDM: House Dust Mite, LIT: The CXCL12 Neutralizing ligand LIT927,

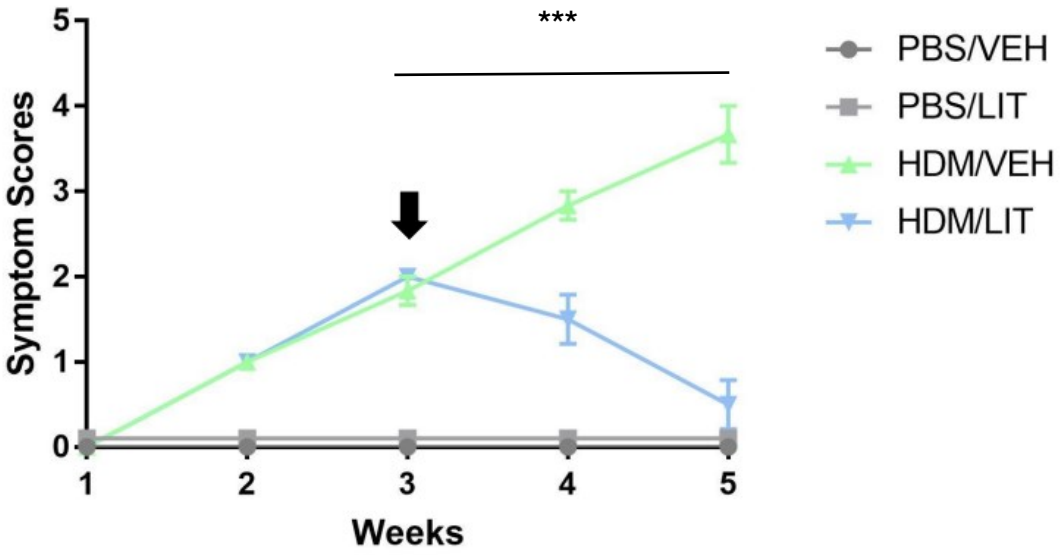

Figure 2.12: Weekly Symptom Scores Across a 5-Week Treatment Regimen. Female C57BL/6 mice (6-8 weeks old) were exposed to either PBS or HDM extract for three consecutive weeks. This was followed by intranasal administration of PBS+VEH, PBS+LIT927, HDM+VEH and HDM+LIT927 Data are derived from two independent experiments with 15 mice per group. ***$p < 0.001$, determined by one-way ANOVA for multiple groups with Tukey's post hoc test. PBS: phosphate-buffered saline; VEH: vehicle control-10% w/v methyl-β-cyclodextrin, HDM: House Dust Mite, LIT: The CXCL12 Neutralizing ligand LIT927,

2.3.6 LIT927 administration reversed HDM induced ASM thickening.

Lung sections from PBS control and HDM-exposed mice were stained for alpha smooth muscle actin α-SMA (red). To measure airway smooth muscle (ASM) thickness, alpha-smooth muscle actin (α-SMA) staining was performed on 10 µm lung sections. The results demonstrated HDM-exposed lungs displayed a thick and continuous layer of smooth muscle around the airways. This was significantly attenuated following treatment with LIT-927. LIT-927 ***p < 0.001, Mice treated with HDM+LIT-927 exhibited ASM thickness similar to those treated with PBS alone or PBS+LIT-927

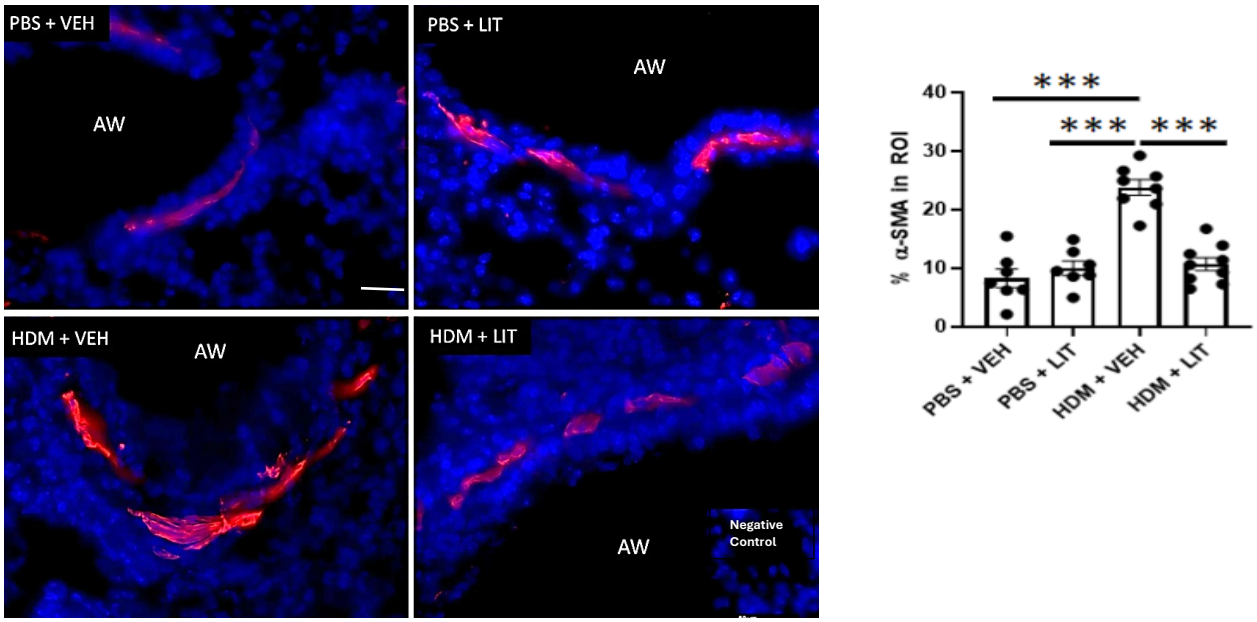

Figure 2.13 Smooth **Muscle Thickening in C57BL/6 Mice Following HDM Exposure and LIT927 Treatment** Female C57BL/6 mice (6-8 weeks old) were exposed to either PBS or HDM extract for three consecutive weeks. This was followed by intranasal administration of PBS+VEH, PBS+LIT927, HDM+VEH and HDM+LIT927 At the end of the protocol, lung sections were stained for the smooth muscle cell marker α-smooth muscle actin (α-SMA; red) to assess thickening of smooth muscle bundles (arrow indicates smooth muscle layer) Images are representative of n=8 from two independent experiments. Scale bar = 25µm. ***p < 0.001, determined by one-way ANOVA for multiple groups with Tukey's post hoc test. AW: airway, PBS: phosphate-buffered saline; VEH: vehicle control-10% w/v methyl-β-cyclodextrin, HDM: House Dust Mite, LIT: The CXCL12 Neutralizing ligand LIT927,

2.3.7 LIT927 Attenuated HDM-induced α-smooth muscle actin positive mural cell Accumulation and Elongation

LIT-927 effectively attenuated the increase in α-smooth muscle actin-positive (α-SMA+) mural cells caused by HDM exposure. Specifically, the introduction of LIT-927 significantly reduced the HDM-induced rise in these cells. Importantly, no side effects were observed with the use of LIT-927. Quantitative analysis was performed using multiple metrics, including horizontal length, perimeter, area, perimeter-to-area ratio, and circularity, to assess alterations in mural cell morphology. Notably, exposure to HDM resulted in significant changes in mural cell shape, characterized by increased horizontal length and area, but decreased perimeter and circularity. These findings suggest that LIT-927 not only reduces the number of α-SMA+ mural cells but also mitigates the morphological changes induced by HDM, highlighting its potential therapeutic role in preventing airway remodeling in asthma.

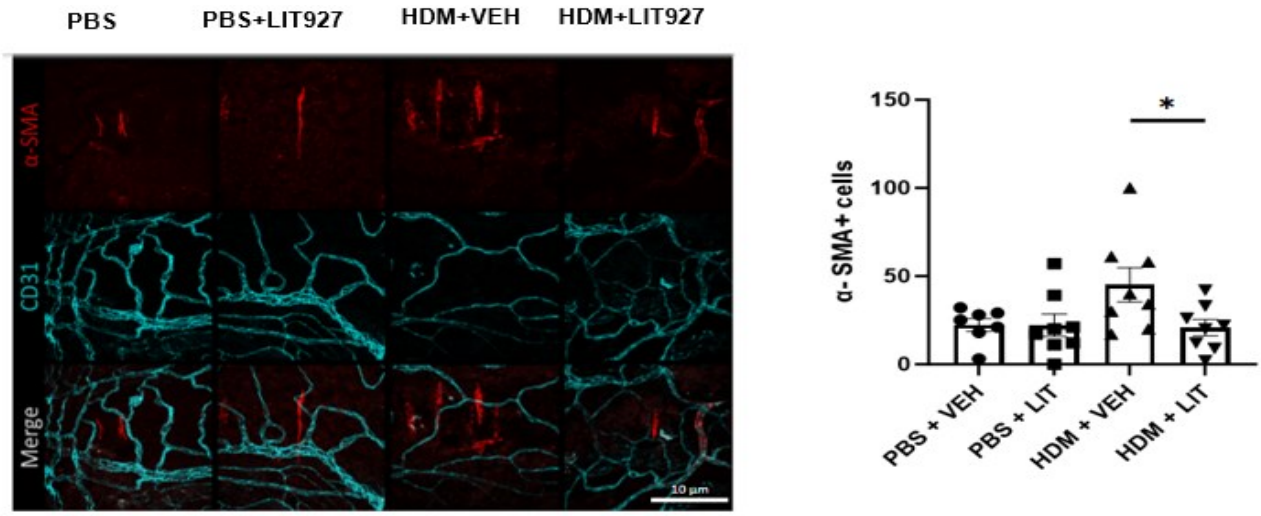

Figure 2.14: α-SMA+ Mural Cell Accumulation Following HDM Exposure and LIT927. Female C57BL/6 mice (6-8 weeks old) were exposed to either PBS or HDM extract for three consecutive weeks. This was followed by intranasal administration of PBS+VEH, PBS+LIT927, HDM+VEH and HDM+LIT927. Post-treatment, trachea and bronchi samples were, processed, and subjected to whole-mount immunostaining targeting mural cell marker α-smooth muscle actin (α-SMA; red) and endothelial cell marker CD31 (cyan), n=7 from two independent experiments. Scale bar=10um. *$p < 0.05$, based on one-way ANOVA, supplemented with the Tukey post hoc test. PBS: phosphate-buffered saline; VEH:

vehicle control-10% w/v methyl-β-cyclodextrin, HDM: House Dust Mite, LIT: The CXCL12 Neutralizing ligand LIT927

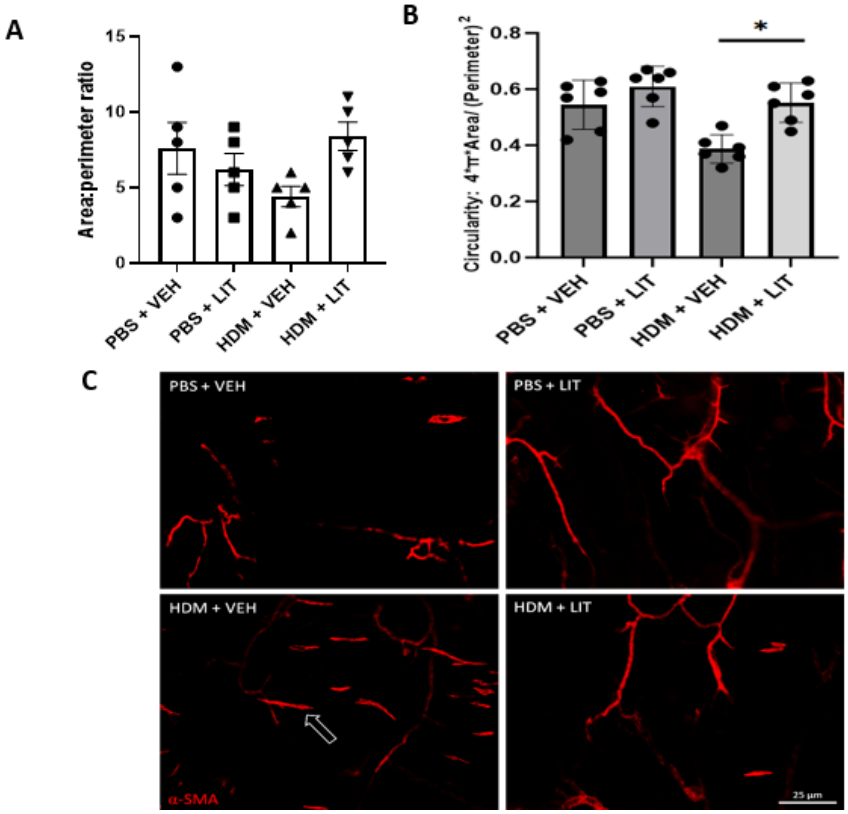

Figure 2.15: α-SMA+ Mural Cell Morphology Following HDM Exposure and LIT927 consecutive weeks. This was followed by intranasal administration of PBS+VEH, PBS+LIT927, HDM+VEH and HDM+LIT927. Post-treatment, trachea and bronchi samples were, processed, and subjected to whole-mount immunostaining targeting mural cell marker α-smooth muscle actin (α-SMA; red) n=7 from two independent experiments, *p < 0.05, based on one-way ANOVA, supplemented with the Tukey post hoc test. **(A)** The Area to Perimeter Ratio for α-SMA+ cells were calculated manually using the Image J software. **(B)** The circularity of α-SMA+ cells were calculated using the circularity plugin on Image J Software. **(C)** accumulation was visualized using florescence microscopy with arrows indicating elongated mural cells, Scale bar=25um. PBS: phosphate-buffered saline; VEH: vehicle control-10% w/v methyl-β-cyclodextrin, HDM: House Dust Mite, LIT: The CXCL12 Neutralizing ligand LIT927

2.3.8 LIT-927 does not attenuate HDM induce increase in immune cell infiltration.

Lungs were removed, and bronchoalveolar lavage (BAL) fluid was collected. The total cell counts, and the percentage of macrophages, eosinophils, and neutrophils were enumerated. Despite the administration of LIT-927, there was no significant reduction in total immune cell counts or the percentages of eosinophils, neutrophils, and macrophages in the BAL fluid of HDM-exposed mice compared to controls.

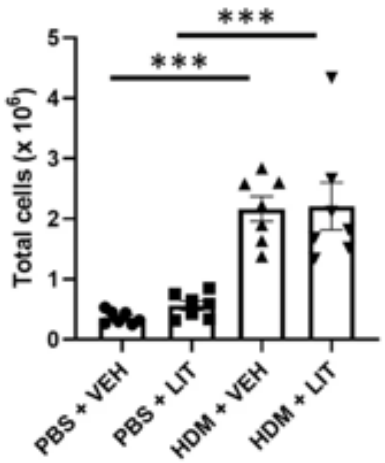

Figure 2.16 Total Immune Cell infiltration following LIT-927 administration.

Female C57BL/6 mice (6-8 weeks old) were exposed to either PBS or HDM extract for three consecutive weeks. This was followed by intranasal administration of PBS+VEH, PBS+LIT927, HDM+VEH and HDM+LIT927 At the end of the protocol, the lungs were removed and bronchoalveolar lavage (BAL) fluid was collected and total cells, were enumerated . Data are derived from two independent experiments with n=7 mice per group. ***p < 0.001, determined by one-way ANOVA for multiple groups with Tukey's post hoc test. PBS: phosphate-buffered saline; VEH: vehicle control-10% w/v methyl-β-cyclodextrin, HDM: House Dust Mite, LIT: The CXCL12 Neutralizing ligand LIT927

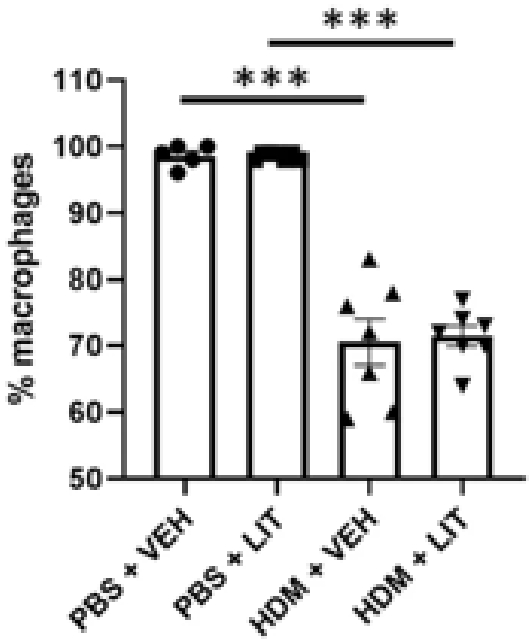

‘

Figure 2.17: Percentage Of Macrophages in BAL after LIT-927 treatment. Female C57BL/6 mice (6-8 weeks old) were exposed to either PBS or HDM extract for three consecutive weeks. This was followed by intranasal administration of PBS+VEH, PBS+LIT927, HDM+VEH and HDM+LIT927 At the end of the protocol, the lungs were removed and bronchoalveolar lavage (BAL) fluid was collected and the percentage of macrophages in BAL, were enumerated. Data are derived from two independent experiments with n=7 mice per group. ***p < 0.001, determined by one-way ANOVA for multiple groups with Tukey's post hoc test. PBS: phosphate-buffered saline; VEH: vehicle control-10% w/v methyl-β-cyclodextrin, HDM: House Dust Mite, LIT: The CXCL12 Neutralizing ligand LIT927

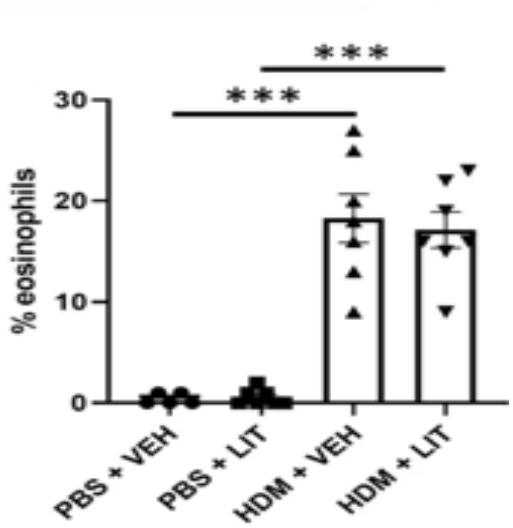

Figure 2.18: Percentage Of Eosinophils in BAL after LIT-927 treatment. Female C57BL/6 mice (6-8 weeks old) were exposed to either PBS or HDM extract for three consecutive weeks. This was followed by intranasal administration of PBS+VEH, PBS+LIT927, HDM+VEH and HDM+LIT927 At the end of the protocol, the lungs were removed and bronchoalveolar lavage (BAL) fluid was collected and the percentage of eosinophils in BAL, were enumerated. Data are derived from two independent experiments with n=7 mice per group. ***p < 0.001, determined by one-way ANOVA for multiple groups with Tukey's post hoc test. PBS: phosphate-buffered saline; VEH: vehicle control-10% w/v methyl-β-cyclodextrin, HDM: House Dust Mite, LIT: The CXCL12 Neutralizing ligand LIT927

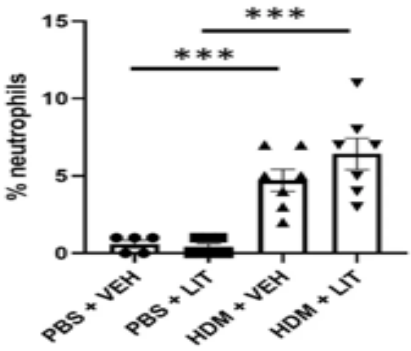

Figure 2.19: Percentage Of Neutrophils in BAL after LIT-927 treatment Female C57BL/6 mice (6-8 weeks old) were exposed to either PBS or HDM extract for three consecutive weeks. This was followed by intranasal administration of PBS+VEH, PBS+LIT927, HDM+VEH and HDM+LIT927 At the end of the protocol, the lungs were removed and bronchoalveolar lavage (BAL) fluid was collected and the percentage of neutrophils in BAL, were enumerated. Data are derived from two independent experiments with n=7 mice per group. ***p < 0.001, determined by one-way ANOVA for multiple groups with Tukey's post hoc test. PBS: phosphate-buffered saline; VEH: vehicle control-10% w/v methyl-β-cyclodextrin, HDM: House Dust Mite, LIT: The CXCL12 Neutralizing ligand LIT927

2.3 Discussion

In this chapter, we explored the impact of the CXCL12 neutralizing ligand, LIT-927, on airway smooth muscle thickening using a mouse model of allergic airway disease. Our primary aim was to evaluate the therapeutic efficacy of LIT-927 in mitigating hallmark features of asthma, such as enhanced airway smooth muscle (ASM) mass, immune cell infiltration, and clinical symptoms indicative of airway hyperresponsiveness.

Exposure to HDM from either Greer (Lenoir, North Carolina, USA) or Citeq (Groningen, Netherlands) Induced Clinical Symptoms of Airway Hyperresponsiveness

We employed the house dust mite (HDM) model because it closely mirrors the multifaceted nature of human asthma triggers (Birrell et al., 2010) Our findings in figures 2.4, 2.5, 2.6, 2.7,2.8 and 2.9 suggest that exposure to HDM allergens from different manufacturers can induce clinical symptoms of dyspnea, increased airway inflammation, and smooth muscle thickening in mice, with no significant difference in response between the suppliers. This supports the use of Dermatophagoides pteronyssinus HDM from either Greer (Lenoir, North Carolina, USA) or Citeq (Groningen, Netherlands) manufacturers in preclinical studies of allergic respiratory disease. This finding is important as there is variation between manufacturers in the specific allergen profile and LPS levels (Birrell et al., 2010)

Exposure to HDM increased CXCR4 and CXCL12 expression after 5 weeks

Our results in figure 2.10 clearly demonstrate that HDM exposure significantly amplifies CXCR4 expression, emphasizing the pivotal role of the CXCL12-CXCR4 signaling axis in asthma pathogenesis. This aligns with existing literature that highlights the significance of this pathway in asthma and fibrotic conditions. For instance, CXCR4 is notably upregulated in lung fibroblasts of idiopathic pulmonary fibrosis (IPF) patients, suggesting its involvement across immune and structural cells within the lung tissue microenvironment (Jaffar et al., 2020). To further explore this axis, we quantified CXCL12 levels using an enzyme-linked immunosorbent assay (ELISA) and found significantly elevated CXCL12 expression in the BAL fluid of mice exposed to HDM for five weeks. This is in agreement with researchers, who reported higher CXCL12 protein levels in asthmatic lungs compared to healthy ones (Negrete-Garcia et al., 2009). Notably we found that CXCL12 levels exceed baseline after three weeks of HDM exposure and this exposure and this is consistent with studies indicating that airway remodeling is not yet established at this early stage (Johnson, 2015)

CXCL12 signaling.

The elevated CXCL12 and CXCR4 expression levels in response to HDM reinforce the crucial role of the CXCL12-CXCR4 signaling pathway in asthma development and progression. Therefore, we investigated the therapeutic potential of CXCL12 inhibition using the neutralizing ligand LIT-927. Collaborating with the Biochemistry Department at Aston University, we used an incremental docking approach to demonstrate that LIT-927 binds securely to a distinct cavity on CXCL12's surface, effectively blocking key interactions between CXCL12 and CXCR4.

This was supported by noticeable differences in the conformation of the CXCL12-LIT-927 complex compared to the CXCL12-CXCR4 complex, as well as the absence of essential salt bridges typically present between the chemokine and the receptor (Stephens et al., 2020). This supports the therapeutic potential of neutralizing ligands, termed "neutraligands," which block the interaction between CXCL12 and its receptors without altering systemic CXCL12 concentrations (Stephens et al., 2020).

There are several advantages to our choice of using LIT-927 to inhibit CXCL12 signaling. Firstly LIT-927 is administered intranasally, targeting the CXCL12 gradient at its primary site of expression. Unlike conventional CXCR4 inhibitors, LIT-927 does not interfere with CXCR4 signaling pathways nor does it stimulate the release of stem cells into circulation, as with the CXCR4 inhibitor AMD300 (De Clercq, 2009) Furthermore, LIT-927 offers oral bioavailability, making it a more patient-friendly option compared to monoclonal antibodies requiring intravenous or subcutaneous administration (W. Zhou et al., 2019)

LIT-927 Attenuates HDM Induced Smooth Muscle Thickening

To assess LIT-927's therapeutic potential, we subjected mice to intranasal HDM exposure for five weeks. From the third week onward, LIT-927 was administered to disrupt the CXCL12 gradient. Our data in figures 2.11 and 2.12 demonstrate that LIT927 administration reversed HDM induced worsening of clinical symptoms. This could be explained by the fact that figure 2.13 revealed that LIT-927 significantly attenuated ASM mass and ameliorated clinical symptoms.

Our findings align with the literature, as in the context of lung fibrosis, CXCL12 promotes the activation and recruitment of fibroblasts and myofibroblasts, essential for extracellular matrix accumulation and fibrosis progression (Phillips et al., 2004). This is further supported by studies using rodent models to mimic IPF, which have shown increased CXCL12 levels in serum and BALF after bleomycin (Heukels et al., 2019).. Furthermore, previous research has shown that targeting the CXCL12-CXCR4 pathway using antagonists and inhibitors like AMD3100 has potential in reducing ASM thickening in fibrotic disorders such as idiopathic pulmonary fibrosis (Shu et al., 2013)

Notably, Chemokine (C-X-C motif) ligand 12 (CXCL12) and its receptor chemokine receptor 4 (CXCR4) have been implicated in the development of bronchial asthma, though the exact molecular mechanisms remain unclear. Chen et al. (2015) demonstrated that CXCL12/CXCR4 signaling contributes to allergic airway inflammation by inducing matrix metalloproteinase 9 (MMP-9) in a mouse model of asthma. Treatment with AMD3100, a specific CXCR4 antagonist, significantly reduced OVA-induced asthmatic symptoms and decreased epithelial MMP-9 expression.

Experiments with a bronchial epithelial cell line (16HBE) revealed that CXCL12/CXCR4 signaling works together with IL-13 to increase epithelial MMP-9 expression. Further mechanistic analysis demonstrated that CXCL12/CXCR4 promotes epithelial MMP-9 expression by inducing and activating ERK1/2. These findings provide new insights into the role of CXCL12/CXCR4 signaling in the pathogenesis of bronchial asthma. (Chen et al., 2015) This underscores CXCL12's involvement in ASM thickening, suggesting its inhibition could be a promising treatment for airway diseases marked by this thickening. Our study further supports this potential therapeutic avenue in asthma, given ASM thickening's known association with worsened asthma symptoms (Bergeron et al., 2010)

LIT-927 Attenuates HDM Induced accumulation and Elongation of α-SMA+ Mural Cells

LIT-927 in figure 2.14 also attenuated the HDM-induced accumulation of α-SMA+ mural cells. This is in agreement with the literature which have shown that CXCR4 inhibition can attenuate fibrosis and the accumulation of α-SMA+ mural cells, in organs like the kidney and liver, (S. Wang et al., 2021) Furthermore, LIT-927 administration in figure 2.15 also reversed the HDM-induced changes in α-SMA+ mural cells morphology, specifically increasing the area-to-perimeter ratio and decreasing their circularity. The change in mural cell shape after CXCL12 inhibition is in agreement with the literature and can be attributed to CXCL12's interaction with the CXCR4 receptor, affecting actin cytoskeleton dynamics (Moyer et al., 2007). Disturbances in this signaling can lead to abnormal cell shapes, hindering mural cells' ability to support vessels. CXCL12 modulates cell spreading and adhesion, possibly by altering integrin and focal adhesion protein activation, affecting cell area and perimeter (Moyer et al., 2007). CXCL12's influence on these parameters determines overall cell morphology, mediating interactions with endothelial cells and impacting vessel functionality (Moyer et al., 2007).

LIT-927 does not attenuate HDM induce increase in immune cell infiltration.

It is worth noting that LIT-927 did not significantly reduce immune cell infiltration and eosinophil counts in the BAL in figures 2.16, 2.17, 2.18 and 2.19. Our findings differ from those of Regenass (2018), who noted reduced eosinophilia post-LIT-927 administration. This discrepancy could be due to differences in treatment timing and study design (Regenass, 2018). For example, unlike Regenass (2018) we began treatment three weeks post-HDM exposure when immune cells might have already infiltrated the airways (Johnson et al., 2015).

Asthma's complex immune reaction involves numerous chemokines and pathways that can potentially offset the loss of CXCL12 signaling, resulting in unchanged immune infiltration levels. Chemokines like CCL11, CCL24, and CCL5 are known to recruit and activate eosinophils (Lambrecht et al., 2019)

In conclusion, our findings highlight the critical role of the CXCL12-CXCR4 signaling axis in asthma and suggest that LIT-927 is a promising therapeutic candidate for treating asthma and lung fibrosis. Its selectivity, oral bioavailability, and ability to specifically target CXCL12 without affecting systemic CXCR4 signaling make it an attractive option. Further research is needed to confirm its efficacy in human patients and optimize its use in various inflammatory lung diseases.

Chapter 3: LIT-927 attenuates vascular remodeling in the mouse model of house dust mite-induced chronic allergic asthma.

3.1 Introduction

Vascular remodelling in asthma is characterized by congestion, inflammatory cell infiltration, Vascular remodeling in asthma is a complex and multifaceted process involving structural and functional changes in the pulmonary vasculature (J. W. Wilson & Kotsimbos, 2003) . The chemokine CXCL12 has been shown to be a potent modulator of vascular remodeling in various fibrotic diseases and cancers, its role in the pathophysiology of asthma and lung fibrosis remains largely underexplored. **This chapter aims to build on Chapter 2's examination of LIT-927's therapeutic potential by focusing on impact of the CXCL12 neutralizing ligand LIT-927 on vascular remodeling in asthma progression in a house dust mite (HDM) model of induced allergic airways inflammation.**

Research on vascular remodeling in asthma is limited due to the challenges associated with existing study methods (Baluk & McDonald, 2022). Whole-mount immunostaining offers several advantages over traditional histopathological methods, which typically require sectioning and staining smaller tissue regions. This method preserves the structural integrity of tissues, providing a comprehensive three-dimensional view of the entire bronchial vascular network, including arteries, veins, and capillaries (Baluk & McDonald, 2022).

Despite these benefits, few studies have employed whole-mount immunostaining for lung vasculature due to the lung's complex and delicate structure, which can be challenging to process and stain without damage. The intricate vascular and airway networks require precise visualization techniques (Baluk & McDonald, 2022) Additionally, we employ precise morphometric measurements for vessel tortuosity, vessel density, branch density, and vessel area, inspired by research on murine retinas and developmental vasculature in fish embryos (Ramos et al., 2018) . To overcome historical challenges in vascular image data analysis, we used both manual and automated analysis protocols as per vascular analysis techniques developed for other organs, such as the brain, heart, kidney, liver, and retina (White et al., 2012).

3.2. Methods

3.2.1 In vivo HDM model

Female C57BL/6 mice (n=30, aged 6–8 weeks) were acquired from Charles River and maintained either at Imperial College London's central animal facility (South Kensington campus) or at Aston University's central animal facility, ensuring specific pathogen-free conditions. These mice were subjected to a 12-hour light-dark regime and were given access to ad libitum food and water. All procedures followed the UK Home Office and Imperial College guidelines as per the Animals (Scientific Procedures) Act 1986. All experiments on animals were conducted according to United Kingdom Home Office regulations (project license P75A73BEB held by the Principal Investigator), and animal handling was performed by qualified personnel. All studies were performed and reported according to the revised ARRIVE guidelines (du Sert et al., 2020).

The HDM extract, sourced from Citeq (Groningen, The Netherlands) was prepared in sterile phosphate-buffered saline (PBS) to attain a 2.5 mg/ml concentration. Mice were intranasally administered 10 µl of this solution. In parallel, control mice (n=15) received an intranasal dose of 10 µl sterile PBS, adhering to an identical protocol. LIT-927, procured from Axon Medchem (Groningen, The Netherlands), was diluted in a VEH of methyl-β-cyclodextrin (Sigma) at 10% w/v to achieve a concentration of 197 ng/ml. This solution (10 µl) was intranasally given to the mice right before their exposure to the allergen.

Figure 3.1: Schematic overview of the dosing strategy. C57BL/6 mice (6-8 weeks old) were exposed to either PBS (10 µL) or HDM extract (25 µg in 10 µL) for three consecutive weeks. This was followed by intranasal administration of 10 µL PBS+VEH (10% w/v methyl-β-cyclodextrin), 10 µL PBS+LIT927 at 197 ng/mL in 10% w/v methyl-β-cyclodextrin), HDM+VEH (25 µg HDM (Citeq) in 10 µL in 10% w/v methyl-β-cyclodextrin) and HDM+LIT927 (25 µg HDM in 10 µL with 197 ng/mL LIT927 in 10% w/v methyl-β-cyclodextrin) Data are derived from two independent experiments with 15 mice per group. .

3.2.2 Sample collection

Mice were euthanized via an intraperitoneal injection of a pentobarbital overdose, ensuring a humane procedure. Subsequent to euthanasia, a variety of samples were collected from each mouse for distinct assessments. Bronchoalveolar lavage fluid was extracted to determine immune cell profiles. For experimental procedures, materials such as those required for lung section immunostaining, flow cytometric analysis, and cell culturing were sourced from the mice. Lungs were surgically excised and then subjected specific immunostaining techniques, elaborated in the following sections.

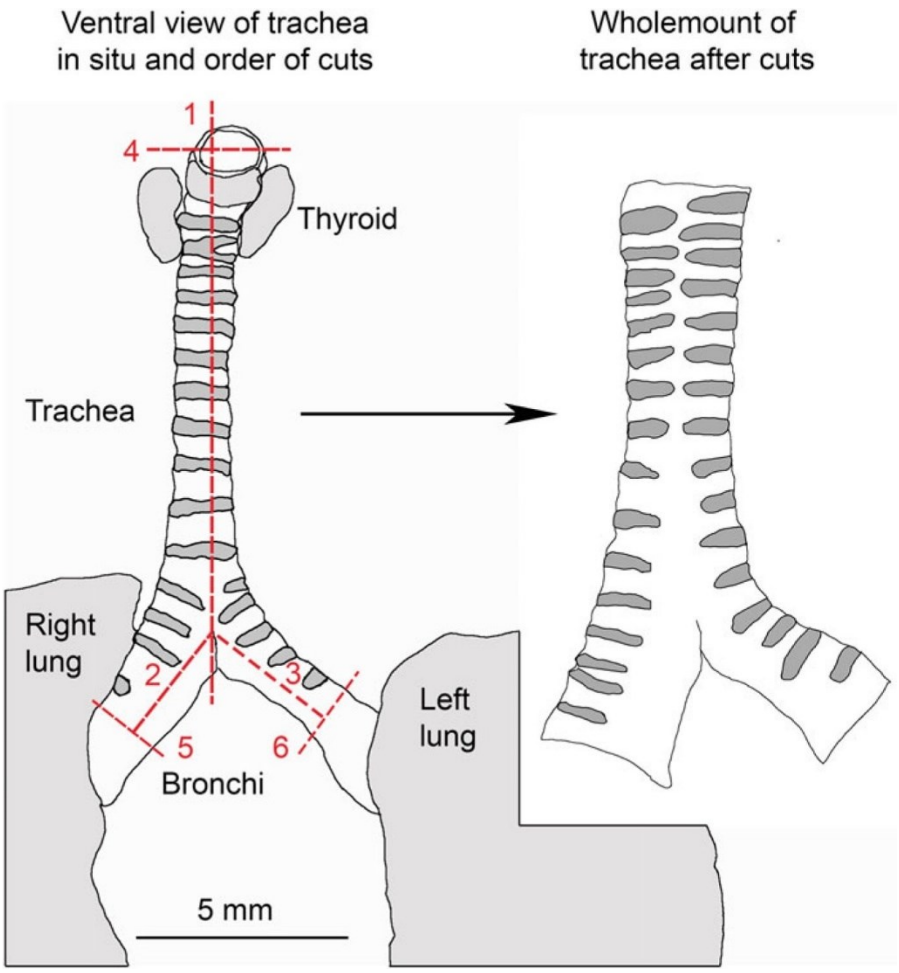

Figure 3.2 Schematic diagram of mouse trachea in situ showing the order of cuts (dashed red lines) to make a wholemount preparation. 1: longitudinal cut along ventral aspect of trachea; 2 and 3: cuts along bronchi; 4: cut across larynx; 5 and 6: cuts across bronchi. The resulting wholemount is shown on the right

3.2.3 Preparation of Lung Sections and Tracheobronchial Whole Mounts

Significant airway portions spanning from the larynx to lung sections were dissected, cleared of excess connective tissue, and secured onto Kwikgard™-coated 6-well plates (WPI). After overnight blocking with 5% NGS/0.3% Triton-X 100 in PBS, tracheal sections were longitudinally bisected and individually stained for pericytes and endothelial cells using primary and secondary antibodies. After blocking, sections were cleansed with PBS and subjected to an overnight incubation with designated primary antibodies (as listed in Table 3.1). Subsequent to another PBS rinse, sections were exposed to secondary antibodies tailored to each primary antibody's origin species. To evaluate specificity, control sections were also processed without primary antibody exposure. After a 2-hour secondary antibody incubation (refer to Table 3.1for details), sections were again rinsed and subsequently mounted with Fluoroshield inclusive of DAPI.

Tracheobronchial whole mounts were examined and imaged utilizing a Zeiss LSM0-510 inverted confocal microscope, comprising a specialized set of lasers and objectives. Image processing was accomplished using LAS X software (Leica).

3.2.4 Immunofluorescence

For the immunohistochemical process, cells first underwent three washing cycles with PBS, each lasting 5 minutes. Following this, a fixation step was performed using a 3% paraformaldehyde (PFA) solution for 15 minutes at room temperature. After washing the fixative off, a blocking step was undertaken to minimize non-specific antibody bindings using a solution of 5% normal goat serum in 0.3% Triton-X-100/PBS, and this was allowed to proceed for 1 hour. The cells were then exposed to the primary antibodies (as detailed in Table 3) for a duration of 2 hours. Post-primary antibody incubation, the cells were washed and treated with the corresponding secondary antibodies for 1 hour at room temperature. To conclude the process, another series of washes was conducted, and the coverslips bearing the cells were mounted onto microscope slides. Mounting was achieved using Fluoroshield (sourced from Sigma-Aldrich)

Antigen Target	***Origin of Antibody***	***Specific Clone***	***Dilution Ratio***	***Provided by***
CD31	Hamster	2H8	1:500	Abcam
α-SMA	Mouse	1A4	1:1000	Sigma-Aldrich

Table 3.1 Antibodies used in immunostaining.

3.2.4 Image J

To analyze the vascular network within the collected images, we employed ImageJ, a powerful open-source image processing software. The parameters of interest included vessel density, vessel diameter vessel branching, and tortuosity. The analysis process began with image acquisition and preprocessing. Images were obtained using a high-resolution microscope and saved in a compatible format, such as TIFF. To ensure consistent analysis, all images were converted to grayscale and subjected to background subtraction using the "Subtract Background" function in ImageJ. Subsequently, the images were enhanced using the "Enhance Contrast" function to ensure uniform intensity distribution across the dataset. For the measurement of vessel density, the preprocessed images were binarized using the "Threshold" function, which highlighted the vessels against the background. The "Analyze Particles" tool was then utilized to measure the area covered by vessels within each image. Vessel density was calculated as the ratio of the vessel area to the total image area, expressed as a percentage. For quantification of vessel diameter using Image J, we measured the straight-line distance between the inner edges of the CD31-positive staining to determine the vessel diameter at multiple points along each vessel. To analyze vessel branching and tortuosity, we processed the binarized images at 20X, using the "Skeletonize" plugin. This plugin converts the vessel structures into a one-pixel-wide skeleton representation, preserving the overall topology of the vascular network. The skeletonized images were then analyzed using the "Analyze Skeleton" plugin, which provided detailed metrics on vessel branching and tortuosity.

For the quantification of vessel branching, we employed both manual counting and automated analysis using the plugin. Manually, branch points were identified and counted by visually inspecting the skeletonized images, ensuring accuracy by cross-referencing with the original preprocessed images. These branch points, or nodes where vessels bifurcate, were normalized to the total vessel length, providing a comprehensive measure of vessel branching density. This manual count provided a direct and detailed measure of vessel branching density. Additionally, the "Analyze Skeleton" plugin automatically identified and counted branch points, offering a complementary and rapid quantification method.

To quantify vessel tortuosity, we calculated the ratio of the vessel path length, as measured along the skeletonized vessel, to the straight-line distance between vessel endpoints. The tortuosity index for each vessel segment was averaged to obtain an overall measure of tortuosity for each image.

3.2. 4 Statistical Analysis

Data analysis was conducted using GraphPad Prism Software version 6 (GraphPad Software, San Diego, CA). For statistical evaluations, we employed the student’s t-test or one-way ANOVA followed by Tukey's post hoc test when applicable. A significance threshold was set at $P < 0.05$. Additionally, Pearson correlation analysis was utilized to determine the relationship between ASM thickening and cell counts. Results are expressed as means ± SE.

3.3 Results

3.3.1 LIT-927 Attenuates HDM Induced Increase in Vessel Density

Vessel density was calculated as the area occupied by vessels divided by the total tissue area. The results showed a significant increase in vessel density in the HDM-exposed group compared to the control group treated with Phosphate-Buffered Saline (PBS) (***$p < 0.001$). This significant increase indicates that HDM exposure leads to a pronounced formation of new blood vessels within the tracheal and bronchial tissues, reflecting an angiogenic response to the allergen. In contrast, the group treated with intranasal LIT-927 during the final three weeks of the five-week HDM exposure protocol exhibited a marked reduction in vessel density. The LIT-927 treated group showed vessel densities that were substantially lower than those observed in the HDM-only group, highlighting the potential of LIT-927 to mitigate HDM-induced vascular changes. The effectiveness of LIT-927 in attenuating vessel density was further validated by whole-mount immunostaining for the endothelial cell marker CD31. The immunostaining clearly showed reduced CD31-positive areas in the LIT-927 treated group compared to the HDM-only group, confirming the quantitative vessel density findings. These observations suggest that LIT-927 exerts a protective effect against the angiogenic response induced by HDM exposure. The reduction in vessel density could be attributed to the anti-inflammatory properties of LIT-927, which might inhibit the pathways responsible for new vessel formation in the inflamed airway tissues.

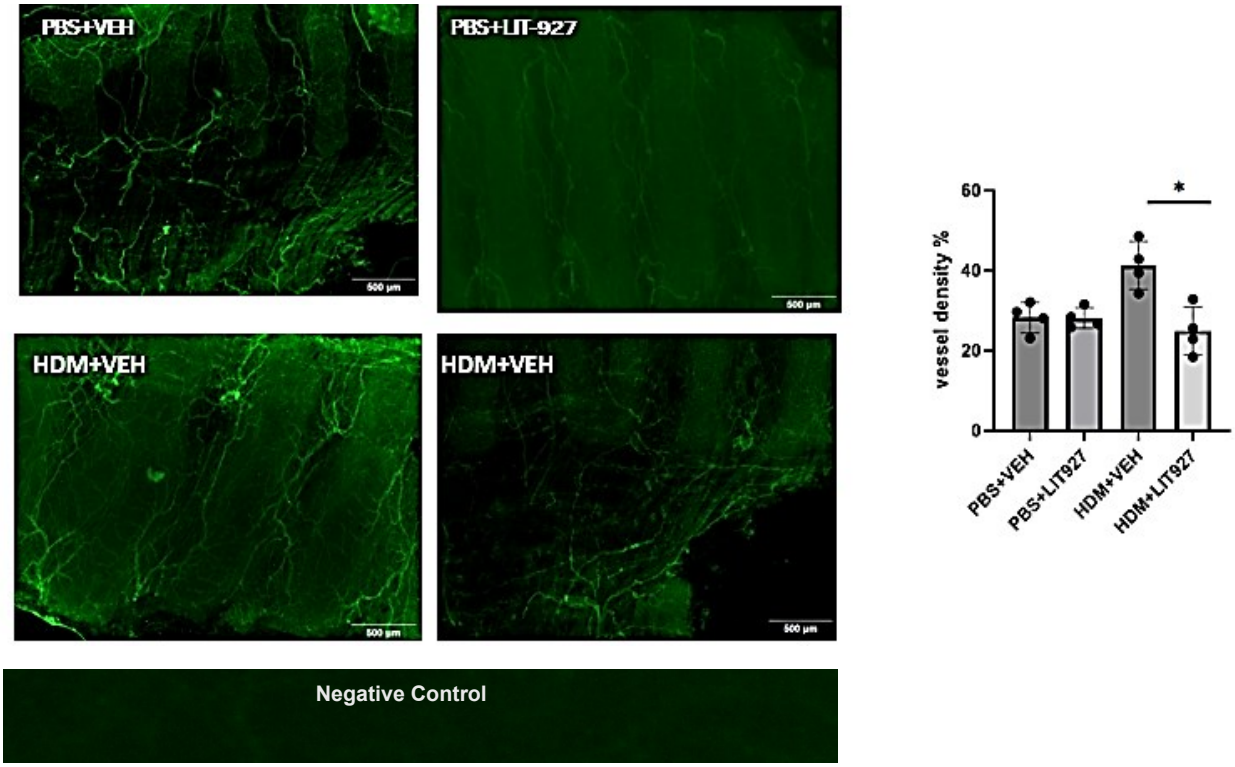

Figure 3.3: Effect of LIT-927 on HDM induced vessel density. C57BL/6mice, aged 6-8 weeks, were analysed after exposure to either PBS or HDM extract on a five-day weekly schedule over five weeks. The final three weeks included intranasal administration of LIT-927 post-treatment, trachea and bronchi samples were, processed, and subjected to whole-mount immunostaining the endothelial cell marker CD31 (green) Scale bar=500um. Data are derived from two independent experiments with n=4 mice per group. .*p < 0.05determined by one-way ANOVA for multiple groups with Tukey's post hoc test. VEH: vehicle control-10% w/v methyl-β-cyclodextrin, HDM: House Dust Mite, LIT: The CXCL12 Neutralizing ligand LIT927

3.3.2 LIT-927 attenuates HDM induced increase in vessel diameter.

In this study, one of our primary objectives was to evaluate the impact of house dust mite (HDM) exposure on vessel diameter in the upper bronchi, which we quantified using whole-mount immunostaining techniques. Using Image J, we measured the straight-line distance between the inner edges of the CD31-positive staining to determine the vessel diameter at multiple points along each vessel.

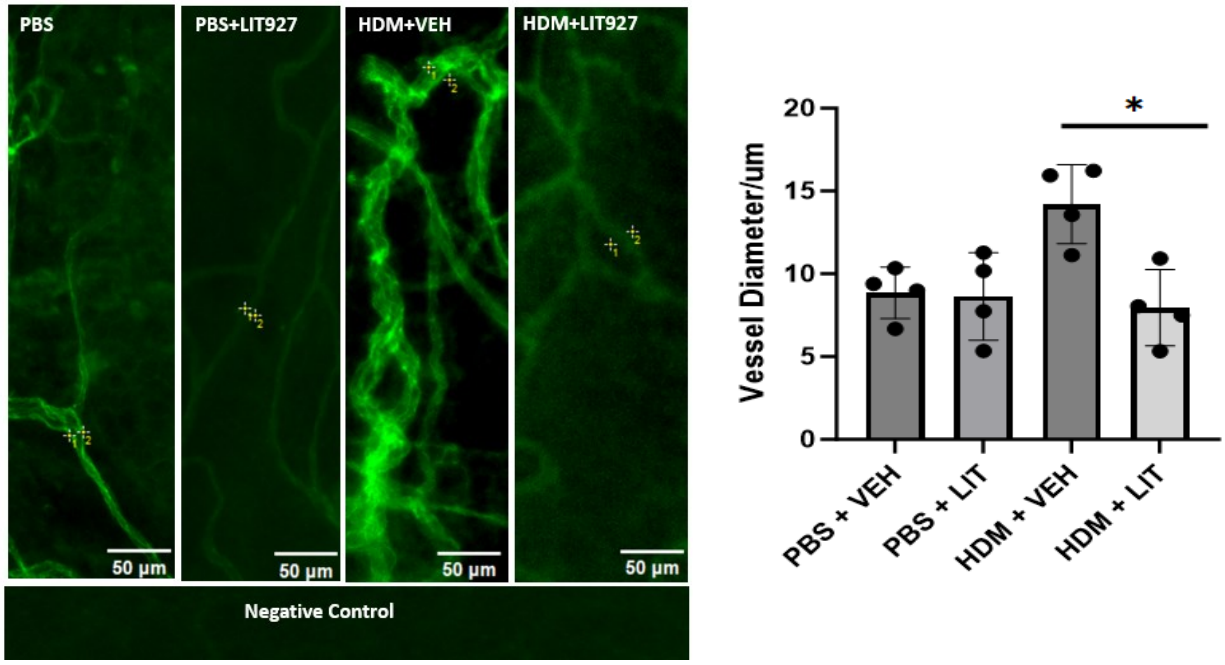

Figure 3.4: Effect of LIT-927 on HDM induced vessel diameterC57BL/6mice, aged 6-8 weeks, were analysed after exposure to either PBS or HDM extract on a five-day weekly schedule over five weeks. The final three weeks included intranasal administration of LIT-927 post-treatment, trachea and bronchi samples were, processed, and subjected to whole-mount immunostaining the endothelial cell marker CD31 (green) Scale bar=50um. Data are derived from two independent experiments with n=4 mice per group. *p < 0.05, determined by one-way ANOVA for multiple groups with Tukey's post hoc test. VEH: vehicle control-10% w/v methyl-β-cyclodextrin, HDM: House Dust Mite, LIT: The CXCL12 Neutralizing ligand LIT927

3.3.3 LIT-927 attenuate HDM induced increase in Vessel Branching and Tortuosity

Using advanced imaging techniques, we demonstrated that treatment with LIT-927 led to a significant reversal in HDM-triggered increases in blood vessel tortuosity and Branching (Figure 3.5). Critically, this effect was observed without any discernible adverse consequences, as Tortuosity is a measure of how twisted or convoluted a vessel path is, and it has important implications for haemodynamics, tissue perfusion, and even pathological states like inflammation or tumour growth. To analyze vessel branching and tortuosity, we processed the binarized images using the "Skeletonize" plugin. This plugin converts the vessel structures into a one-pixel-wide skeleton representation, preserving the overall topology of the vascular network. The skeletonized images were then analyzed using the "Analyze Skeleton" plugin, which provided detailed metrics on vessel branching and tortuosity. For the quantification of vessel branching, we employed both manual counting and automated analysis using the plugin. Manually, branch points were identified and counted by visually inspecting the skeletonized images, ensuring accuracy by cross-referencing with the original preprocessed images. These branch points, or nodes were defined as points where the vessels bifurcate. The number of branches were normalized to the total vessel length, providing a comprehensive measure of vessel branching density. This manual count provided a direct and detailed measure of vessel branching density. Additionally, the "Analyze Skeleton" plugin automatically identified and counted branch points, offering a complementary and rapid quantification method. To quantify vessel tortuosity, we calculated the ratio of the vessel path length, as measured along the skeletonized vessel, to the straight-line distance between vessel endpoints. The tortuosity index for each vessel segment was averaged to obtain an overall measure of tortuosity for each image.

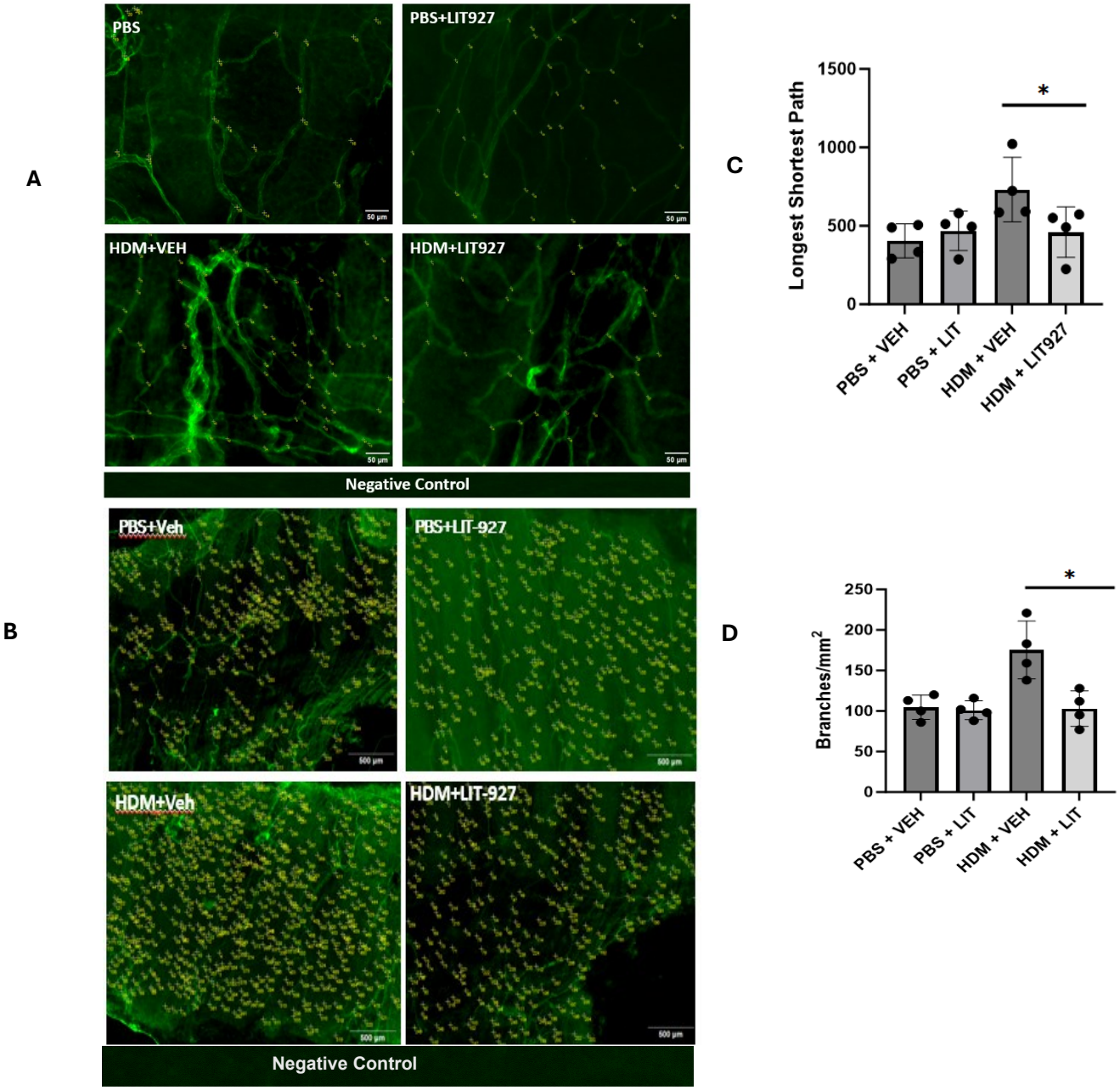

Figure 3.5: Impact of LIT927 on Vessel Branching and Tortuosity C57BL/6 mice, aged 6-8 weeks, were analyzed after exposure to either PBS or HDM extract on a five-day weekly schedule over five weeks. During the final three weeks, intranasal administration of LIT-927 was conducted. Post-treatment, trachea and bronchi samples were processed and subjected to whole-mount immunostaining using the endothelial cell marker CD31 (green). **A:** Vessel branching, and tortuosity were analyzed using the Skeletonize Plugin at 20X magnification (scale bar = 50 µm). Branch points, or nodes where vessels bifurcate, are highlighted in yellow. **B:** Vessel branching was quantified manually at 4X magnification (scale bar = 500 µm). Branch points, or nodes where vessels bifurcate, are highlighted in yellow. **C:** To quantify vessel tortuosity, the ratio of the vessel path length (measured along the skeletonized vessel) to the straight-line distance between vessel endpoints was calculated. The tortuosity index for each vessel segment was averaged to obtain an overall measure of tortuosity for each image. **D:** The number of branches was normalized to the total vessel length, providing a comprehensive measure of vessel branching density. Data are derived from two independent experiments with n=4 mice per group. *$p < 0.05$, determined by one-way ANOVA for multiple groups with Tukey's post hoc test. **VEH:** vehicle control-10% w/v methyl-β-cyclodextrin, **HDM:** House Dust Mite, **LIT:** The CXCL12 Neutralizing Ligand LIT927

3.3 Discussion

This chapter examines the impact of the CXCL12 neutralizing ligand, LIT-927, on vascular remodeling in an HDM model of asthma. The scarcity of studies in this area is largely due to the limitations of traditional methods for studying vascular remodeling. To address this, we optimized a novel whole-mount immunostaining technique to examine vascular remodeling in the bilateral bronchi. This approach provided a three-dimensional perspective of the bronchial vasculature, revealing that LIT-927 effectively attenuates HDM-induced changes in vessel morphology, including tortuosity, vessel density, branch density, and vessel diameter.

Vessel Density

In our study, fluorescently labeled antibodies targeting CD31, enabled detailed visualization of the vasculature. Whole-mount staining allows observation of structures in their entirety, in 3D, without sectioning. Vessel density was calculated as the area occupied by vessels divided by the total tissue area. As per figure 3.3 Vessel Density was significantly increased in the HDM-exposed group compared to the control group treated with phosphate-buffered saline (PBS). This finding aligns with the existing literature, which links increased vascular density with asthma. Studies using monoclonal antibodies targeting factor VIII, collagen type IV, and CD31 have consistently shown that asthmatic patients exhibit an increased number of vessels and vascular area compared to healthy controls (Bailey et al., 2009; Rossi et al., 2019; Schmidt & von Hochstetter, 1995; Woodfin et al., 2007)

For example in patients with mild to moderate asthma, a significant increase in vessel number and/or percent vascular area and an increased average capillary dimension can be observed compared to healthy controls (Grainge et al., 2011). A relationship between increased bronchial micro vascularity and the severity of asthma has also been found (Zanini et al., 2010)The marked increase in vessel density in response to HDM can be attributed to a coordinated remodeling process initiated by inflammation commonly associated with asthma. This inflammation arises from the release of pro-inflammatory cytokines and growth factors upon HDM exposure, notably interleukin-1 (IL-1), interleukin-6 (IL-6), CXCL12, and vascular endothelial growth factor (VEGF) (Lambrecht et al., 2019). These factors influence endothelial cells, prompting proliferation and migration, which collectively give rise to new blood vessels (Lambrecht et al., 2019).

To determine the impact of CXCL12 inhibition on vascular remodeling, we treated mice with the CXCL12 neutralizing ligand LIT-927. Inhibiting CXCL12 effectively attenuated the induced increase in vessel density. This finding aligns with existing literature highlighting the CXCL12/CXCR4 pathway's role in angiogenesis and its potential as a therapeutic target in various diseases. For example, elevated levels of CXCL12 and CXCR4 in lung cancer correlate with heightened tumor resilience, angiogenesis, and metastasis, influencing lung vessel density (Y. Shi et al., 2020)

Vessel Diameter

Vessel diameter is a critical factor influenced by inflammatory cytokines, affecting flow rate, shear stress, blood pressure, and vascular resistance. During inflammation, vasodilation occurs, increasing vessel diameter and facilitating the movement of immune cells to the affected areas (Zanini et al., 2010). To accomplish this, we stained the tissue sections with CD31, a marker for endothelial cells, which allowed for clear visualization of the blood vessels. Using ImageJ, we measured the straight-line distance between the inner edges of the CD31-positive staining to determine the vessel diameter at multiple points along each vessel. This measurement technique enabled us to quantify alterations in vessel diameter accurately and confirm that HDM increased vessel diameter. Our findings in figure 3.4 are consistent with existing research, which confirms that vessel diameters are increased in asthmatic patients compared to healthy controls (Chu et al., 2001). In agreement with our findings studies have highlighted that asthmatic patients have enlarged vessels (Claesson-Welsh et al., 2021) . Enlarged vessels in asthmatic patients have also been associated with heightened permeability due to compromised epithelial integrity due to pro inflammatory cytokines (Chu et al., 2001). Notably, increased vessel diameter in asthma and other inflammatory diseases is consistently associated with heightened vascular permeability as mediators such as histamine, bradykinin, and various cytokines can induce plasma extravasation (Chu et al., 2001).

LIT-927 effectively attenuated the house dust mite (HDM)-induced increase diameter increase of these vessels. These findings are consistent with an expanding body of literature emphasizing CXCL12's multifaceted roles in vascular biology. CXCL12 is crucial for angiogenesis, potentially leading to larger-diameter vessels as new vasculature matures and expands (Chang et al., 2020). In vitro studies have demonstrated that CXCL12 can increase the diameter of blood vessels and the permeability of human endothelial cell monolayers and reducing the levels of occludin, thereby increasing endothelial permeability (Ahirwar et al., 2018)

Vessel Tortuosity and Branching

To further explore vascular changes, we used the Longest Shortest Path (LSP) metric to assess blood vessel tortuosity. Tortuosity measures how twisted or convoluted a vessel path is, with significant implications for hemodynamics, tissue perfusion, and pathological states like inflammation or tumor growth (Gifre-Renom & Jones, 2021). In network analysis, the LSP is the path that requires the most "hops" or segments between any two nodes (branching points or termini of vessels) while still representing the shortest possible route between those two nodes (Gifre-Renom & Jones, 2021). A longer LSP indicates a more tortuous network, which could correspond to alterations in flow resistance, shear stress, and endothelial cell function (Gifre-Renom & Jones, 2021).. This is particularly relevant in pathological states where blood vessel tortuosity is often increased, such as cardiovascular diseases, diabetes, and cancer. Our findings in figure 3.5 align with studies showing that inflammation in the retina, is associated with increased vascular tortuosity (Ramos et al., 2018)

We also manually counted bifurcation points to investigate vessel branching, which serves as a quantitative metric to assess the complexity and bifurcation of the blood vascular network in tissues (G. Wang et al., 2023). This measure provides insights into the functional capacity and spatial arrangement of vessels, playing a pivotal role in respiratory diseases like asthma (G. Wang et al., 2023). Increased vessel branching in asthma is likely an outcome of airway inflammation and remodeling, facilitated by cytokine-mediated inflammatory signaling and changes in extracellular matrix components (G. Wang et al., 2023).

The exact mechanisms behind the increased tortuosity and branching of vessels during inflammation are not fully understood. The spatial distribution of capillary networks also determines the regional variability of oxygen and nutrient delivery (Ramos et al., 2018). Increased blood vessel tortuosity and branching may indicate endothelial cell activation, pathogenic microvascular remodeling, or arterialization of collateral micro vessels due to ischemia (Chang et al., 2020).

While the broader roles of CXCL12 in angiogenesis and endothelial cell function have been studied in the literature, its impact on vessel tortuosity and branching remains less clear. This reduction in tortuosity in pathological conditions may be partially attributed to the fact that CXCL12 facilitates endothelial cell proliferation and migration, fundamental steps in angiogenesis (Ahirwar et al., 2018). Newly sprouting vessels in pathological settings are often more tortuous, especially when rapid vascular remodeling is required, such as in chronic inflammation or tumors (Y. Shi et al., 2020)

Moreover, inflammatory cytokines such as CXCL12 can lead to increased branches and more convoluted vascular pathways as the vasculature adapts to the altered local environment (Ramos et al., 2018). The confluence of these factors culminates in increased vessel tortuosity, changing the geometry and subsequently, the hemodynamic factors like flow and shear stress within those vessels (Ramos et al., 2018).

In conclusion, our study reveals that LIT-927 has a potent effect in mitigating HDM-induced vascular remodeling it is crucial to note that the formation and maintenance of blood vessels in the lungs involve a complex interplay of various signaling pathways and factors. Therefore, more research is needed to fully understand the specific outcomes of inhibiting CXCR4 on blood vessel branching and to explore the broader therapeutic applications of LIT-927 in lung diseases.

Chapter 4: LIT-927 attenuates pericyte migration in vivo and in vitro.

4.1 Introduction

In Chapters 2 and 3, we unveiled the significant potential of the CXCL12 neutralizing ligand LIT-927 in attenuating HDM-induced bronchial and vascular remodeling. These findings are promising, yet the exact cellular targets and molecular pathways responsible for LIT-927's therapeutic effects remain to be fully understood. Therefore, this chapter aims to uncover these mechanisms, with a particular focus on pericytes, pivotal players in asthma-related bronchial and vascular remodeling.

Pericytes, often referred to as the gatekeepers of microvascular stability, are integral to numerous physiological and pathological processes. These include angiogenesis, vascular development, wound healing, and cancer metastasis. During inflammatory episodes in the lungs, pericytes exhibit notable migratory behavior, moving from the vasculature towards the airway wall. This migration significantly contributes to airway remodeling, a hallmark of chronic respiratory diseases such as asthma and chronic obstructive pulmonary disease (Rowley et al., 2015). The importance of understanding pericyte behavior in such contexts cannot be overstated, as it provides insights into disease progression and potential therapeutic interventions.

One of the key factors influencing pericyte migration is the chemokine CXCL12, known for its potent ability to enhance this migration. This suggests CXCL12 as a potential therapeutic target for a variety of diseases (Anastasiadou et al., 2024). In the context of lung inflammation, CXCL12's role extends beyond attracting immune cells; it also recruits and activates structural cells such as fibroblasts and pericytes, contributing to tissue remodeling and fibrosis (Bignold et al., 2022) This dual functionality underscores the complexity and significance of CXCL12 in chronic inflammatory conditions.

The primary objective of this chapter is to investigate how CXCL12 and its neutralizing ligand LIT-927 influence pericyte migration in vivo and in vitro. This dual approach allows us to dissect the cellular and molecular intricacies of pericyte behavior in a controlled environment while also validating these findings in a more complex, living system. This research holds considerable relevance, as it will help identify the underlying factors prompting pericytes to transition from the vascular system to fibrotic zones, thereby shedding light on new therapeutic approaches for chronic respiratory diseases.

4.2 Methods

4.2.1 In vivo HDM model

Female C57BL/6 mice (n=30, aged 6–8 weeks) were acquired from Charles River and maintained either at Imperial College London's central animal facility (South Kensington campus) or at Aston University's central animal facility, ensuring specific pathogen-free conditions. These mice were subjected to a 12-hour light-dark regime and were given access to ad libitum food and water. All procedures followed the UK Home Office and Imperial College guidelines as per the Animals (Scientific Procedures) Act 1986. All experiments on animals were conducted according to United Kingdom Home Office regulations (project license P75A73BEB held by the Principal Investigator), and animal handling was performed by qualified personnel. All studies were performed and reported according to the revised ARRIVE guidelines (du Sert et al., 2020).

The HDM extract, sourced from Citeq (Groningen, The Netherlands) was prepared in sterile phosphate-buffered saline (PBS) to attain a 2.5 mg/ml concentration. Mice were intranasally administered 10 µl of this solution. In parallel, control mice (n=15) received an intranasal dose of 10 µl sterile PBS, adhering to an identical protocol. LIT-927, procured from Axon Medchem (Groningen, The Netherlands), was diluted in a VEH of methyl-β-cyclodextrin (Sigma) at 10% w/v to achieve a concentration of 197 ng/ml. This solution (10 µl) was intranasally given to the mice right before their exposure to the allergen.

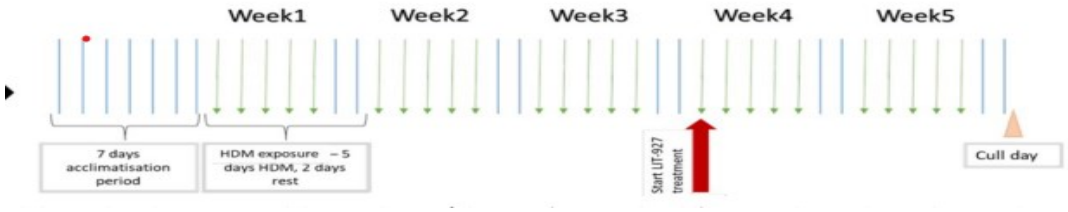

Figure 4.1: Schematic overview of the dosing strategy. C57BL/6 mice (6-8 weeks old) were exposed to either PBS (10 µL) or HDM extract (25 µg in 10 µL) for three consecutive weeks. This was followed by intranasal administration of 10 µL PBS+VEH (10% w/v methyl-β-cyclodextrin), 10 µL PBS+LIT927 at 197 ng/mL in 10% w/v methyl-β-cyclodextrin), HDM+VEH (25 µg HDM (Citeq) in 10 µL in 10% w/v methyl-β-cyclodextrin) and HDM+LIT927 (25 µg HDM in 10 µL with 197 ng/mL LIT927 in 10% w/v methyl-β-cyclodextrin) Data are derived from two independent experiments with 15 mice per group. .

4.2.2 Sample collection

Mice were euthanized via an intraperitoneal injection of a pentobarbital overdose, ensuring a humane procedure. Subsequent to euthanasia, a variety of samples were collected from each mouse for distinct assessments. Bronchoalveolar lavage fluid was extracted to determine immune cell profiles. For experimental procedures, materials such as those required for lung section immunostaining, flow cytometric analysis, and cell culturing were sourced from the mice. Lungs were surgically excised and then subjected to specific immunostaining techniques, elaborated in the following sections. For flow cytometric evaluations or immunomagnetic separation of CD146+ cells, whole lung tissues were enzymatically digested. These CD146+ cells were then further cultured for subsequent analyses.

4.2.3 Preparation of Single-Cell Suspensions from Murine Lungs

To access the pleural cavity, a bilateral thoracotomy was executed. Subsequently, a minute incision was made in the left ventricle. Using a 21G needle paired with a 10 ml syringe, the circulatory system was perfused with 10 ml of ice-cold PBS via the right ventricle. Following perfusion, the lungs were carefully excised and deposited into an Eppendorf tube containing 0.5 ml DMEM fortified with penicillin/streptomycin (pen/strep, 1%).

For tissue disaggregation, the lungs were meticulously minced utilizing scissors. Thereafter, 0.5 ml of DMEM pen/strep enriched with Liberase™ thermolysin (0.195WU/ml, Roche Diagnostics) and DNAse I (Sigma-Aldrich) was introduced. This mix was then incubated at a temperature of 37 °C for a duration of 45 minutes.

To halt the enzymatic reaction, 1 ml of fetal bovine serum (FBS) complemented with EDTA (5 mM) was introduced, and subsequently, the samples were maintained on ice. For mechanical dissociation of the tissue, the digested matter was compelled through a 100 µm cell strainer (Miltenyi) with the aid of a syringe plunger. Post dissociation, the material was washed twice utilizing RPMI buffer (comprising RPMI, pen/strep, HEPES at 25 mM, EDTA at 5 mM, and FBS at 10%). The washing was performed at a centrifugation speed of 1200 rpm, at 4 °C, lasting 6 minutes. Finally, the cell suspension was filtered via a 70 µm filter (Miltenyi), resulting in a homogenous single-cell suspension.

4.2.4 Flow Cytometric Staining of Murine Lung Cells

Cellular suspensions were adjusted to concentrations ranging from 10 to 50 × 10^6 cells/ml using a staining buffer formulated with PBS, 10% FBS, and 5 mM EDTA. Fc receptors on cells were blocked using anti-CD26/32 (1:100 dilution, Biolegend) by incubating for 10 minutes on ice.

Subsequently, cells were portioned into V-bottomed 96-well plates (Corning), allocating 100 µl per well. The cells were centrifuged at 1200 rpm for 5 minutes at 4 °C. After centrifugation, the supernatant was discarded, and the cells were resuspended in staining buffer that was pre-loaded with fluorophore-conjugated antibodies (refer to figure 2.1). The cells, in this antibody-containing solution, were left to incubate on ice for 30 minutes, shielded from light.

Post incubation, cells underwent two wash cycles to eliminate any unattached antibodies. For each wash, the staining buffer was used, followed by centrifugation to pellet the cells. After the washing steps, the cells were fixed using IC fixation buffer (eBioscience), dispensing 100 µl per well. This fixing step took place on ice in the dark for 20 minutes. Thereafter, the cells were washed and then resuspended in 200 µl of PBS. Following staining and fixation, samples were preserved at 4 °C, ensuring protection from light until they were analyzed using flow cytometry.

The table below lists the antibodies used for staining murine lung cells, along with their specific targets, clones, conjugated fluorophores, dilutions, and suppliers.

Antibody	Target	Clone	Fluorophore	Dilution (µl/100 µl)	Supplier
CD31	Endothelial cells	390	FITC*	2	Biolegend
			PerCp-Cy5.5**	1.25	Biolegend
CD45	Pan-leukocytes	30-F11	PerCp-Cy5.5	1.25	Biolegend
CD146	Pericytes	ME-9F1	PE-Cy7	1.25	Biolegend
			FITC	1	
PDGFRβ	Pericytes	APB5	APC	5	Biolegend
Ter119	Erythrocytes	TER-119	PerCP-Cy5.5	1.25	Biolegend

Table 4.1 Flow Cytometry Antibody Panel for Murine Lung Cells. The diagram represents the antibody panel used for distinguishing specific cell populations within murine lung tissue. The antibodies target endothelial cells (CD31), pan-leukocytes (CD45), pericytes (CD146, PDGFRβ), and erythrocytes (Ter119). Fluorophores such as FITC, PerCp-Cy5.5, PE-Cy7, and APC are conjugated to these antibodies to facilitate detection and differentiation. The asterisk (*) denotes the use of FITC as part of the dump channel with the LEGENDScreen™, while the double asterisk (**) indicates the application of PerCp-Cy5.5 for endothelial cell exclusion in other assays. All antibodies were sourced from Biolegend.

4.2.5 Flow Cytometry Analysis

For accurate determination and compensation, single color compensation controls utilizing VersaComp antibody capture beads (sourced from Beckman Coulter) were prepared. Additionally, Fluorescence Minus One (FMO) control were set up concurrently, adhering to the same staining protocol as the samples. All control samples, post-staining, were preserved at 4°C, ensuring they were protected from light. Flow cytometry examinations were executed on instruments including the BD LSR Fortessa and the Cytoflex flow cytometer. These instruments were equipped with multiple lasers: a 405 nm, 488 nm (with filters at 530/30 for FITC/AF488 and 695/40 for PerCp-Cy5.5), 561 nm (with filters at 585/15 for PE and 780/60 for PE-Cy7), and 640 nm (with a filter at 670/14 for APC).

Subsequent to data acquisition, analysis was conducted using the FlowJo software, developed by Treestar. Comprehensive information regarding the antibodies employed in this study is available in figures 2.1 and 2.2.

Antibody	**Clone**	**Fluorophore**	**Dilution (µl/100 µl)**	**Supplier**
CD13	R3-242	PE	2	BD Pharmingen
CXCR4	L276F12	PE	2.5	Biolegend
Podoplanin	8.1.1	PE	2	Biolegend

Table 4.2: Antibody Panel for Pulmonary Pericyte Phenotypic Assessment via Flow Cytometry. The chart displays a curated set of antibodies specifically chosen to evaluate markers indicative of the pulmonary pericyte phenotype. The antibodies target CD13, CXCR4, and Podoplanin, with each conjugated to a PE fluorophore for detection. Information regarding the clone, dilution, and supplier for each antibody is provided. Both BD Pharmingen and Biolegend served as sources for the antibodies.

4.2.6 Pericyte Enrichment

To facilitate the LEGEND Screen™ and cell culture experiments, murine lung samples were enriched for Mesenchymal Stem Cells (MSCs) by employing a negative selection strategy. Specifically, CD45+ and ter119+ cell populations were removed using the EasySep™ Mouse Mesenchymal Stem/Progenitor Cell Enrichment Kit in conjunction with the EasySep™ magnet. This approach ensures a higher concentration of MSCs by depleting unwanted cell populations. Mesenchymal Stem Cell (MSC)-enriched lung suspensions were seeded in T25 culture flasks, dedicating one flask per mouse, using pericyte growth medium (sourced from PromoCell GmbH). One-week post-seeding, cultures underwent a wash with sterile, warm PBS followed by a medium replacement. The medium refreshment occurred biweekly until the cell confluence reached between 80% to 90%. Subsequent to reaching the desired confluency, cells were subjected to trypsinization using 0.25% Trypsin-EDTA solution (from Sigma Aldrich) and allowed to incubate for 5 minutes at 37°C. To halt the action of trypsin, a neutralizing solution containing DMEM with 10% FBS and 1% pen/strep was used. The cells were then transferred to a T75 flask for continued culture. After undergoing three passages, cells were seeded on gelatin-coated coverslips inside 12-well plates at a density of 0.1×106 cells/well, and subsequently cultured in pericyte growth medium until they achieved 90% confluence.

4.2.7 Immunofluorescence

Lungs excised from mice were preserved in a sucrose solution to facilitate cryopreservation. After rinsing away the sucrose with PBS, the samples were encapsulated in TissueTek OCT (Sakura) and subsequently frozen at -80°C. Sections of 10 µm thickness were prepared using a Leica cryostat and adhered to Superfrost Plus slides (Fisher Scientific), which were then stored at -80°C. Before staining, slides were equilibrated to ambient temperature. Tissue sections were demarcated with a hydrophobic pen. A 5% NGS and 0.3% Triton-X mixture in PBS was used to block and permeabilize the sections for a minimum of 2 hours. After blocking, sections were cleansed with PBS and subjected to an overnight incubation with designated primary antibodies (as listed in Table 3). Subsequent to another PBS rinse, sections were exposed to secondary antibodies tailored to each primary antibody's origin species. To evaluate specificity, control sections were also processed without primary antibody exposure. After a 2-hour secondary antibody incubation (refer to Table 2.3 for details), sections were again rinsed and subsequently mounted with Fluoroshield inclusive of DAPI.

For the immunohistochemical process, cells first underwent three washing cycles with PBS, each lasting 5 minutes. Following this, a fixation step was performed using a 3% paraformaldehyde (PFA) solution for 15 minutes at room temperature. After washing the fixative off, a blocking step was undertaken to minimize non-specific antibody bindings using a solution of 5% normal goat serum in 0.3% Triton-X-100/PBS, and this was allowed to proceed for 1 hour. The cells were then exposed to the primary antibodies (as detailed in Table 3) for a duration of 2 hours.

Post-primary antibody incubation, the cells were washed and treated with the corresponding secondary antibodies for 1 hour at room temperature. To conclude the process, another series of washes was conducted, and the coverslips bearing the cells were mounted onto microscope slides. Mounting was achieved using Fluoroshield (sourced from Sigma-Aldrich), which contains the nucleic acid stain, 4',6-diamidino-2-phenylindole (DAPI). For immunostained sections, imaging was executed on a TCS SP8 FALCON Leica confocal microscope, equipped with a specific laser and objective configuration.

Antigen Target	***Origin of Antibody***	***Specific Clone***	***Dilution Ratio***	***Provided by***
NG2	Rabbit	AB5320	1:250	Millipore
CD31	Hamster	2H8	1:500	Abcam
CXCR4	Rat	2B11	1:200	eBioscience
α-SMA	Mouse	1A4	1:1000	Sigma-Aldrich

Table 4.3 Antibodies used in immunostaining.

4.2.8 Cell culture

Human placental pericyte cells (HPLPCs) were procured from Promocell (Heidelberg, Germany) and were initially received at passage 2. For the purpose of this study, they were expanded until passage 10. Culture conditions entailed the use of pericyte-specific growth media (Promocell, Heidelberg, Germany), supplemented with 1% antibiotic–antimycotic (ThermoFisher, Massachusetts, US). For optimal cell adherence, both flasks and well plates were pre-coated with a 5% gelatin solution, prepared in autoclaved distilled water. For passaging, trypsin–EDTA (Sigma-Aldrich Ltd., St. Louis, USA) was employed to facilitate cell detachment from the culture substrate.

4.2.9 Growth Factor Treatment

Various recombinant growth factors and cytokines were used to treat HPLPCs for 24hrs in serum free DMEM. Table 2.4 contains an overview of the concentration used for each growth factor. Table 2.5 provides an overview of the inhibitors used throughout the thesis.

Growth Factor	Concentration ng/l	Manafacturer
TGF-B	1, 10, 100	Biolegend, California, USA
TNFA	1, 10, 100	Biolegend, California, USA
CXCL12	1, 10, 100, 500	Biolegend, California, USA
PDGFBB	1, 10, 100	Biolegend, California, USA

Table 4.4: Growth factor concentrations

Inhibitor	Concentration	Manufacturer
LIT-927	10um/ml	Axon Medchem (Groningen, The Netherlands)
SB203580	1um/ml	Cell Signalling Technology (Danvers, Massachusetts, USA.)
AMD3100	1um/ml	Cell Signalling Technology (Danvers, Massachusetts, USA.)
ARRY	1um/ml	Cell Signalling Technology (Danvers, Massachusetts, USA.)
LY294002	1um/ml	Cell Signalling Technology (Danvers, Massachusetts, USA.)

Table 4.5: Inhibitors concentrations

4.2.10 Transwell Migration Assay

Cells were harvested using trypsin-EDTA, centrifuged, and re-suspended in serum-free medium. 25,000 cells in 300 µl of serum-free medium were seeded into the upper chamber of 12-well transwell inserts (8.0 µm pore size, Corning, USA) to a concentration of 5×10^5 cells/ml. One hundred µl of cells were then added to the Transwell inserts (Corning).

The plates were incubated at 37 °C and in a 5% CO_2 atmosphere for 24 h. After 24 h, medium containing residual cells was removed from the upper chamber of the Transwell using a pipette, then a cotton swab, before fixation in methanol for a minimum of 10 min. Filters were removed from each insert, washed in ddH_2O and mounted on individual slides using Fluoroshield containing DAPI to provide nuclear staining. Slides were stored at − 20 °C until image acquisition. Cells were visualized at 20X using a Leica DM2500 fluorescence microscope (Leica Microsystems, Milton Keynes, UK). Cells on the inferior side of the filter were imaged at. Images were then processed using ImageJ software (NIH). Separate ‘particles’ were counted as single cells. Five random fields of view per insert were captured for subsequent quantification. The average number of migrated cells for each condition was calculated.

4.2.11 MTT viability assay

In order to evaluate cell viability, an MTT assay was employed. This assay leverages the ability of viable cells to convert MTT (3-(4,5-dimethylthiazol-2-yl)-2,5-diphenyltetrazolium bromide) into formazan crystals. The cells were first prepared in serum-free DMEM and subsequently seeded at a density of 5,000 cells per well in a 96-well plate. After allowing a period for adherence and proliferation—typically 24 hours in a 37°C incubator with 5% CO_2—the cells were exposed to specific test compounds. Following this treatment, the MTT solution was added to each well and the plate was incubated for several hours, as recommended by the MTT manufacturer's guidelines. Post-incubation, the medium was carefully discarded and a solubilizing agent, often dimethyl sulfoxide (DMSO), was introduced to dissolve the formazan crystals formed by live cells. The absorbance of each well was then measured using a spectrophotometer or plate reader, typically at 570 nm. The resulting absorbance values serve as an indicator of cell viability, with higher absorbance suggesting greater cell viability.

4.2.12 Statistical Analysis

Data analysis was conducted using GraphPad Prism Software version 6 (GraphPad Software, San Diego, CA). For statistical evaluations, we employed the student’s t-test or one-way ANOVA followed by Tukey's post hoc test when applicable. A significance threshold was set at $P < 0.05$. Additionally, Pearson correlation analysis was utilized to determine the relationship between ASM thickening and cell counts. Results are expressed as means ± SE.

4.3 Results

4.3.1 Murine Lung Pericytes Express Mesenchymal Cell Markers

The lungs of female C57BL/6 mice, aged 6-8 weeks, were carefully extracted, and subsequently subjected to flow cytometry analysis to determine the expression patterns of pericyte markers in mouse lung pericytes. Pulmonary pericytes were reliably identified as cells exhibiting the following marker profile: CD45-/CD31-/Ter119-/PDGFRβ+/CD146+. This combination of markers effectively distinguished pulmonary pericytes from other cell types within the lung tissue. A more detailed analysis was then conducted using the Biolegend LegendScreen™ (Fig. 4.2B).

Since pericytes are considered MSC-like cells residing in the perivascular niche of various tissues, including the lung, the expression of classic MSC markers was compared with antigens that pericytes expressed in this assay. For the characterization of pericyte cell surface markers, murine pulmonary pericytes identified as CD45-/CD31-/Ter119-/CD146+/PDGFRβ+ were screened for 252 markers using the LEGENDScreen™ panel (Fig.4.2A). This screen demonstrated that CD45-/CD31-/Ter119-/PDGFRβ+/CD146+ pericytes lacked markers typically associated with hematopoietic cells, affirming their non-hematopoietic nature. Furthermore, the presence of markers characteristic of mesenchymal cells was confirmed on these pulmonary pericytes. This assay revealed that murine pulmonary pericytes highly express the integrins CD29 and CD49a, both of which are reported to be expressed by MSCs.

Other highly expressed markers included CD47, CD105, CD266, and Ly-51. Pericytes were also found to express CD107a and CD107b, which are lysosomal degranulation markers known as LAMP1 and LAMP2 (Fig. 4.2C).

This comprehensive flow cytometry analysis provides valuable insights into the precise identification and characterization of pulmonary pericytes within lung tissue, highlighting their unique marker expression profile and distinguishing them from other cell types.

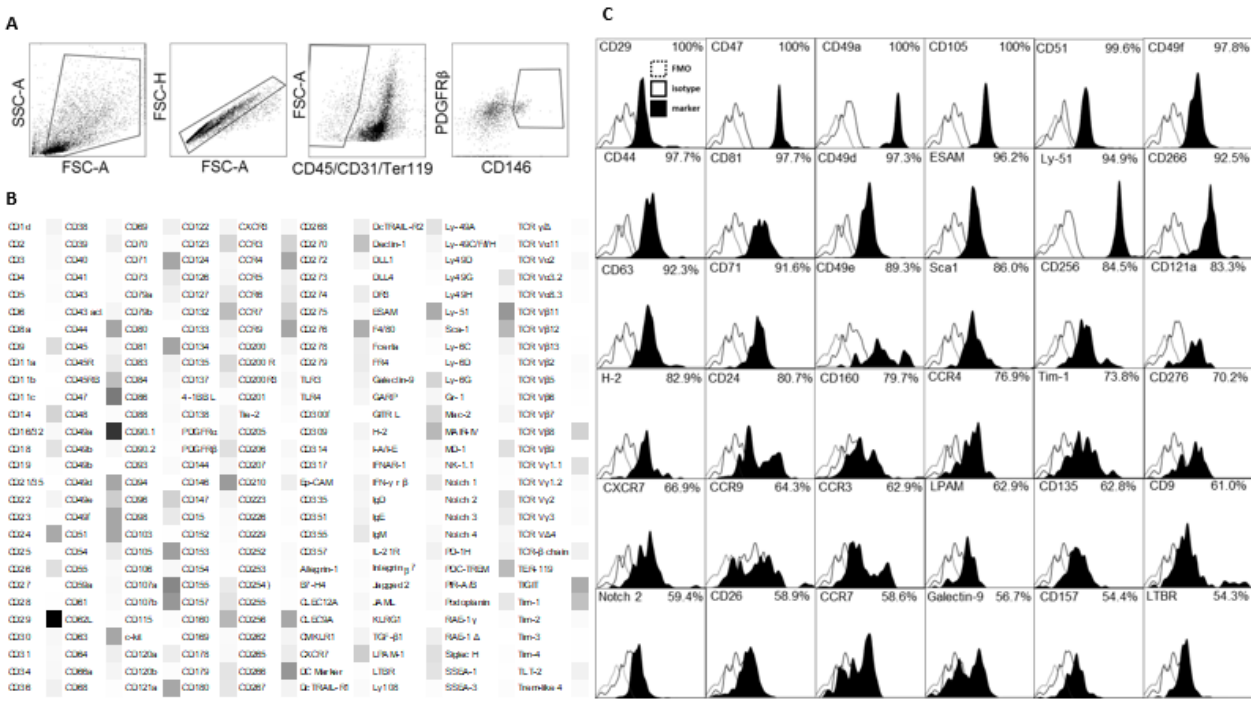

Figure 4.2: Murine Pulmonary Pericyte Characterization via Biolegend LegendScreenTM. pericytes were comprehensively characterized using flow cytometry. The lungs of female C57BL/6 mice, aged 6-8 weeks, were carefully extracted, and subsequently subjected to flow cytometry analysis. **(A)**: Pulmonary pericytes were reliably identified as cells that exhibited the following marker profile: CD45-/CD31-/Ter119-/PDGFRβ+/CD146+. Fluorescence minus one (FMO) control were employed to ensure the specificity of marker expression. Additional parameters such as forward scatter (FSC) and side scatter (SSC) were used for further characterization. **(B)**: A more detailed analysis using the Biolegend LegendScreenTM **(C)**: Histograms were employed to visually represent the distribution of expression levels for markers that were highly expressed by these pulmonary pericytes.

4.3.2 Pericyte Transition to a Migratory Phenotype Following HDM Exposure In Vivo

To investigate the mechanism behind the enhanced migratory capacity of pulmonary pericytes from HDM-exposed mice, flow cytometry was used to assess pericytes (negative for CD31, CD45, and Ter119) for key surface markers defining the pericyte phenotype (CD146, PDGFRβ) and markers associated with cell migration (CD13, podoplanin; Fig. 4.3 E, F). In HDM-exposed lungs, pericytes constituted a smaller proportion of lung cells ($p < 0.01$; Fig. 4.3B) due to the influx of inflammatory cells. However, the expression levels of the pericyte markers PDGFRβ and CD146 remained unchanged after the induction of allergic airway disease (Fig. 4.3C, D). To further examine the migratory phenotype in pulmonary pericytes, flow cytometry was used to assess the expression of the cell migration markers CD13 (Fig. 4.3 E) and podoplanin (Fig. 4.3F). Pericytes in the lungs of HDM-exposed mice showed significantly higher levels of these migratory markers, as determined by median fluorescence intensity (MFI; $p < 0.05$). Figure 4.4 further confirms that HDM exposure induces a migratory phenotype in pericytes. Pericytes were exposed to HDM in vivo, then isolated using magnetic sorting. These isolated pericytes were subsequently subjected to a Transwell assay with fetal calf serum (FCS) as the chemoattractant. The results showed a significant increase in migration, with ***$p < 0.001$. Figure 4.5 further confirms that pericytes exhibit a migratory phenotype in response to inflammation. Pericyte migration is mediated by the CXCL12/CXCR4 pathway, as pericytes isolated from murine whole lung digests using the gating strategy described in Figure 4.3 displayed increased CXCR4 expression in response to HDM ($p < 0.05$; Fig. 4.5).

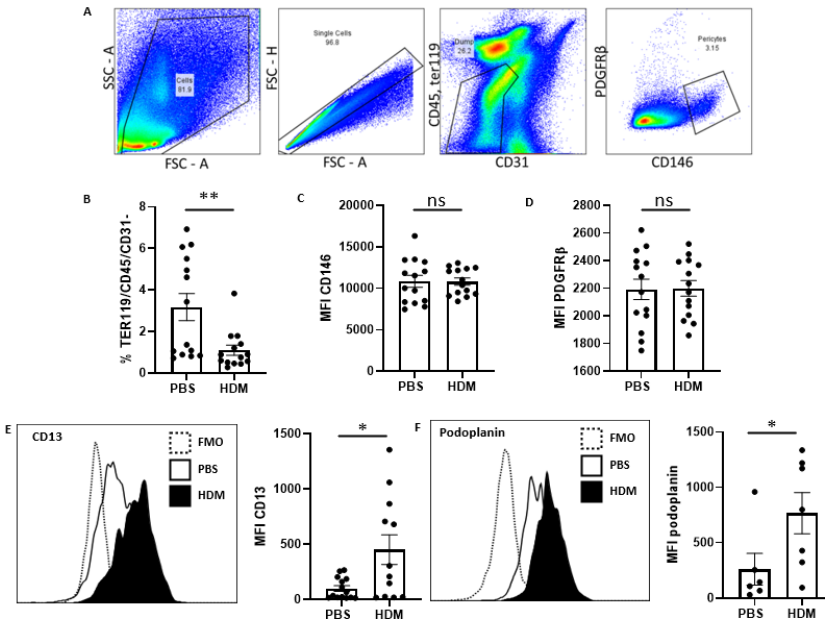

Figure 4.3: Flow Cytometry Characterization of Murine Lung Pericytes following HDM Exposure In Vivo. **(A)**. Pericytes were identified based on specific criteria, including being whole, single cells (FSC, SSC), negative for the markers ter119, CD31, and CD45, and positive for the markers CD146 and PDGFRβ. **(B)**: The proportion of ter119-/CD31-CD45- cells was determined, and the median fluorescence intensity (MFI) of CD146 **(C)** and PDGFRβ **(D)** was analyzed using FlowJo software. This analysis involved a sample size of n=14 per group and was representative of three independent experiments. **(E, F)**: Flow cytometry was also employed to evaluate pericytes in terms of the MFI of CD13 and podoplanin, with analysis again conducted using FlowJo software. Similar sample sizes (n=14 per group) were used, and the results were representative of three independent experiments. Noteworthy findings indicated by statistical significance include *p<0.05, **p<0.01, and ***p<0.001. Additional abbreviations and terms used in the figure include FCS (fetal calf serum), FMO (fluorescence minus one control), FSC (forward scatter), HDM (house dust mite), MFI (median fluorescence intensity), PBS (phosphate-buffered saline), and SSC (side scatter). This figure provides critical insights into the dynamic changes in pericyte phenotype induced by HDM exposure in vivo.

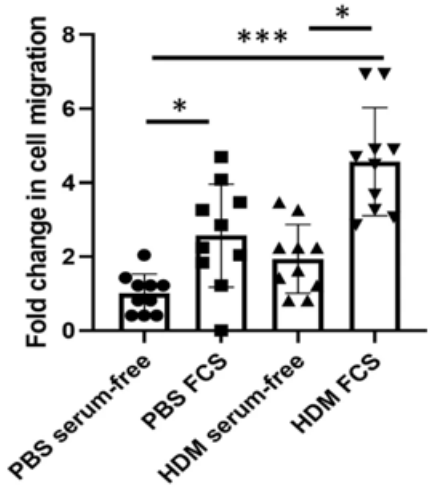

Figure 4.4: Effect of HDM on pericyte migration in ex vivo trans well assay. Female C57BL/6 mice (6–8 weeks old) were subjected to intranasal delivery of sterile PBS or house dust mite extract (HDM) 5 days a week for 5 consecutive weeks. Lung tissue was digested and pericytes were obtained by magnetic sorting, then subjected to a Transwell assay using fetal calf serum (FCS) as the chemoattractant. n = 10 per group, representative of four independent experiments. *p < 0.05, **p < 0.01, ***p < 0.001.

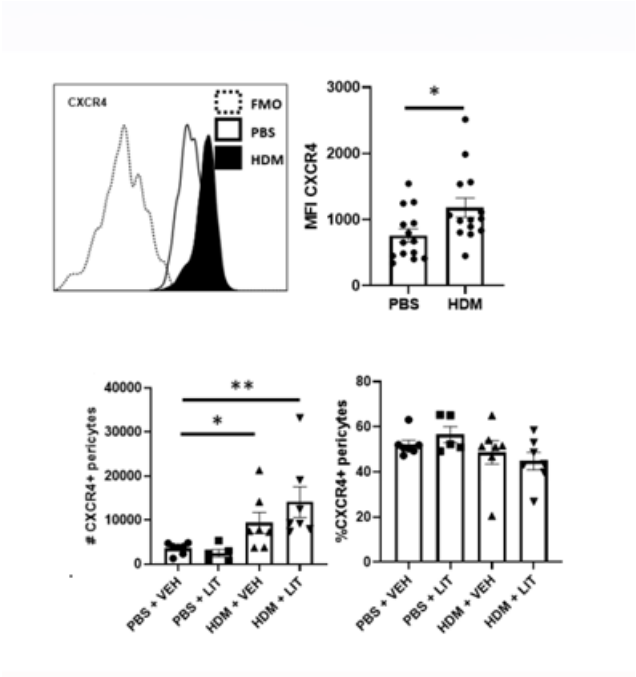

Figure 4.5: Pericyte Migration Governed by the CXCL12/CXCR4 Pathway The experimental design involved female C57BL/6 mice aged 6–8 weeks. The mice were subjected to intranasal administration of either sterile PBS (10 µl) or house dust mite extract (HDM; 25 µg in 10 µl) for 5 days each week, consistently over 5 consecutive weeks. Subsequently, at the conclusion of the protocol, lung tissue was harvested, and pericytes were assessed using flow cytometry. The analysis focused on determining the median fluorescence intensity of CXCR4, with FlowJo software employed for data analysis. The sample size for this analysis consisted of $n = 14$, which was representative of findings from three independent experiments. Statistical significance was indicated by $*p < 0.05$.

4.3.3 Reversal of CXCL12-Induced Migration of Human Placental Pericytes by LIT927 Administration in vitro and in vivo Under Fibrotic Conditions"

In vivo, HDM exposure caused an increase in NG2 expression, while LIT-927 attenuated the HDM-induced accumulation of NG2+ pericytes in the airway wall (Figure 4.6). To further understand the pathways involved in pericyte migration towards 300 ng/ml CXCL12, we conducted Transwell (Figure 4.9) and scratch assays (Figure 4.7). Cell migration towards CXCL12, assessed via the scratch assay, showed a significant reduction when treated with LIT-927 (Figure 4.7).

Supporting these findings, CXCL12-induced migration in the Transwell assay was significantly inhibited ($p < 0.01$) when human pericytes were exposed to LIT-927, AMD3100, and downstream MAPK inhibitors for the ERK, PI3K/AKT, and P38 pathways. Visualization was performed at 20X magnification using a Leica DM2500 fluorescence microscope (Leica Microsystems, Milton Keynes, UK). Single cells were counted as separate "particles," with five random fields of view per insert captured for subsequent quantification. The average number of migrated cells for each condition was calculated. There was no difference in pericyte migration between exposure to AMD3100, MAPK inhibitors, and LIT-927, highlighting the effectiveness of LIT-927 as an alternative therapeutic option. A concentration of 10 μM of LIT-927 significantly ($p < 0.05$) reversed the effect of CXCL12 on pericyte migration. Unlike MAPK inhibitors, LIT-927 specifically inhibits CXCL12-induced migration. There was no significant difference between pericytes exposed to LIT-927 alone and those exposed to serum-free DMEM.

Pericytes were pretreated for 24 hours with pro-fibrotic cytokines, specifically TNF-α, TGF-β, and CXCL12, to stimulate a fibrotic response. Appropriate concentrations were determined by the MTT assay (Figure 4.9). The therapeutic potential of LIT-927 was assessed by evaluating the migration of pretreated human placental pericytes towards CXCL12 and a range of inhibitors (AMD3100 and downstream MAPK inhibitors for the ERK, PI3K/AKT, and P38 pathways) (Figures 4.10, 4.11, 4.12).

Our findings indicate that pericytes pretreated with TNF-α, TGF-β, and CXCL12 exhibited a significantly enhanced migratory response towards CXCL12, 10% FCS, and serum-free media compared to those that weren't pretreated. This increased migratory ability when exposed to CXCL12 suggests a crucial role for CXCL12 in pericyte migration. Migration followed a similar trend in pericytes that were not pretreated. There was no difference in pericyte migration between exposure to AMD3100 and LIT-927, underscoring the effectiveness of LIT-927 as an alternative therapeutic option. A concentration of 10 μM of LIT-927 significantly ($p < 0.05$) reversed the effect of CXCL12 on pericyte migration. Unlike MAPK inhibitors, LIT-927 is only effective in the presence of CXCL12. There was no significant difference between pericytes exposed to LIT-927 alone and those exposed to serum-free DMEM. These results collectively underscore the role of the CXCL12/CXCR4 pathway in pericyte migration and the potential of LIT-927 as a therapeutic agent in modulating this process.

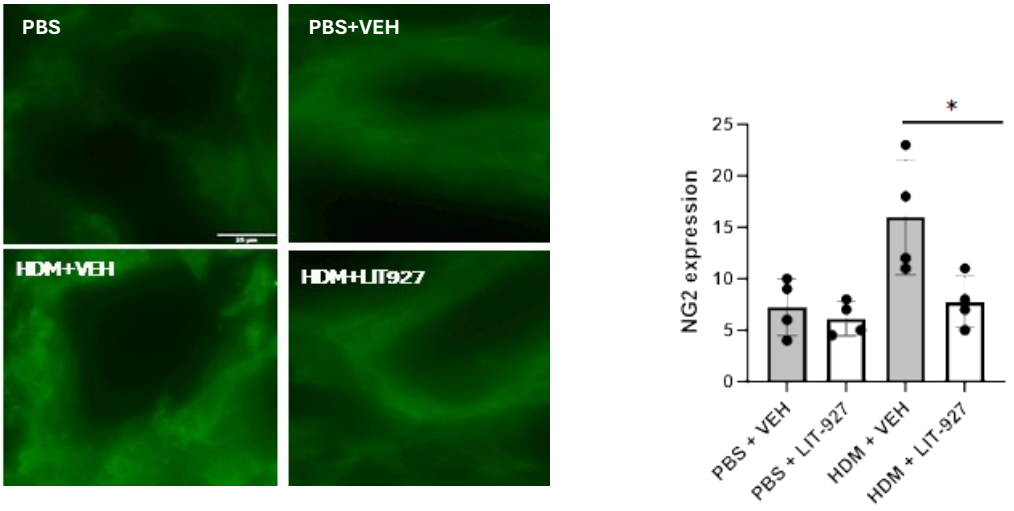

Figure 4.6: Immunostaining and Quantification of NG2 Expression in Pericytes
Female C57BL/6 mice (6-8 weeks old) were exposed to either PBS or HDM extract for three consecutive weeks. This was followed by intranasal administration of PBS+VEH, PBS+LIT927, HDM+VEH and HDM+LIT927 At the end of the protocol, Lung sections obtained were stained for the pericyte marker NG2 (green). NG2 marker expression was quantified using Image J. =. Scale bar: 25 µm. Data are derived from two independent experiments with n=4 mice per group. ***p < 0.001, determined by one-way ANOVA for multiple groups with Tukey's post hoc test. PBS: phosphate-buffered saline; VEH: vehicle control-10% w/v methyl-β-cyclodextrin, HDM: House Dust Mite, LIT: The CXCL12 Neutralizing ligand LIT927

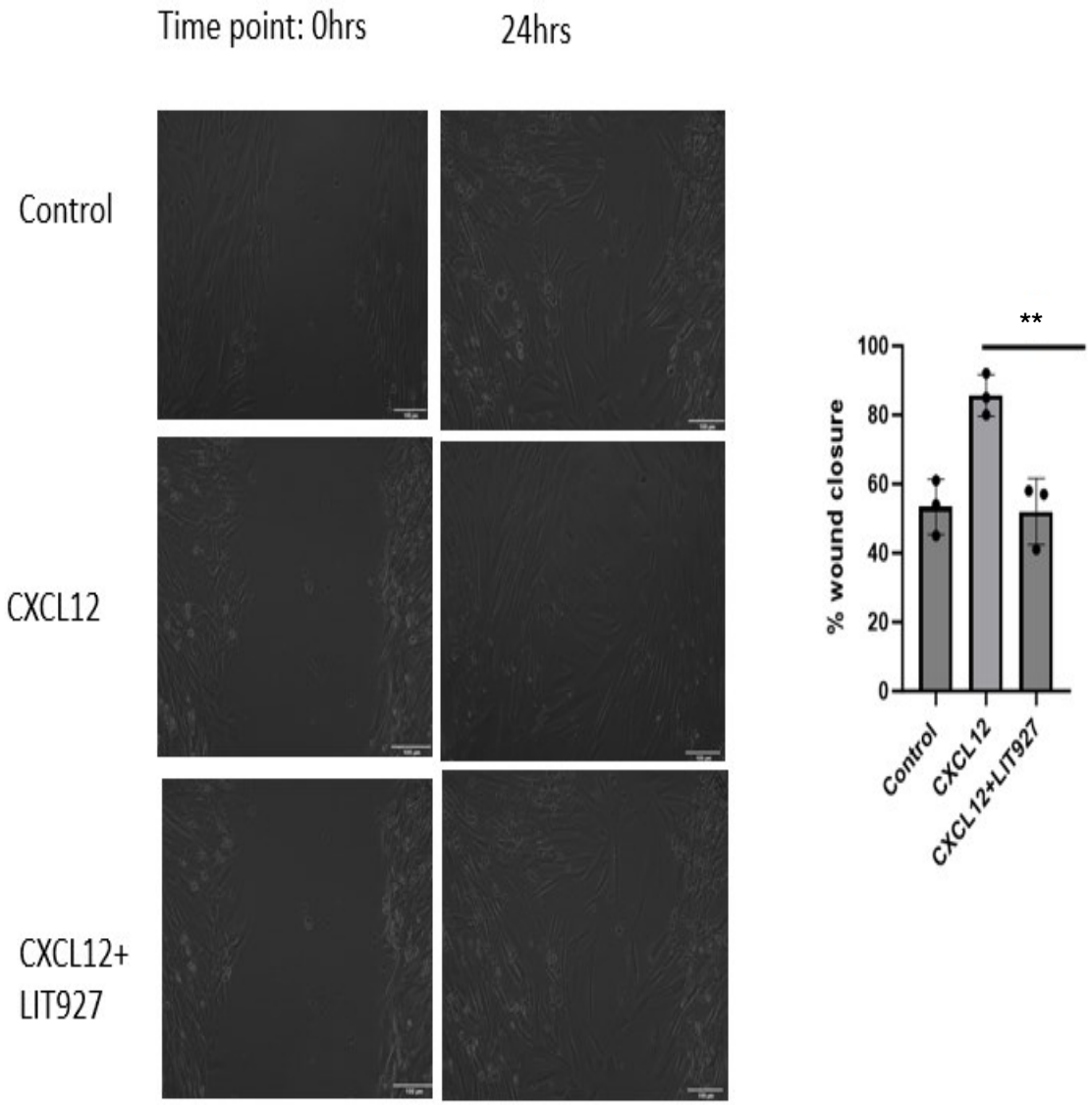

Figure 4.7: Assessment of Human Placental Pericyte Migration After Treatment with CXCL12 and LIT-927 Human placental pericytes were treated for 24 hours with CXCL12 and the neutralizing ligand LIT-927. Cell migration was assessed after 24 hours using the scratch assay, and the percentage of wound/scratch closure was quantified using Image J. Data are derived from two independent experiments with n=3. Statistical significance was determined with **p < 0.01, using one-way ANOVA for multiple groups with Tukey's post hoc test. Scale bar: 100 µm.

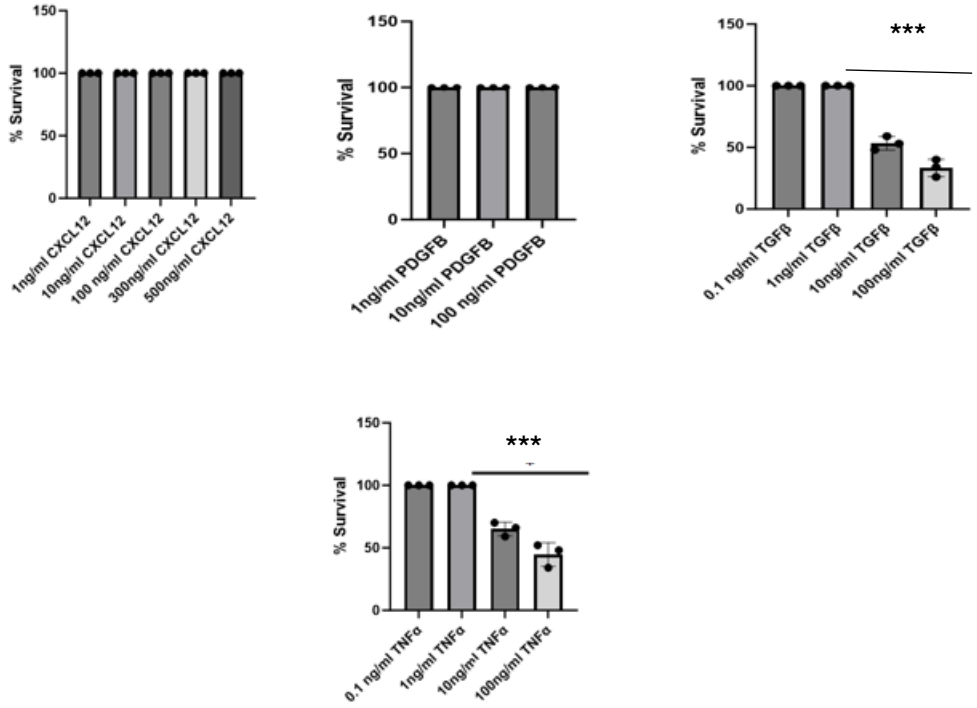

Figure 4.8: MTT assay of Human Placental Pericytes Treated with Pro-Fibrotic Cytokines. Human placental pericytes were treated for 24 hours with pro-fibrotic cytokines at different concentrations. Survival was assessed via the MTT assay. Data are derived from two independent experiments with n=3. Statistical significance was determined with ***p < 0.001, using one-way ANOVA for multiple groups with Tukey's post hoc test.

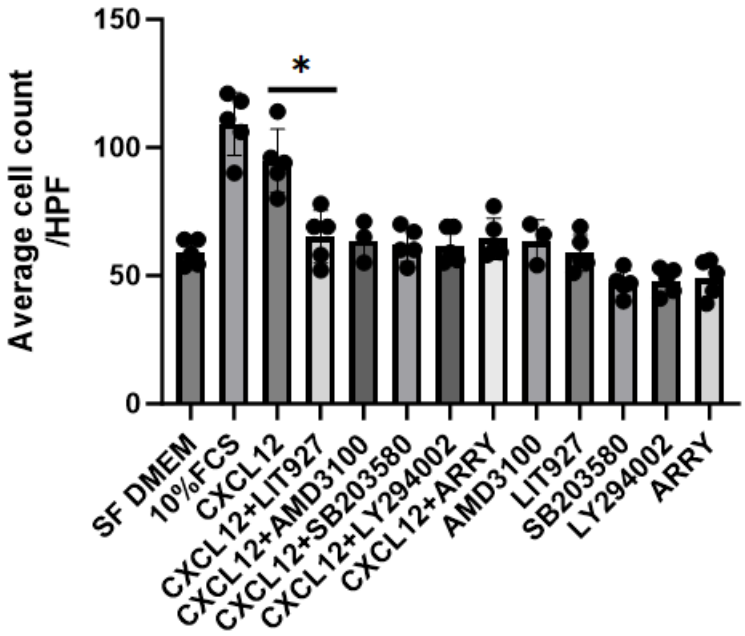

Figure 4.9: Assessment of CXCL12-Induced Migration of Human Placental Pericytes and the Effect of Inhibitors Using a Transwell Assay. human placental pericyte migration towards CXCL12 and a range of inhibitors was assessed. Using a Transwell assay. LIT-927 was found to suppress CXCL12-induced migration. The data were obtained from two independent experiments, each with n=5. Statistical significance was determined with *p < 0.05, using one-way ANOVA followed by Tukey's post hoc test.

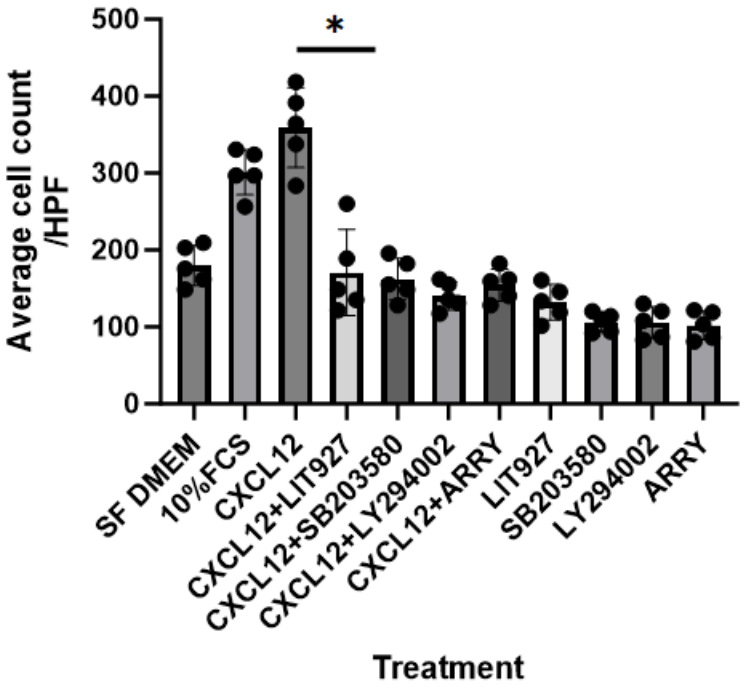

Figure 4.10: Suppression of CXCL12-Induced Migration of CXCL12 Pre-Treated Human Placental Pericytes by LIT-927 in a Transwell Assay. CXCL12 pre-treated human placental pericyte migration towards CXCL12 and a range of inhibitors was assessed. The migratory behavior of human placental pericytes in response to CXCL12 and selected inhibitors was investigated using a Transwell assay. Data are derived from two independent experiments with n=5. Statistical significance was determined with *$p < 0.05$, using one-way ANOVA for multiple groups with Tukey's post hoc test.

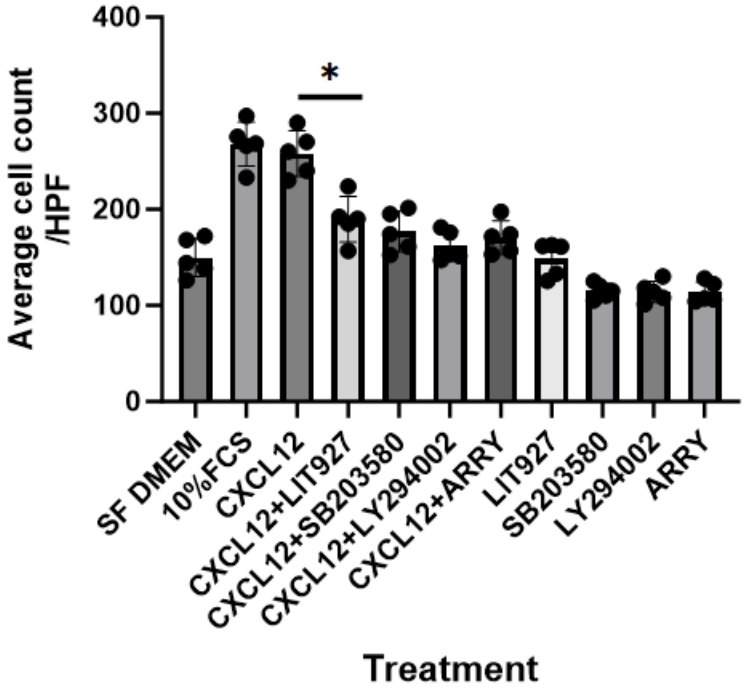

Figure 4.11: Suppression of CXCL12-Induced Migration of TNF-α Treated Human Placental Pericytes by LIT-927 in a Transwell Assay. TNF-α pre-treated human placental pericyte migration towards CXCL12 and a range of inhibitors was assessed. The migratory behavior of human placental pericytes in response to CXCL12 and selected inhibitors was investigated using a Transwell assay. Data are derived from two independent experiments with n=5. Statistical significance was determined with *$p < 0.01$, using one-way ANOVA for multiple groups with Tukey's post hoc test.

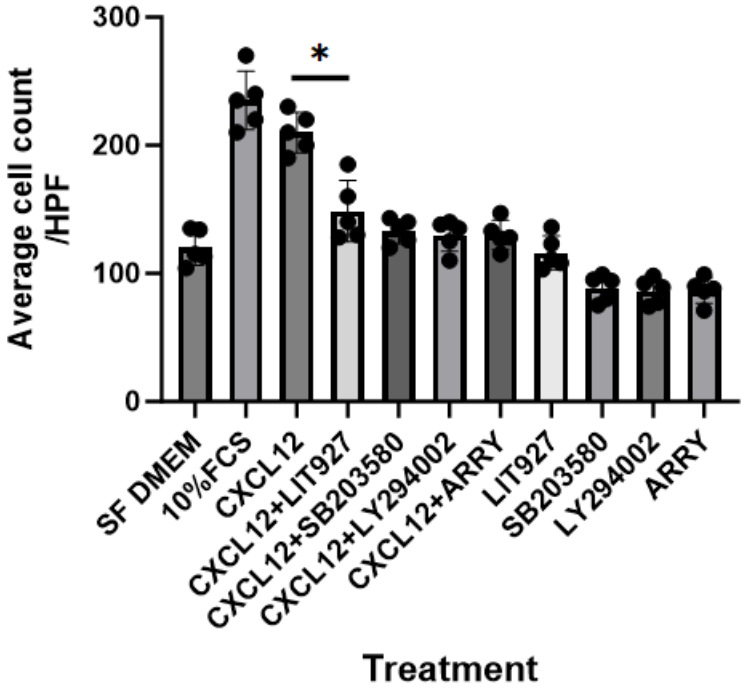

Figure 4.12: Suppression of CXCL12-Induced Migration of TGF-β Treated Human Placental Pericytes by LIT-927 in a Transwell Assay. TGF-β pre-treated human placental pericyte migration towards CXCL12 and a range of inhibitors was assessed. The migratory behavior of human placental pericytes in response to CXCL12 and selected inhibitors was investigated using a Transwell assay. Data are derived from two independent experiments with n=5. Statistical significance was determined with *p < 0.05, using one-way ANOVA for multiple groups with Tukey's post hoc test.

4.4 Discussion

This chapter delves deeper into the mechanisms by which LIT-927 exerts its effects on pericytes, both in vivo and in vitro, situating these findings within the broader context of existing literature.

Identification of Murine Pericyte Markers

To understand the factors influencing pericyte migration, we conducted a comprehensive screening of cell surface markers on freshly isolated murine lung pericytes. This study contributes to the limited but growing body of literature on murine pericyte markers, providing crucial insights into their phenotype and function.

Our findings in figure 4.2 are consistent with the current literature, demonstrating that murine pulmonary pericytes lack CD31, CD34, CD45, CD62L, CD71, CD106, c-kit, and CD133 expression, but express CD49b, CD63, CD90, CD105, and CD146 (Dellavalle, 2007). Additionally, they exhibit weak CD54 expression (Turley et al., 2015). According to the International Society of Cellular Therapy (ISCT) definition of human (Dominici, 2006), murine pulmonary pericytes can be classified as a subset of MSCs based on their expression of CD105, CD73, and CD90, and the absence of CD45, CD34, CD11b, CD79a, CD19, and HLA-DR, despite also being CD14 positive.

Our research aligns with and extends the findings of de Souza et al. (2016), who described pericytes as mesenchymal stromal cells that lack certain hematopoietic and endothelial cell markers but express others like CD146 and PDGFRβ (de Souza et al., 2016). Moreover, our study highlights that while both MSCs and pericytes share many markers, unique markers like CD140b (PDGFR-β) are specific to pericytes. This distinction is critical for accurately identifying and studying pericytes in various disease models and underscores the potential for developing targeted therapies.

The scarcity of literature on murine pericyte markers compared to human markers may be due to the difficulties in acquiring mouse pericytes and the general preference to initiate preliminary tests on murine models before proceeding with human studies. Our findings showed that murine pericytes do not express markers like CD31, CD34, and CD45, but do express CD49b, CD63, and CD90 (Morikawa et al., 2009). . Additionally, in our assay, pericytes showed moderate Sca1 expression but little to no PDGFRα expression. Other MSC markers, including CD9, CD24, CD44, CD47, CD49e, CD81, and CD98 (Rostovskaya & Anastassiadis, 2012), were also identified on mouse pulmonary pericytes. Additionally, pericytes expressed the signaling receptor Notch2 and CD51, an integrin expressed on Nestin+/CD146+ pericyte-like MSCs (Pinho, 2013)

Overall, our research contributes valuable insights into the unique marker expression profile of murine pulmonary pericytes, distinguishing them from other cell types. This comprehensive characterization provides a foundation for further studies on pericyte function and potential therapeutic applications.

HDM-Induced Pericyte Migration

Following the validation of a flow cytometry panel to identify murine pulmonary pericytes, we subjected mice to an HDM-driven model of chronic allergic inflammation to assess the impact of a Th2-polarized immune environment on pericyte phenotype and function. Assessments of marker expression on pericytes revealed significant increases in CD13 (Rahman, 2014) and podoplanin (Ward, 2019) (Figure 4.3), and CXCR4 (Figure 4.5). These markers have all been implicated in mesenchymal cell migration. This increase in migration was functionally observed when sorted pericytes from the lungs exposed to HDM showed increased migratory capacity ex vivo in a Transwell assay (Figure 4.4). In vivo, increased pericyte migration in response to inflammation was further confirmed by the fact that HDM caused an accumulation of NG2+ pericytes (Figure 4.6). In line with our observations, recent studies have identified pericytes as a primary source of myofibroblasts in other fibrotic diseases, including kidney and liver fibrosis. In the context of tissue injury, inflammation, and fibrosis, pericytes have demonstrated the ability to differentiate into fibroblasts, playing a crucial role in wound healing. Immunohistochemical studies of dermal scars indicate that pericytes migrate into the perivascular space before transforming into fibroblast-like cells (Sundberg et al., 2002).

More recent research has identified pericytes as a significant source of myofibroblasts in mouse models of renal (S. L. Lin, 2008) and hepatic fibrosis (Mederacke et al., 2013). Lin and colleagues used chimeric mice with GFP-tagged collagen type 1α1 (coll1a1) to demonstrate that pericytes differentiate into myofibroblasts in kidney fibrosis. Following ureteral obstruction, coll1a1-GFP-expressing pericytes were identified as the primary source of scar-forming myofibroblasts. In 2010, further studies by this group utilized Cre fate tracking techniques to show that FoxD1-positive and PDGFR-β cells (perivascular cells) proliferate and differentiate into alpha-smooth muscle actin (α-SMA) positive myofibroblasts during fibrosis. These perivascular cells were found to be responsible for more than 95% of scar-forming myofibroblasts in this fibrotic model.

Mederacke et al. (2013) demonstrated, using Cre-transgenic mice, that liver-resident pericytes (hepatic stellate cells) account for approximately 90% of tissue myofibroblasts in models of liver fibrosis induced by toxins, cholestasis, and non-alcoholic steatohepatitis. More recently, Johnson et al. (2015) explored the role of PDGF-B/PDGFRβ signaling in maintaining pericyte-endothelial cell interactions in a mouse model of allergic lung disease. They found that inhibiting PDGFRβ led to significant pericyte uncoupling from the vasculature, increased airway smooth muscle thickening, and worsened lung dysfunction. This study was the first to show that pericytes migrate from the tissue vasculature contributing to airway remodeling by integrating into smooth muscle bundles. However, the mechanism driving this migration was not identified.

Building on previous studies demonstrating MSC migration in response to (C. Hu, 2013), we examined the regulation of the CXCL12/CXCR4 pathway in HDM-exposed mice. Pericytes from the inflamed lung exhibited higher levels of CXCR4 than those from control mice. Immunostained lung sections showed the accumulation of NG2+/CXCR4+ pericytes in the airway smooth muscle of HDM-exposed mice.

These results suggest that the CXCR4/CXCL12 axis is functionally relevant in pericyte chemotaxis in this disease model. Although the role of this axis in pulmonary pericyte migration during inflammation is not well understood, substantial literature supports its involvement in recruiting bone marrow mesenchymal stem cells in response to injury. Previous studies have shown that CXCL12 transcript and protein levels increase under hypoxic conditions, leading to the recruitment of circulating CXCR4-expressing progenitor cells to the injury site, where they participate in tissue regeneration. Similarly, CXCL12 levels have been shown to increase following bone fractures (Hamdan et al., 2014). Although these injuries are different from the HDM model of inflammation used in this study, these findings strongly suggest that CXCL12 significantly influences pericyte/MSC recruitment in response to injury. Previous studies have assessed the effect of CXCL12 on pericytes using a CXCR4 inhibitor, AMD3100. This research showed that CXCL12 contributes to the differentiation of bone marrow stem cells into pericytes and increases the number of pericytes at fibrotic tumor sites (Hamdan et al., 2014). However, since AMD3100 has been shown to induce the egress of bone marrow MSC into peripheral blood (Kumar & Ponnazhagan, 2012), its effect could be detrimental in the context of allergic asthma.

Our findings are important as they offer an alternative approach to counteract the negative effects of AMD3100. Recent research has developed a novel neutraligand molecule, LIT-927, modified from chalcone 4 to enhance bioavailability (Regenass, 2018). LIT-927 has shown efficacy in a mouse model of pulmonary hypertension by reducing pericyte migration toward blood vessels and mitigating the vascular remodeling typical of this disease (Bordenave et al., 2020).

Profibrotic cytokine pretreatment -Induced Pericyte Migration and this was attenuated by LIT927.

Pericytes from the inflamed lung exhibited higher levels of CXCR4 than those from control mice (Figure 4.5). This finding aligns with previous studies demonstrating MSC migration in response to CXCL12 (C. Hu, 2013), By examining the regulation of the CXCL12/CXCR4 pathway in HDM-exposed mice, our study builds on existing literature, reinforcing the significance of this pathway in pericyte migration

Scratch Assays (Figure 4.7) and Transwell assays (Figure 4.9,4.10,4.11 and 4.12) provided further insights into the effects of CXCL12 on human pericyte migration. LIT-927 effectively reversed the migration-promoting effects of CXCL12, suggesting its potential as a therapeutic alternative. To further investigate the impact of a pro-fibrotic inflammatory environment on pericytes, we examined the effects of pre-treating human pericytes with TGF-β, TNF-α, and CXCL12. These cytokines significantly enhanced pericyte migratory responses, and the increase in migration was reversed by LIT-927, underscoring the fact therapeutic potential of LIT-927.

CXCL12-induced migration was significantly inhibited ($p<0.05$) when human pericytes were exposed to AMD3100 and downstream MAPK inhibitors for the ERK, PI3K/AKT, and P38 pathways, indicating these pathways play a significant role in pericyte migration. There was no difference in pericyte migration upon exposure to AMD3100 and LIT927, emphasizing the effectiveness of LIT927 as an alternative therapeutic option. A concentration of 10 μM of LIT927 was able to significantly ($p<0.05$) reverse the effect of CXCL12 on pericyte migration. There was no significant difference between pericytes exposed to CXCL12+LIT927 and those exposed to serum-free DMEM. Notably, there was also no significant difference in migration between pericytes exposed to CXCL12+LIT927 and pericytes exposed to CXCL12 and MAPK inhibitors, indicating that LIT927 is an effective alternative to MAPK inhibitors

Our findings align with the literature, where CXCL12 expression has been shown to increase following bone fracture, highlighting the role of CXCL12 in pericyte/MSC recruitment in response to injury. Previous studies have utilized a CXCR4 inhibitor, AMD3100, to assess the effect of CXCL12 on pericytes. This study demonstrated that CXCL12 contributes to the differentiation of bone marrow stem cells into pericytes and overall increases the number of pericytes present at the site of the fibrotic tumour. However, AMD3100 has been shown to induce

Interestingly, there was a significant reduction in migration when pericytes were exposed to MAPK inhibitors (without CXCL12 as a chemokine) vs serum-free DMEM. This aligns with evidence that inhibiting MAPK pathways such as ERK, PI3K/AKT, and the P38 pathway is difficult to achieve locally without significant side effects, making them unattractive therapeutic targets. For that reason, we attempted to inhibit the CXCL12 pathway in vitro using LIT927, which locally neutralizes CXCL12. The CXCR4 antagonist AMD3100 is also known to induce a rapid release of CXCL12 from bone marrow stroma to the circulation, leading to the release of stem cells into the circulation over their anchorage in bone marrow niches. Therefore, chemokine blockade could be an interesting strategy to be used as an alternative to conventional receptor blockade.

Inhibiting CXCL12 is therapeutically advantageous as CXCL12 plays a nonredundant homeostatic role and it is closely associated with tissue injury and several diseases, including chronic inflammation, autoimmune diseases (such as lupus erythematosus), cancer, atherosclerosis, and AIDS.

Chapter 5- General Discussion and Conclusions

5.1 Conclusions

This PhD thesis successfully achieved its aims, significantly contributing to the understanding of chronic allergic airway disease, particularly through the exploration of the CXCL12/CXCR4 signaling pathway and the role of CXCR4+ pericytes. We demonstrated that CXCR4+ pericytes play a crucial role in inflammation-driven tissue and vascular remodeling. Our findings highlight CXCL12 neutralization as a novel therapeutic target for chronic allergic airway disease. Specifically, we showed how pulmonary pericytes migrate to the airway wall and contribute to both structural and vascular changes observed in persistent allergic airway inflammation. Identifying LIT-927 as a viable pharmacological target offers a promising intervention for mitigating airway and vascular remodeling.

Our hypothesis was that HDM exposure induces structural changes in the lung by increasing CXCL12 levels, leading to airway smooth muscle thickening and vascular remodeling, driven by pericyte uncoupling and migration. Our results confirmed that treatment with LIT-927 disrupts the CXCL12 chemokine gradient, prevents pericyte migration, reduces smooth muscle thickening and vascular remodeling, and improves lung function. In conclusion, targeting CXCR4+ pericytes presents a promising strategy for treating chronic allergic airway diseases.

5.2 General Discussion

In this thesis, we explored the therapeutic effects of the novel CXCL12 neutralizing agent, LIT-927, on airway remodeling in allergic airway diseases. Our research focused on three critical parameters: bronchial remodeling, vascular remodeling, and pericyte migration. The most important observation from our research is the demonstration that LIT-927, by inhibiting CXCL12, can simultaneously attenuate bronchial and vascular remodeling and disrupt pericyte migration. This multifaceted impact positions LIT-927 as a highly promising therapeutic agent for asthma, suggesting a more integrated approach in treating the disease.

Why is this Research important?

Investigating LIT-927 as a therapeutic target for asthma is crucial because many asthmatics experience a progressive decline in lung function over time (Bousquet et al., 2007). About 4% of asthmatics continue to grapple with poorly managed asthma and significant impairment of quality of life, underscoring the need for more potent and novel treatments for lung fibrosis (Morales, 2013) Previous studies have underscored CXCL12 as a pivotal factor in angiogenesis, inflammation, and fibrosis. However, our research uniquely demonstrates the comprehensive impact of CXCL12 inhibition on bronchial remodeling, vascular remodeling, and pericyte migration. Our findings are important as they offer an alternative approach to counteract the negative effects of AMD3100 A comparative analysis reveals distinct advantages of LIT-927 over traditional CXCL12 and CXCR4 inhibitors. LIT-927 offers several advantages over traditional treatments. Unlike CXCR4 inhibitors such as AMD3100, which can promote the release of CXCL12 from bone marrow, LIT-927 selectively targets CXCL12, ensuring that CXCR4 signaling remains unaffected.

This selectivity reduces the likelihood of off-target effects (Daubeuf et al., 2013) In terms of administration, LIT-927's oral bioavailability provides a convenient option compared to some monoclonal antibodies (mAbs) that require intravenous or subcutaneous administration (Daubeuf et al., 2013). Preliminary evidence indicates that LIT-927 has a promising safety profile. This stands in contrast to other strategies, such as RNA-based methods, which might introduce unforeseen off-target consequences or trigger immune responses (Daubeuf et al., 2013). The precision targeting of LIT-927 enhances its potential for use in combination with other treatments for lung diseases without increasing the risk of amplified toxicity (Daubeuf et al., 2013). Finally, LIT-927 boasts greater stability and cost-effectiveness compared to mAbs or RNA-based therapeutics (Daubeuf et al., 2013).

Situating the findings within the literature

. Recent research has developed a novel neutraligand molecule, LIT-927, which was modified from chalcone 4 to enhance bioavailability (Regenass, 2018) LIT-927 has shown efficacy in a mouse model of pulmonary hypertension by reducing pericyte migration toward blood vessels and mitigating the vascular remodeling typical of this disease (Bordenave et al., 2020). In the context of HDM-driven allergic inflammation, we chose to administer LIT-927 intranasally to disrupt the CXCL12 gradient at the site of expression in the airway wall's inflammatory exudates.

Additionally, we administered this compound therapeutically, after the initiation but before the full establishment of airway remodeling (Johnson, 2004) This approach demonstrated that LIT-927 significantly reduced symptom scores in treated mice and substantially decreased the airway smooth muscle burden. Mechanistically, this was associated with a significant reduction in the number of pericytes uncoupling from the pulmonary vasculature. The attenuation of bronchial remodeling by LIT-927 aligns with earlier studies highlighting the role of CXCL12 in fibrosis and tissue remodeling. CXCL12 has been implicated in promoting fibroblast activity and collagen deposition, both of which are crucial in the development of bronchial remodeling (F. Li et al., 2020).

Our study builds on this by showing that neutralizing CXCL12 can effectively reduce these fibrotic processes, providing a novel therapeutic approach for asthma. This finding is significant because it suggests that targeting CXCL12 can reverse structural changes in the airways, potentially improving lung function and quality of life for asthmatics. In terms of vascular remodeling, our findings are consistent with existing literature that positions the CXCL12/CXCR4 axis as a key player in angiogenesis and vascular integrity. Studies have shown that elevated levels of CXCL12 and CXCR4 correlate with increased angiogenesis and vessel formation in various diseases, including cancer and chronic inflammation (Chang et al., 2020). By demonstrating that LIT-927 can attenuate vascular remodeling, we provide evidence that targeting CXCL12 can disrupt these processes, offering a potential therapeutic strategy for diseases characterized by abnormal vascular remodeling, such as asthma.

This is particularly important as it highlights a novel approach to managing the vascular aspects of asthma, which have been less studied compared to bronchial changes.

The impact of LIT-927 on pericyte migration adds a new dimension to our understanding of the role of pericytes in asthma. Pericytes are known to differentiate into myofibroblasts, contributing to tissue fibrosis and remodeling (Johnson et al., 2015). Our findings that LIT-927 significantly affects pericyte behavior and reduces their migration underscore the importance of CXCL12 in pericyte dynamics. This is particularly relevant as it highlights a novel mechanism by which CXCL12 inhibition can mitigate both bronchial and vascular remodeling in asthma. This observation is crucial because it identifies a new target for therapeutic intervention that could potentially address multiple aspects of airway remodeling simultaneously.

Table 5.1 illustrates the role of CXCR4 inhibitors in organ fibrosis, situating our findings within the broader context of CXCR4/CXCL12 research.

Type of fibrosis	**Research models**	**CXCR4 inhibitors**	**Function**	**Reference**
Pulmonary fibrosis	Human lung fibroblasts	AMD3100, CXCR4 siRNA	Effective inhibition of CXCL12-induced CTGF upregulation	(C.-H. Lin et al., 2014)
IPF in mice	Lung fibroblasts	F-PAMD (a siRNA carrier)	In vitro studies show substantial cellular uptake and anti-fibrotic effects	(Y. Wang et al., 2019)
Pulmonary fibrosis	BLM-induced pulmonary fibrosis mice model	AMD3100	Reduced BLM-induced pulmonary inflammation	(Watanabe et al., 2007)
Pulmonary fibrosis	BLM-induced pulmonary fibrosis mice model	AMD3100	Restrained fibrotic lesion, limited fibrocyte migration	(Makino et al., 2013)
COPD	COPD patient-derived fibrocytes	AMD3100	Reduced fibrocyte migration	(Dupin et al., 2016)

Table 5.1 illustrates the role of CXCR4 inhibitors in organ fibrosis, situating our findings within the broader context of CXCR4/CXCL12 research.

This thesis advances the field by providing robust evidence for the comprehensive therapeutic potential of CXCL12 inhibition in asthma. Our findings lay the groundwork for developing more effective, multifaceted treatment strategies for allergic airway diseases and possibly other fibrotic conditions. By situating our results within the broader context of CXCL12/CXCR4 research, we highlight the significant potential of LIT-927 as a groundbreaking therapeutic agent in the fight against asthma and related diseases. This integrated approach to understanding and targeting airway remodeling processes offers a promising path forward in improving the management and outcomes of asthma.

Advantages of My Study and Contribution to the Literature

Table 5.2 situates our findings within the field by providing a clear, direct comparison between LIT-927 and other traditional inhibitors, emphasizing the advantages of LIT-927 in various critical aspects relevant to clinical and therapeutic settings.

Feature	**LIT-927**	**AMD3100 (CXCR4 inhibitor)**
Selectivity	Targets CXCL12 exclusively, preserving CXCR4 signaling and reducing off-target effects (Regenass, 2018)	Non-selective, may disrupt CXCR4 signaling and release CXCL12 from bone marrow (Daubeuf et al., 2013)
Oral Bioavailability	Can be administered orally, offering ease of use and patient convenience (Regenass, 2018)	Often requires intravenous or subcutaneous administration (Daubeuf et al., 2013)
Safety Profile	Shows a promising safety profile with fewer potential off-target effects or immune responses (Regenass, 2018)	May introduce unforeseen off-target effects or trigger immune responses (Daubeuf et al., 2013)
Combination Therapy Potential	Enhances potential for use in combination therapies for lung diseases without increasing toxicity (Regenass, 2018)	Combination may lead to amplified toxicity (Daubeuf et al., 2013)
Stability & Cost-Effectiveness	Offers greater stability and cost-effectiveness compared to monoclonal antibodies (mAbs) or RNA-based therapies (Regenass, 2018)	Less stable and more expensive, particularly mAbs and RNA-based therapies (Daubeuf et al., 2013)

Table 5.2 situates our findings within the field by providing a clear, direct comparison between LIT-927 and other traditional inhibitors,

Advantages of the HDM Model as the Method Chosen in this Thesis

Our study utilized the mouse model of house dust mite-induced chronic allergic asthma (HDM model), which offers several distinct advantages over the commonly used ovalbumin (OVA) model. The HDM model more accurately replicates the complex nature of human asthma triggers. Unlike the OVA model, which relies on a single protein and often requires adjuvants like aluminum hydroxide to provoke significant allergic responses (Aun et al., 2017), the HDM model uses extracts that contain a complex mixture of proteins, lipids, and endotoxins. This complexity closely mirrors the diversity of allergens encountered by humans (Birrell et al., 2010; Rowley et al., 2015).

The HDM model effectively induces hallmark pathological features of asthma, such as goblet cell hyperplasia, airway remodeling, and eosinophilic inflammation, often without the need for adjuvants. Additionally, it allows for chronic exposure studies that more authentically represent the progression and long-term effects of human asthma (Aun et al., 2017; Birrell et al., 2010; Rowley et al., 2015). While the OVA model has significantly advanced our understanding of asthma's molecular and cellular mechanisms, the HDM model offers a nuanced representation of real-world allergen exposures and resultant pathophysiological processes, providing a more comprehensive platform for asthma research.

Advantages and Strengths of Flow Cytometry Methods Used

Our study employed advanced flow cytometry techniques, which provided several advantages for investigating the roles of pericytes and the effects of LIT-927. Flow cytometry allowed for precise quantification and characterization of cell populations, including CXCR4+ pericytes, within complex tissue environments. This method enabled the identification of specific cellular responses to HDM exposure and LIT-927 treatment, offering high-resolution insights into cell behavior and interactions that are crucial for understanding the mechanisms of asthma and vascular remodeling. Furthermore, The Biolegend LegendScreen™ is highly regarded for its comprehensive immune profiling and biomarker discovery capabilities. It includes a vast array of validated antibodies, allowing extensive profiling of various immune cell markers, which ensures reliable and reproducible results. Designed for high-throughput screening, it facilitates the simultaneous analysis of multiple markers, making it suitable for large-scale studies. The kit is user-friendly, with detailed protocols and support provided by Biolegend, and it offers customization options to tailor the screen to specific research needs. Additionally, the LegendScreen™ is cost-effective as it bundles a comprehensive panel of antibodies, reducing overall research costs compared to purchasing individual antibodies separately. It is optimized for flow cytometry, ensuring seamless integration into existing workflows and enhancing data analysis capabilities. Biolegend's commitment to continuous innovation ensures that researchers have access to the latest discoveries and emerging markers, making the LegendScreen™ a valuable resource for advancing research in immunology and related fields.

Advantages of Whole Mount Immunostaining to Study Vascular Remodeling

Our study significantly contributes to the literature on vascular remodeling in asthma, an underexplored but critical area. The use of whole mount immunostaining provided a comprehensive and detailed view of vascular changes, offering a non-invasive alternative to traditional methods. Most current techniques, such as biopsies from post-mortem resections, lung resection studies, fiberoptic bronchoscopy, and high-magnification video bronchoscopy bronchial biopsies, are invasive and not feasible for continuous studies or broader patient groups (Zanini et al., 2010). Additionally, factors like smoking and cardiovascular conditions can complicate interpretations in humans, making standardized evaluation methods challenging (Zanini et al., 2010). Our use of whole mount immunostaining allowed for a detailed analysis of vascular structures and their remodeling in response to chronic allergic inflammation and treatment with LIT-927. This approach provided new insights into the dynamics of vascular remodeling, contributing valuable data to the field, and highlighting the potential of LIT-927 as a therapeutic intervention.

Overall Contributions

In summary, this PhD thesis achieved its aims and made significant contributions to the existing literature. By utilizing the HDM model, advanced flow cytometry, and whole mount immunostaining, our study provided a comprehensive analysis of the mechanisms underlying chronic allergic airway disease and vascular remodeling. Our findings align with the hypothesis that HDM exposure induces structural changes in the lung via increased CXCL12 levels, leading to airway smooth muscle thickening and vascular remodeling driven by pericyte migration. Treatment with LIT-927 effectively mitigated these effects, offering a promising therapeutic strategy. This research fills a significant knowledge gap and lays the groundwork for future studies, particularly those exploring the long-term impact of LIT-927 and its combination with existing asthma therapies. By advancing our understanding of the CXCL12/CXCR4 axis and its role in asthma and vascular remodeling, this thesis provides a foundation for developing more effective treatments for chronic allergic airway diseases.

5.3 Limitations and Disruptions

Single Concentration and Duration of LIT-927 Treatment

Our study focused on investigating the effects of LIT-927 treatment at a specific concentration and duration. While the results provide valuable insights, it's important to acknowledge that broader and more extensive dose- and time-response experiments are warranted. Such experiments would enable a more comprehensive exploration of the potential therapeutic benefits of CXCL12 neutralization in the context of allergic asthma. Different concentrations and treatment durations may reveal dose-dependent or time-dependent responses that could be crucial for optimizing treatment strategies.

Limited Assessment of Lung Function

In this study, we did not employ invasive measures of lung function to fully evaluate the impact of LIT-927 treatment. Lung function assessments, such as pulmonary function tests or plethysmography, can provide critical data on airway responsiveness, resistance, and compliance. Incorporating these measures would have allowed for a more thorough understanding of how LIT-927 treatment influences lung function in the context of allergic asthma. Future studies with comprehensive lung function assessments could provide a more holistic view of treatment effects.

Impact on Inflammatory Cell Influx

Although our study examined several aspects of the immune response in the context of LIT-927 treatment, we did not specifically evaluate its impact on the influx of CXCR4+ inflammatory cells, particularly monocyte-derived macrophages. This is an important consideration since these cells play a significant role in the inflammatory processes associated with allergic asthma. While preliminary assessments indicated minimal effects on cell egress from circulation, a more detailed investigation of the specific effects of LIT-927 on the recruitment and activation of these cells in lung tissues would enhance our understanding of the treatment's mechanisms.

Limited Effects Beyond Large Airways

Our findings suggest that intranasally delivered LIT-927 has relatively minor effects beyond the large airways. While this information provides valuable insights into the localized impact of the treatment, it also highlights the need for further research to explore potential systemic effects or impacts on other regions of the respiratory system. A more comprehensive assessment of LIT-927's effects throughout the entire respiratory tract could provide a more nuanced understanding of its therapeutic potential.

It is notable that this thesis was also impacted by significant disruptions.

such as:

Disruptions Due to the SARS-CoV-2 Pandemic: The study faced significant disruptions caused by the SARS-CoV-2 pandemic, including lockdowns and restrictions. The closure of Aston University and personal health concerns delayed laboratory work and data analysis. Cell culture experiments, which required weeks to initiate, were particularly affected. Social distancing measures further limited laboratory access and reduced research time. International travel restrictions also prevented important training for lung function measurements.

Brexit-Related Delays: Brexit had a notable impact on the study, especially regarding the shipping of cells and reagents. Previously fast deliveries took weeks to months, affecting experiment timelines and cell culture. Problems with customs clearance resulted in non-viable materials, causing additional delays and disruptions.

Technical Limitations: Technical constraints also influenced the research. Access to a high-resolution confocal microscope was limited due to a lack of required training. The available confocal microscope produced low-resolution images and couldn't image DAPI, impacting sample analysis. The unavailability of a live cell imaging system and issues with the CytoFlex flow cytometer further hindered experiments, as the flow cytometer was frequently out of service or provided inaccurate results.

5.4 Future

To extend the current findings and build a robust body of research around the therapeutic impacts of LIT-927 and the CXCL12/CXCR4 axis, several experimental directions and research themes could be pursued in detail.

Expansion in the Inflammatory State Due to Soluble Factors and the Impact of LIT-927

The primary objective here is to determine whether the expansion in the inflammatory state is due to soluble factors and to elucidate the roles and impacts of these factors. Additionally, assessing the therapeutic potential of LIT-927 in modulating these soluble factors and mitigating inflammation is crucial. Identifying and understanding the soluble factors involved in the inflammatory state will provide insights into the mechanisms driving inflammation and vascular changes. Assessing the impact of LIT-927 on these factors could lead to targeted therapeutic interventions that reduce inflammation and improve vascular integrity in diseases such as allergic asthma.

The study will start with sample collection and preparation. Using HDM-induced asthma models in mice, bronchoalveolar lavage fluid (BALF), blood serum, and tissue samples will be collected from control, HDM-exposed, and LIT-927 treated animals. For human samples, airway lavage fluids, blood samples, and biopsies will be obtained from patients with allergic asthma, healthy controls, and patients treated with LIT-927.

Following sample collection, proteomics analysis will be performed using mass spectrometry-based proteomics on BALF and serum samples to identify differentially expressed proteins and soluble factors. Label-free quantification or isotopic labeling methods will be used for comparative analysis. Additionally, cytokine and chemokine profiling will be conducted utilizing multiplex immunoassays (e.g., Luminex, ELISA) to quantify levels of key cytokines and chemokines (e.g., TNF-α, IL-1β, IL-6, CXCL12) in the collected samples. Metabolomics studies will also be conducted to identify metabolic changes and soluble metabolites associated with the inflammatory state using techniques such as GC-MS or LC-MS.

Imaging and localization studies will be conducted next. RNA in situ hybridization will be used to localize mRNA expression of key soluble factors in tissue sections to identify the cellular sources of these factors. Immunohistochemical staining on tissue sections will help visualize and quantify the protein expression of identified soluble factors using specific antibodies to detect cytokines, chemokines, and other inflammatory mediators. Fluorescence microscopy will be employed to image the distribution and localization of labeled soluble factors in tissues and cell cultures using fluorescently labeled antibodies or probes. Functional studies will involve culturing pericytes, endothelial cells, and immune cells (e.g., monocytes, macrophages) and treating them with identified soluble factors at various concentrations. Changes in cell behavior, including migration, proliferation, and activation, will be assessed using functional assays (e.g., scratch assay, Transwell migration, proliferation assays).

The impact of LIT-927 on cell behavior will be assessed by treating cells with LIT-927 in the presence of these soluble factors and comparing the results with untreated controls and those treated with other inhibitors. Neutralization experiments will use neutralizing antibodies or small molecule inhibitors, including LIT-927, to block the activity of specific soluble factors in cell cultures and animal models, evaluating the impact on inflammation and vascular integrity. Signal pathway analysis will investigate the signaling pathways activated by soluble factors in pericytes and endothelial cells using Western blotting, qPCR, and immunofluorescence, identifying key mediators and downstream effectors involved in the inflammatory response and the modulation by LIT-927.

In vivo validation will involve assessing the effects of neutralizing specific soluble factors or modulating their levels using genetic approaches (e.g., knockout models, siRNA) or pharmacological agents, including LIT-927, in HDM-induced asthma models. Clinical outcomes, including airway hyperresponsiveness, inflammation, and vascular integrity, will be assessed. Therapeutic interventions will evaluate the potential of LIT-927 in reducing inflammation and improving vascular health in animal models and potentially in clinical trials, comparing its efficacy with other therapeutic agents targeting the same or different pathways. Comprehensive statistical analysis will compare levels of soluble factors between control, HDM-exposed, and LIT-927 treated groups, using appropriate statistical tests to determine significance. Bioinformatics tools will be applied to integrate proteomics, metabolomics, and imaging data, identifying pathways and networks involved in the inflammatory response and the therapeutic effects of LIT-927.

The expected outcomes include the identification of key soluble factors contributing to the inflammatory state in allergic asthma, mechanistic insights into how these factors drive inflammation, pericyte behavior, and vascular changes, and the identification of potential therapeutic targets for intervention. The study will also assess the efficacy of LIT-927 in modulating these targets to reduce inflammation and improve vascular integrity.

Role of Pericytes in Vascular Integrity

Investigating the specific functions of pericytes in maintaining vascular integrity under normal and inflammatory conditions is another critical area of study. Clarifying the role of pericytes in vascular health and disease could lead to new strategies for preventing or reversing the vascular damage seen in allergic asthma and other inflammatory conditions.

In vitro studies will involve culturing human pericytes and endothelial cells together to form a co-culture system, assessing the integrity of the endothelial monolayer by measuring trans-endothelial electrical resistance (TEER) and permeability assays using FITC-dextran. In vivo studies will use animal models of allergic asthma, such as HDM-induced asthma in mice, to evaluate vascular integrity by examining the leakage of Evans blue dye and performing histological analysis of blood vessel structure. Markers of interest will include measuring expression levels of tight junction proteins (e.g., ZO-1, occludin) and extracellular matrix components (e.g., collagen, fibronectin) using immunofluorescence and Western blotting. The effects of LIT-927 on vascular

integrity under both normal and inflammatory conditions will be assessed by comparing treated and untreated groups.

Influence of Inflammatory Mediators on Pericyte Function

Exploring how inflammatory mediators influence pericyte behavior, particularly their migration and transition into myofibroblasts during fibrosis, is essential for understanding these dynamics and providing insights into how inflammatory responses contribute to fibrotic remodeling. This may identify new therapeutic targets within these pathways. The study design involves treating pericytes with various pro-inflammatory and pro-fibrotic cytokines (e.g., TNF-α, TGF-β, IL-1β) and analyzing changes in cell behavior. Migration assays, such as scratch assays and Transwell migration assays, will quantify pericyte migration in response to cytokine treatment. The transition of pericytes into myofibroblasts will be assessed by measuring markers such as α-SMA and collagen I am using immunofluorescence and qPCR. Signal pathway analysis will use pharmacological inhibitors and siRNA to dissect the signaling pathways (e.g., MAPK, PI3K/AKT) involved in cytokine-induced pericyte behavior.

CXCL12 Signaling in Pericyte Dynamics and Monocyte Transmigration

Examining the role of CXCL12 signaling in pericyte-mediated control of monocyte transmigration during inflammatory responses could uncover new mechanisms by which CXCL12 influences immune cell behavior and tissue remodeling in fibrotic diseases. The study design includes using Transwell systems to study monocyte transmigration across endothelial-pericyte co-cultures in the presence of CXCL12, measuring the effect of LIT-927 and other inhibitors on this process. Live-cell imaging will observe real-time interactions between pericytes, endothelial cells, and monocytes during transmigration. Molecular analysis will involve analyzing changes in expression of adhesion molecules (e.g., ICAM-1, VCAM-1) and chemokine receptors (e.g., CXCR4) on monocytes and pericytes using flow cytometry and immunofluorescence. Pathway inhibition will investigate the involvement of specific signaling pathways in CXCL12-induced transmigration using pathway-specific inhibitors and genetic knockdown approaches.

Dosage and Concentration Optimization

Determining the optimal concentrations and dosing schedules for CXCL12/CXCR4 antagonists, such as LIT-927, in the treatment of various fibrotic diseases is crucial for maximizing therapeutic efficacy while minimizing side effects. Precise dosage optimization will ensure effective inhibition of CXCL12/CXCR4 signaling without adverse effects, enhancing patient outcomes. The study design involves in vitro dosage optimization using relevant cell lines (e.g., fibroblasts, pericytes) and primary cells from fibrotic tissues. Dose-response curves will be generated by treating cells with varying concentrations of LIT-927 and other CXCL12/CXCR4 antagonists to determine the IC50 (half-maximal inhibitory concentration) for each compound. Cell viability assays will assess cell viability at each concentration using assays such as MTT, WST-1, or trypan blue exclusion to ensure that therapeutic doses are non-cytotoxic. Functional assays using 3D spheroids ex vivo will evaluate the effects of different concentrations on cell migration, proliferation, and collagen production.

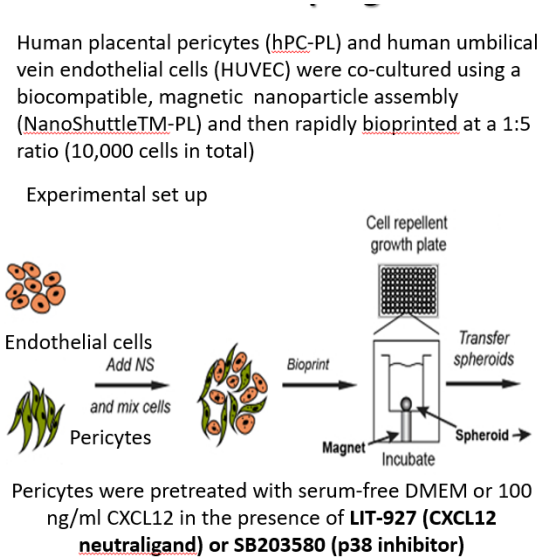

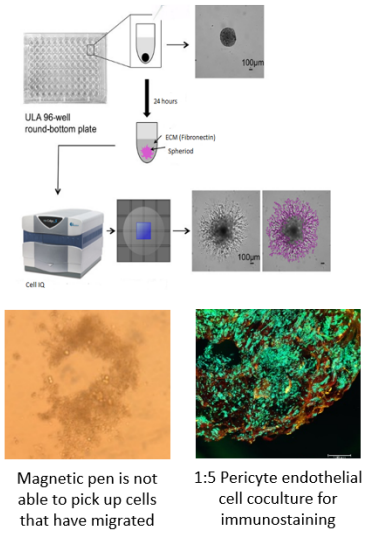

Magnetic pen is not able to pick up cells that have migrated

1:5 Pericyte endothelial cell coculture for immunostaining

Figure 5.1: Protocol for 3D models of pericytes and endothelial via NanoShuttle TM-PL system (bio-printing of spheroids) to enable a large-scale therapeutic testing on the impact of LIT-297 in vitro via the NanoShuttle TM-PL system (bio-printing of spheroids)

In vivo dosage optimization will use mouse models. The therapeutic efficacy will be assessed at different doses by evaluating fibrosis markers (e.g., collagen deposition via Masson's trichrome staining, hydroxyproline content) and functional outcomes (e.g., lung function tests) Pharmacokinetics (PK) and pharmacodynamics (PD) studies will be performed to understand the absorption, distribution, metabolism, and excretion of LIT-927, correlating these parameters with therapeutic efficacy to identify optimal dosing regimens. Furthermore, Clinical trials will start with Phase I trials to conduct initial dose-finding studies in healthy volunteers to assess safety, tolerability, and pharmacokinetics. Phase II trials will evaluate the efficacy and safety of optimized doses in patients with fibrotic diseases, utilizing biomarkers and imaging techniques (e.g., MRI, CT) to monitor fibrosis progression and response to treatment. Phase III trials will confirm the therapeutic benefits and safety profile of the optimized dosing regimen in a larger patient population.

Molecular Mechanisms of CXCL12/CXCR4

Conducting detailed studies to unravel the molecular pathways and interactions involved in the CXCL12/CXCR4 signaling axis will enable the development of more targeted therapies and may reveal additional therapeutic targets within these pathways. This could lead to more effective interventions for fibrotic diseases and other conditions where CXCL12/CXCR4 signaling plays a crucial role.

The study design includes signaling pathway analysis using mass spectrometry-based proteomics and phosphoproteomics to identify proteins and phosphorylation events regulated by CXCL12/CXCR4 signaling. Western blotting and immunoprecipitation will validate key signaling molecules identified from proteomics studies, and co-immunoprecipitation will study protein-protein interactions within the signaling pathway. Gene expression profiling will conduct RNA-sequencing (RNA-seq) to analyze global gene expression changes in response to CXCL12 stimulation and LIT-927 treatment, identifying key transcriptional regulators and downstream target genes.

Functional assays will involve using luciferase reporter constructs to study the activation of specific transcription factors (e.g., NF-κB, STAT3) in response to CXCL12/CXCR4 signaling. Knockdown/knockout studies will utilize siRNA, shRNA, or CRISPR/Cas9 technologies to knockdown or knockout key signaling molecules in vitro and in vivo, assessing the impact on fibrosis-related processes such as cell migration, proliferation, and extracellular matrix production. Chemical inhibitors will be applied to

dissect the roles of different signaling pathways (e.g., ERK, PI3K/AKT, JAK/STAT) in CXCL12/CXCR4-mediated effects.

Advanced imaging and single-cell analysis will use live-cell imaging techniques to visualize real-time dynamics of CXCL12/CXCR4 signaling in single cells, employing fluorescent biosensors to monitor signaling events such as calcium flux and second messenger production. Single-cell RNA-sequencing will analyze the heterogeneity of CXCL12/CXCR4 signaling across different cell populations within fibrotic tissues, identifying cell type-specific responses and interactions.

Animal models and translational studies will develop transgenic and knockout mouse models to study the in vivo roles of CXCL12/CXCR4 signaling components in fibrosis, analyzing tissue samples using histology, immunohistochemistry, and molecular techniques. Human tissue samples will validate key findings from animal models in human tissue samples obtained from patients with fibrotic diseases, using techniques such as immunohistochemistry, in situ hybridization, and laser capture microdissection to analyze CXCL12/CXCR4 signaling at the tissue and cellular levels.

Expected Outcomes

Through these comprehensive studies, the expected outcomes include the identification of key soluble factors contributing to the inflammatory state in allergic asthma, mechanistic insights into how these factors drive inflammation, pericyte behavior, and vascular changes, and the identification of potential therapeutic targets for intervention. The study will also determine the optimal concentrations and dosing schedules for LIT-927 and other CXCL12/CXCR4 antagonists, enhancing their therapeutic efficacy and safety profiles. Detailed understanding of the molecular mechanisms and pathways involved in CXCL12/CXCR4 signaling will provide a foundation for the development of more targeted and effective therapies. Additionally, new therapeutic targets within the CXCL12/CXCR4 signaling axis and related pathways will be identified, paving the way for novel treatment strategies for fibrotic diseases and other inflammatory conditions.

In conclusion, pursuing these comprehensive studies in , we aim to advance the therapeutic potential of LIT-927 and deepen our understanding of the CXCL12/CXCR4 axis, ultimately improving treatment outcomes for patients with fibrotic and inflammatory diseases.

Bibliography

Ahirwar, D. K., Nasser, M. W., Ouseph, M. M., Elbaz, M., Cuitiño, M. C., Kladney, R. D., Varikuti, S., Kaul, K., Satoskar, A. R., Ramaswamy, B., Zhang, X., Ostrowski, M. C., Leone, G., & Ganju, R. K. (2018). Fibroblast-Derived CXCL12 Promotes Breast Cancer Metastasis by Facilitating Tumor Cell Intravasation. *Oncogene*, *37*(32), 4428–4442. https://doi.org/10.1038/s41388-018-0263-7

Aliverti, A. (2016). The respiratory muscles during exercise. *Breathe*, *12*(2), 165–168. https://doi.org/10.1183/20734735.008116

Anastasiadou, D. P., Quesnel, A., Duran, C. L., Filippou, P. S., & Karagiannis, G. S. (2024). An emerging paradigm of CXCL12 involvement in the metastatic cascade. *Cytokine & Growth Factor Reviews*, *75*, 12–30. https://doi.org/10.1016/j.cytogfr.2023.10.003

Antar, S. A., Ashour, N. A., Marawan, M. E., & Al-Karmalawy, A. A. (2023). Fibrosis: Types, Effects, Markers, Mechanisms for Disease Progression, and Its Relation with Oxidative Stress, Immunity, and Inflammation. *International Journal of Molecular Sciences*, *24*(4), Article 4. https://doi.org/10.3390/ijms24044004

Arboleda-Velasquez, J. F., Primo, V., Graham, M., James, A., Manent, J., & D'Amore, P. A. (2014). Notch Signaling Functions in Retinal Pericyte Survival. *Investigative Ophthalmology & Visual Science*, *55*(8), 5191–5199. https://doi.org/10.1167/iovs.14-14046

Armani-Tourret, M., Zhou, Z., Gasser, R., Staropoli, I., Cantaloube-Ferrieu, V., Benureau, Y., Garcia-Perez, J., Pérez-Olmeda, M., Lorin, V., Puissant-Lubrano, B., Assoumou, L., Delaugerre, C., Lelièvre, J.-D., Lévy, Y., Mouquet, H., Martin-Blondel, G., Alcami, J.,

Arenzana-Seisdedos, F., Izopet, J., … Lagane, B. (2021). Mechanisms of HIV-1 evasion to the antiviral activity of chemokine CXCL12 indicate potential links with pathogenesis. *PLoS Pathogens*, *17*(4), e1009526. https://doi.org/10.1371/journal.ppat.1009526

Armulik, A., Genové, G., & Betsholtz, C. (2011). Pericytes: Developmental, physiological, and pathological perspectives, problems, and promises. *Developmental Cell*, *21*(2), 193–215. https://doi.org/10.1016/j.devcel.2011.07.001

Aun, M. V., Bonamichi-Santos, R., Arantes-Costa, F. M., Kalil, J., & Giavina-Bianchi, P. (2017). Animal models of asthma: Utility and limitations. *Journal of Asthma and Allergy*, *10*, 293–301. https://doi.org/10.2147/JAA.S121092

Bailey, S., Boustany, S., Burgess, J., Hirst, S., Sharma, H., Simcock, D., Suravaram, P., & Weckmann, M. (2009). Airway vascular reactivity and vascularisation in human chronic airway disease. *Pulmonary Pharmacology & Therapeutics*, *22*, 417–425. https://doi.org/10.1016/j.pupt.2009.04.007

Baluk, P., & McDonald, D. M. (2022). Imaging Blood Vessels and Lymphatics in Mouse Trachea Wholemounts. *Methods in Molecular Biology (Clifton, N.J.)*, *2441*, 115–134. https://doi.org/10.1007/978-1-0716-2059-5_10

Baos, S., Calzada, D., Cremades-Jimeno, L., Sastre, J., Picado, C., Quiralte, J., Florido, F., Lahoz, C., & Cárdaba, B. (2018). Nonallergic Asthma and Its Severity: Biomarkers for Its Discrimination in Peripheral Samples. *Frontiers in Immunology*, *9*, 1416. https://doi.org/10.3389/fimmu.2018.01416

Bårnes, C. B., & Ulrik, C. S. (2015). Asthma and Adherence to Inhaled Corticosteroids: Current Status and Future Perspectives. *Respiratory Care*, *60*(3), 455–468. https://doi.org/10.4187/respcare.03200

Baxi, S. N., & Phipatanakul, W. (2010). The Role of Allergen Exposure and Avoidance in Asthma. *Adolescent Medicine: State of the Art Reviews*, *21*(1), 57–ix.

Bergeron, C., Tulic, M. K., & Hamid, Q. (2010). Airway remodelling in asthma: From benchside to clinical practice. *Canadian Respiratory Journal : Journal of the Canadian Thoracic Society*, *17*(4), e85–e93.

Bergers, G., & Song, S. (2005). The role of pericytes in blood-vessel formation and maintenance. *Neuro-Oncology*, *7*(4), 452–464. https://doi.org/10.1215/S1152851705000232

Bignold, R., Shammout, B., Rowley, J. E., Repici, M., Simms, J., & Johnson, J. R. (2022). Chemokine CXCL12 drives pericyte accumulation and airway remodeling in allergic airway disease. *Respiratory Research*, *23*, 183. https://doi.org/10.1186/s12931-022-02108-4

Birrell, M. A., Oosterhout, A. J. M. V., & Belvisi, M. G. (2010). Do the current house dust mite-driven models really mimic allergic asthma? *European Respiratory Journal*, *36*(5), 1220–1221. https://doi.org/10.1183/09031936.00069110

Bordenave, J., Thuillet, R., Tu, L., Phan, C., Cumont, A., Marsol, C., Huertas, A., Savale, L., Hibert, M., Galzi, J.-L., Bonnet, D., Humbert, M., Frossard, N., & Guignabert, C. (2020). Neutralization of CXCL12 attenuates established pulmonary hypertension in rats. *Cardiovascular Research*, *116*(3), 686–697. https://doi.org/10.1093/cvr/cvz153

Bousquet, J., Rabe, K., Humbert, M., Chung, K. F., Berger, W., Fox, H., Ayre, G., Chen, H., Thomas, K., Blogg, M., & Holgate, S. (2007). Predicting and evaluating response to omalizumab in patients with severe allergic asthma. *Respiratory Medicine*, *101*(7), 1483–1492. https://doi.org/10.1016/j.rmed.2007.01.011

Boyman, O., Kaegi, C., Akdis, M., Bavbek, S., Bossios, A., Chatzipetrou, A., Eiwegger, T., Firinu, D., Harr, T., Knol, E., Matucci, A., Palomares, O., Schmidt-Weber, C., Simon, H.-U., Steiner, U. C., Vultaggio, A., Akdis, C. A., & Spertini, F. (2015). EAACI IG Biologicals task force paper on the use of biologic agents in allergic disorders. *Allergy*, *70*(7), 727–754. https://doi.org/10.1111/all.12616

Brown, L. S., Foster, C. G., Courtney, J.-M., King, N. E., Howells, D. W., & Sutherland, B. A. (2019). Pericytes and Neurovascular Function in the Healthy and Diseased Brain. *Frontiers in Cellular Neuroscience*, *13*. https://doi.org/10.3389/fncel.2019.00282

Bülow, R. D., & Boor, P. (2019). Extracellular Matrix in Kidney Fibrosis: More Than Just a Scaffold. *Journal of Histochemistry and Cytochemistry*, *67*(9), 643–661. https://doi.org/10.1369/0022155419849388

Bush, A. (2019). Pathophysiological Mechanisms of Asthma. *Frontiers in Pediatrics*, *7*. https://www.frontiersin.org/articles/10.3389/fped.2019.00068

Busillo, J. M., & Benovic, J. L. (2007). Regulation of CXCR4 Signaling. *Biochimica et Biophysica Acta*, *1768*(4), 952–963. https://doi.org/10.1016/j.bbamem.2006.11.002

Cabral-Pacheco, G. A., Garza-Veloz, I., Castruita-De la Rosa, C., Ramirez-Acuña, J. M., Perez-Romero, B. A., Guerrero-Rodriguez, J. F., Martinez-Avila, N., & Martinez-Fierro, M. L. (2020). The Roles of Matrix Metalloproteinases and Their Inhibitors in Human Diseases. *International Journal of Molecular Sciences*, *21*(24), 9739. https://doi.org/10.3390/ijms21249739

Cao, L., Zhou, Y., Chen, M., Li, L., & Zhang, W. (2021). Pericytes for Therapeutic Approaches to Ischemic Stroke. *Frontiers in Neuroscience*, *15*. https://doi.org/10.3389/fnins.2021.629297

Caporarello, N., D'Angeli, F., Cambria, M. T., Candido, S., Giallongo, C., Salmeri, M., Lombardo, C., Longo, A., Giurdanella, G., Anfuso, C. D., & Lupo, G. (2019). Pericytes in Microvessels: From "Mural" Function to Brain and Retina Regeneration. *International Journal of Molecular Sciences*, *20*(24), 6351. https://doi.org/10.3390/ijms20246351

Cappella, A., & Durham, S. R. (2012). Allergen immunotherapy for allergic respiratory diseases. *Human Vaccines & Immunotherapeutics*, *8*(10), 1499–1512. https://doi.org/10.4161/hv.21629

Capuano, F., Loke, Y.-H., & Balaras, E. (2019). Blood Flow Dynamics at the Pulmonary Artery Bifurcation. *Fluids*, *4*(4), Article 4. https://doi.org/10.3390/fluids4040190

Carlsson, R., Enström, A., & Paul, G. (2023). Molecular Regulation of the Response of Brain Pericytes to Hypoxia. *International Journal of Molecular Sciences*, *24*(6). https://doi.org/10.3390/ijms24065671

Chang, C.-W., Seibel, A. J., Avendano, A., Cortes-Medina, M., & Song, J. W. (2020). Distinguishing Specific CXCL12 Isoforms on Their Angiogenesis and Vascular Permeability Promoting Properties. *Advanced Healthcare Materials*, *9*(4), e1901399. https://doi.org/10.1002/adhm.201901399

Chen, H., Xu, X., Teng, J., Cheng, S., Bunjhoo, H., Cao, Y., Liu, J., Xie, J., Wang, C., Xu, Y., & Xiong, W. (2015). CXCR4 inhibitor attenuates allergen-induced lung inflammation by down-regulating MMP-9 and ERK1/2. *International Journal of Clinical and Experimental Pathology*, *8*(6), 6700–6707.

Chiaverina, G., di Blasio, L., Monica, V., Accardo, M., Palmiero, M., Peracino, B., Vara-Messler, M., Puliafito, A., & Primo, L. (2019). Dynamic Interplay between Pericytes and Endothelial Cells during Sprouting Angiogenesis. *Cells*, *8*(9), 1109. https://doi.org/10.3390/cells8091109

Chu, H. W., Kraft, M., Rex, M. D., & Martin, R. J. (2001). Evaluation of Blood Vessels and Edema in the Airways of Asthma Patients: Regulation With Clarithromycin Treatment. *CHEST*, *120*(2), 416–422. https://doi.org/10.1378/chest.120.2.416

Chute, M., Aujla, P., Jana, S., & Kassiri, Z. (2019). The Non-Fibrillar Side of Fibrosis: Contribution of the Basement Membrane, Proteoglycans, and Glycoproteins to Myocardial Fibrosis. *Journal of Cardiovascular Development and Disease*, *6*(4), 35. https://doi.org/10.3390/jcdd6040035

Claesson-Welsh, L., Dejana, E., & McDonald, D. M. (2021). Permeability of the Endothelial Barrier: Identifying and Reconciling Controversies. *Trends in Molecular Medicine*, *27*(4), 314–331. https://doi.org/10.1016/j.molmed.2020.11.006

Colas, L., Hassoun, D., & Magnan, A. (2020). Needs for Systems Approaches to Better Treat Individuals With Severe Asthma: Predicting Phenotypes and Responses to Treatments. *Frontiers in Medicine*, *7*, 98. https://doi.org/10.3389/fmed.2020.00098

Daneman, R., & Prat, A. (2015). The Blood–Brain Barrier. *Cold Spring Harbor Perspectives in Biology*, *7*(1), a020412. https://doi.org/10.1101/cshperspect.a020412

Darby, I. A., Laverdet, B., Bonté, F., & Desmoulière, A. (2014). Fibroblasts and myofibroblasts in wound healing. *Clinical, Cosmetic and Investigational Dermatology*, *7*, 301–311. https://doi.org/10.2147/CCID.S50046

Daubeuf, F., Hachet-Haas, M., Gizzi, P., Gasparik, V., Bonnet, D., Utard, V., Hibert, M., Frossard, N., & Galzi, J.-L. (2013). An Antedrug of the CXCL12 Neutraligand Blocks Experimental Allergic Asthma without Systemic Effect in Mice *. *Journal of Biological Chemistry*, *288*(17), 11865–11876. https://doi.org/10.1074/jbc.M112.449348

De Clercq, E. (2009). Anti-HIV drugs: 25 compounds approved within 25 years after the discovery of HIV. *International Journal of Antimicrobial Agents*, *33*(4), 307–320. https://doi.org/10.1016/j.ijantimicag.2008.10.010

de Souza, L. E. B., Malta, T. M., Kashima Haddad, S., & Covas, D. T. (2016). Mesenchymal Stem Cells and Pericytes: To What Extent Are They Related? *Stem Cells and Development*, *25*(24), 1843–1852. https://doi.org/10.1089/scd.2016.0109

De Troyer, A., & Boriek, A. M. (2011). Mechanics of the respiratory muscles. *Comprehensive Physiology*, *1*(3), 1273–1300. https://doi.org/10.1002/cphy.c100009

Delgado-Martín, C., Escribano, C., Pablos, J. L., Riol-Blanco, L., & Rodríguez-Fernández, J. L. (2011). Chemokine CXCL12 Uses CXCR4 and a Signaling Core Formed by Bifunctional Akt, Extracellular Signal-regulated Kinase (ERK)1/2, and Mammalian Target of

Rapamycin Complex 1 (mTORC1) Proteins to Control Chemotaxis and Survival Simultaneously in Mature Dendritic Cells. *The Journal of Biological Chemistry*, *286*(43), 37222–37236. https://doi.org/10.1074/jbc.M111.294116

Dellavalle, A. (2007). Pericytes of human skeletal muscle are myogenic precursors distinct from satellite cells. *Nat Cell Biol*, *9*. https://doi.org/10.1038/ncb1542

Dharmage, S. C., Perret, J. L., & Custovic, A. (2019). Epidemiology of Asthma in Children and Adults. *Frontiers in Pediatrics*, *7*, 246. https://doi.org/10.3389/fped.2019.00246

Doeing, D. C., & Solway, J. (2013). Airway smooth muscle in the pathophysiology and treatment of asthma. *Journal of Applied Physiology*, *114*(7), 834–843. https://doi.org/10.1152/japplphysiol.00950.2012

Dominici, M. (2006). Minimal criteria for defining multipotent mesenchymal stromal cells. The International Society for Cellular Therapy position statement. *Cytotherapy*, *8*. https://doi.org/10.1080/14653240600855905

Du, W., Zhou, L., Ni, Y., Yu, Y., Wu, F., & Shi, G. (2017). Inhaled corticosteroids improve lung function, airway hyper-responsiveness and airway inflammation but not symptom control in patients with mild intermittent asthma: A meta-analysis. *Experimental and Therapeutic Medicine*, *14*(2), 1594–1608. https://doi.org/10.3892/etm.2017.4694

Duong, T. E., & Hagood, J. S. (2018). Epigenetic Regulation of Myofibroblast Phenotypes in Fibrosis. *Current Pathobiology Reports*, *6*(1), 79. https://doi.org/10.1007/s40139-018-0155-0

Dupin, I., Allard, B., Ozier, A., Maurat, E., Ousova, O., Delbrel, E., Trian, T., Bui, H.-N., Dromer, C., Guisset, O., Blanchard, E., Hilbert, G., Vargas, F., Thumerel, M., Marthan, R., Girodet, P.-O., & Berger, P. (2016). Blood fibrocytes are recruited during acute exacerbations of chronic obstructive pulmonary disease through a CXCR4-dependent pathway. *The Journal of Allergy and Clinical Immunology*, *137*(4), 1036-1042.e7. https://doi.org/10.1016/j.jaci.2015.08.043

Eklund, L., Kangas, J., & Saharinen, P. (2017). Angiopoietin–Tie signalling in the cardiovascular and lymphatic systems. *Clinical Science (London, England : 1979)*, *131*(1), 87–103. https://doi.org/10.1042/CS20160129

Eldridge, L., & Wagner, E. M. (2019). Angiogenesis in the lung. *The Journal of Physiology*, *597*(4), 1023–1032. https://doi.org/10.1113/JP275860

Fahy, J. V. (2015). Type 2 inflammation in asthma—Present in most, absent in many. *Nature Reviews. Immunology*, *15*(1), 57–65. https://doi.org/10.1038/nri3786

Ferland-McCollough, D., Slater, S., Richard, J., Reni, C., & Mangialardi, G. (2017). Pericytes, an overlooked player in vascular pathobiology. *Pharmacology & Therapeutics*, *171*, 30–42. https://doi.org/10.1016/j.pharmthera.2016.11.008

Figueiredo, A. M., Villacampa, P., Diéguez-Hurtado, R., José Lozano, J., Kobialka, P., Cortazar, A. R., Martinez-Romero, A., Angulo-Urarte, A., Franco, C. A., Claret, M., Aransay, A. M., Adams, R. H., Carracedo, A., & Graupera, M. (2020). Phosphoinositide 3-Kinase–Regulated Pericyte Maturation Governs Vascular Remodeling. *Circulation*, *142*(7), 688–704. https://doi.org/10.1161/CIRCULATIONAHA.119.042354

Foong, R.-X., du Toit, G., & Fox, A. T. (2017). Asthma, Food Allergy, and How They Relate to Each Other. *Frontiers in Pediatrics*, *5*, 89. https://doi.org/10.3389/fped.2017.00089

Forno, E., & Celedón, J. C. (2009). Asthma and Ethnic Minorities: Socioeconomic Status and Beyond. *Current Opinion in Allergy and Clinical Immunology*, *9*(2), 154–160.

Fu, J., Liang, H., Yuan, P., Wei, Z., & Zhong, P. (2023). Brain pericyte biology: From physiopathological mechanisms to potential therapeutic applications in ischemic stroke. *Frontiers in Cellular Neuroscience*, *17*, 1267785. https://doi.org/10.3389/fncel.2023.1267785

Gaengel, K., Genové, G., Armulik, A., & Betsholtz, C. (2009). Endothelial-Mural Cell Signaling in Vascular Development and Angiogenesis. *Arteriosclerosis, Thrombosis, and Vascular Biology*, *29*(5), 630–638. https://doi.org/10.1161/ATVBAHA.107.161521

García-Cuesta, E. M., Santiago, C. A., Vallejo-Díaz, J., Juarranz, Y., Rodríguez-Frade, J. M., & Mellado, M. (2019). The Role of the CXCL12/CXCR4/ACKR3 Axis in Autoimmune Diseases. *Frontiers in Endocrinology*, *10*. https://doi.org/10.3389/fendo.2019.00585

Gardiner, T. A., Gibson, D. S., De Gooyer, T. E., De La Cruz, V. F., McDonald, D. M., & Stitt, A. W. (2005). Inhibition of Tumor Necrosis Factor-α Improves Physiological Angiogenesis and Reduces Pathological Neovascularization in Ischemic Retinopathy. *The American Journal of Pathology*, *166*(2), 637–644. https://doi.org/10.1016/S0002-9440(10)62284-5

Garrison, A. T., Bignold, R. E., Wu, X., & Johnson, J. R. (2023). Pericytes: The lung-forgotten cell type. *Frontiers in Physiology*, *14*. https://www.frontiersin.org/articles/10.3389/fphys.2023.1150028

Gencer, S., Evans, B. R., van der Vorst, E. P. C., Döring, Y., & Weber, C. (2021). Inflammatory Chemokines in Atherosclerosis. *Cells*, *10*(2), 226. https://doi.org/10.3390/cells10020226

Gevaert, P., Wong, K., Millette, L. A., & Carr, T. F. (2022). The Role of IgE in Upper and Lower Airway Disease: More Than Just Allergy! *Clinical Reviews in Allergy & Immunology*, *62*(1), 200–215. https://doi.org/10.1007/s12016-021-08901-1

Gifre-Renom, L., & Jones, E. A. V. (2021). Vessel Enlargement in Development and Pathophysiology. *Frontiers in Physiology*, *12*, 639645. https://doi.org/10.3389/fphys.2021.639645

Gil, E., Venturini, C., Stirling, D., Turner, C., Tezera, L. B., Ercoli, G., Baker, T., Best, K., Brown, J. S., & Noursadeghi, M. (2022). Pericyte derived chemokines amplify neutrophil recruitment across the cerebrovascular endothelial barrier. *Frontiers in Immunology*, *13*, 935798. https://doi.org/10.3389/fimmu.2022.935798

Gillich, A., Zhang, F., Farmer, C. G., Travaglini, K. J., Tan, S. Y., Gu, M., Zhou, B., Feinstein, J. A., Krasnow, M. A., & Metzger, R. J. (2020). Capillary cell-type specialization in the alveolus. *Nature*, *586*(7831), 785–789. https://doi.org/10.1038/s41586-020-2822-7

Gonzalez-Uribe, V., Romero-Tapia, S. J., & Castro-Rodriguez, J. A. (2023). Asthma Phenotypes in the Era of Personalized Medicine. *Journal of Clinical Medicine*, *12*(19), 6207. https://doi.org/10.3390/jcm12196207

Gordon, E., Schimmel, L., & Frye, M. (2020). The Importance of Mechanical Forces for in vitro Endothelial Cell Biology. *Frontiers in Physiology*, *11*, 684. https://doi.org/10.3389/fphys.2020.00684

Goumans, M.-J., & ten Dijke, P. (2018). TGF-β Signaling in Control of Cardiovascular Function. *Cold Spring Harbor Perspectives in Biology*, *10*(2), a022210. https://doi.org/10.1101/cshperspect.a022210

Grainge, C. L., Lau, L. C. K., Ward, J. A., Dulay, V., Lahiff, G., Wilson, S., Holgate, S., Davies, D. E., & Howarth, P. H. (2011). Effect of bronchoconstriction on airway remodeling in asthma. *The New England Journal of Medicine*, *364*(21), 2006–2015. https://doi.org/10.1056/NEJMoa1014350

Grant, T., Croce, E., & Matsui, E. C. (2022). Asthma and the social determinants of health. *Annals of Allergy, Asthma & Immunology*, *128*(1), 5–11. https://doi.org/10.1016/j.anai.2021.10.002

Guo, F., Wang, Y., Liu, J., Mok, S. C., Xue, F., & Zhang, W. (2016). CXCL12/CXCR4: A symbiotic bridge linking cancer cells and their stromal neighbors in oncogenic communication networks. *Oncogene*, *35*(7), 816–826. https://doi.org/10.1038/onc.2015.139

Haddad, M., & Sharma, S. (2024). Physiology, Lung. In *StatPearls*. StatPearls Publishing. http://www.ncbi.nlm.nih.gov/books/NBK545177/

Han, S., & Mallampalli, R. K. (2015). The Role of Surfactant in Lung Disease and Host Defense against Pulmonary Infections. *Annals of the American Thoracic Society*, *12*(5), 765–774. https://doi.org/10.1513/AnnalsATS.201411-507FR

Harker, J. A., & Lloyd, C. M. (2023). T helper 2 cells in asthma. *The Journal of Experimental Medicine*, *220*(6), e20221094. https://doi.org/10.1084/jem.20221094

Harrell, C. R., Simovic Markovic, B., Fellabaum, C., Arsenijevic, A., Djonov, V., & Volarevic, V. (2018). Molecular mechanisms underlying therapeutic potential of pericytes. *Journal of Biomedical Science*, *25*(1), 21. https://doi.org/10.1186/s12929-018-0423-7

Herrera, J., Henke, C. A., & Bitterman, P. B. (2018). Extracellular matrix as a driver of progressive fibrosis. *The Journal of Clinical Investigation*, *128*(1), 45–53. https://doi.org/10.1172/JCI93557

Heukels, P., Moor, C. C., von der Thüsen, J. H., Wijsenbeek, M. S., & Kool, M. (2019). Inflammation and immunity in IPF pathogenesis and treatment. *Respiratory Medicine*, *147*, 79–91. https://doi.org/10.1016/j.rmed.2018.12.015

Hu, C. (2013). CXCL12/CXCR4 axis promotes mesenchymal stem cell mobilization to burn wounds and contributes to wound repair. *J Surg Res*, *183*. https://doi.org/10.1016/j.jss.2013.01.019

Hu, X., Li, J., Fu, M., Zhao, X., & Wang, W. (2021). The JAK/STAT signaling pathway: From bench to clinic. *Signal Transduction and Targeted Therapy*, *6*(1), 1–33. https://doi.org/10.1038/s41392-021-00791-1

Humeniuk, P., Dubiela, P., & Hoffmann-Sommergruber, K. (2017). Dendritic Cells and Their Role in Allergy: Uptake, Proteolytic Processing and Presentation of Allergens. *International Journal of Molecular Sciences*, *18*(7), 1491. https://doi.org/10.3390/ijms18071491

Ince, L. M., Pariollaud, M., & Gibbs, J. E. (2018). Lung physiology and defense. *Current Opinion in Physiology*, *5*, 9–15. https://doi.org/10.1016/j.cophys.2018.04.005

Ivins, S., Chappell, J., Vernay, B., Suntharalingham, J., Martineau, A., Mohun, T. J., & Scambler, P. J. (2015). The CXCL12/CXCR4 Axis Plays a Critical Role in Coronary Artery Development. *Developmental Cell*, *33*(4), 455–468. https://doi.org/10.1016/j.devcel.2015.03.026

Jacobson, G. A., Raidal, S., Hostrup, M., Calzetta, L., Wood-Baker, R., Farber, M. O., Page, C. P., & Walters, E. H. (2018). Long-Acting β2-Agonists in Asthma: Enantioselective Safety Studies are Needed. *Drug Safety*, *41*(5), 441–449. https://doi.org/10.1007/s40264-017-0631-1

Jaffar, J., Griffiths, K., Oveissi, S., Duan, M., Foley, M., Glaspole, I., Symons, K., Organ, L., & Westall, G. (2020). CXCR4+ cells are increased in lung tissue of patients with idiopathic pulmonary fibrosis. *Respiratory Research*, *21*, 221. https://doi.org/10.1186/s12931-020-01467-0

Janssens, R., Struyf, S., & Proost, P. (2018). The unique structural and functional features of CXCL12. *Cellular & Molecular Immunology*, *15*(4), 299–311. https://doi.org/10.1038/cmi.2017.107

Johnson, J. R. (2004). Continuous exposure to house dust mite elicits chronic airway inflammation and structural remodeling. *Am J Respir Crit Care Med*, *169*. https://doi.org/10.1164/rccm.200308-1094OC

Johnson, J. R. (2015). Pericytes contribute to airway remodeling in a mouse model of chronic allergic asthma. *Am J Physiol Lung Cell Mol Physiol*, *308*. https://doi.org/10.1152/ajplung.00286.2014

Karnati, S., Seimetz, M., Kleefeldt, F., Sonawane, A., Madhusudhan, T., Bachhuka, A., Kosanovic, D., Weissmann, N., Krüger, K., & Ergün, S. (2021). Chronic Obstructive Pulmonary Disease and the Cardiovascular System: Vascular Repair and Regeneration as a Therapeutic Target. *Frontiers in Cardiovascular Medicine*, *8*, 649512. https://doi.org/10.3389/fcvm.2021.649512

Kisler, K., Nikolakopoulou, A. M., & Zlokovic, B. V. (2021). Microglia have a grip on brain microvasculature. *Nature Communications*, *12*(1), 5290. https://doi.org/10.1038/s41467-021-25595-3

Klain, A., Dinardo, G., Salvatori, A., Indolfi, C., Contieri, M., Brindisi, G., Decimo, F., Zicari, A. M., & Miraglia del Giudice, M. (2022). An Overview on the Primary Factors That Contribute to Non-Allergic Asthma in Children. *Journal of Clinical Medicine*, *11*(21), 6567. https://doi.org/10.3390/jcm11216567

Koch, C., & Engele, J. (2020). Functions of the CXCL12 Receptor ACKR3/CXCR7-What Has Been Perceived and What Has Been Overlooked. *Molecular Pharmacology*, *98*(5), 577–585. https://doi.org/10.1124/molpharm.120.000056

Krock, B. L., Skuli, N., & Simon, M. C. (2011). Hypoxia-Induced Angiogenesis. *Genes & Cancer*, *2*(12), 1117–1133. https://doi.org/10.1177/1947601911423654

Kropp, M., Golubnitschaja, O., Mazurakova, A., Koklesova, L., Sargheini, N., Vo, T.-T. K. S., de Clerck, E., Polivka, J., Potuznik, P., Polivka, J., Stetkarova, I., Kubatka, P., & Thumann, G. (2023). Diabetic retinopathy as the leading cause of blindness and early predictor of cascading complications—Risks and mitigation. *The EPMA Journal*, *14*(1), 21–42. https://doi.org/10.1007/s13167-023-00314-8

Krüger-Genge, A., Blocki, A., Franke, R.-P., & Jung, F. (2019). Vascular Endothelial Cell Biology: An Update. *International Journal of Molecular Sciences*, *20*(18), 4411. https://doi.org/10.3390/ijms20184411

Kudo, M., Ishigatsubo, Y., & Aoki, I. (2013). Pathology of asthma. *Frontiers in Microbiology*, *4*. https://www.frontiersin.org/articles/10.3389/fmicb.2013.00263

Kulkarni, T., O'Reilly, P., Antony, V. B., Gaggar, A., & Thannickal, V. J. (2016). Matrix Remodeling in Pulmonary Fibrosis and Emphysema. *American Journal of Respiratory Cell and Molecular Biology*, *54*(6), 751–760. https://doi.org/10.1165/rcmb.2015-0166PS

Kumar, S., & Ponnazhagan, S. (2012). Mobilization of bone marrow mesenchymal stem cells in vivo augments bone healing in a mouse model of segmental bone defect. *Bone*, *50*. https://doi.org/10.1016/j.bone.2012.01.027

Kutcher, M. E., Kolyada, A. Y., Surks, H. K., & Herman, I. M. (2007). Pericyte Rho GTPase Mediates Both Pericyte Contractile Phenotype and Capillary Endothelial Growth State. *The American Journal of Pathology*, *171*(2), 693. https://doi.org/10.2353/ajpath.2007.070102

Lama, J., & Planelles, V. (2007). Host factors influencing susceptibility to HIV infection and AIDS progression. *Retrovirology*, *4*, 52. https://doi.org/10.1186/1742-4690-4-52

Lambrecht, B. N., Hammad, H., & Fahy, J. V. (2019). The Cytokines of Asthma. *Immunity*, *50*(4), 975–991. https://doi.org/10.1016/j.immuni.2019.03.018

LeBlanc, A. J., Krishnan, L., Sullivan, C. J., Williams, S. K., & Hoying, J. B. (2012). Microvascular Repair: Post-Angiogenesis Vascular Dynamics. *Microcirculation (New York, N.Y. : 1994)*, *19*(8), 10.1111/j.1549-8719.2012.00207.x. https://doi.org/10.1111/j.1549-8719.2012.00207.x

Lekeux, P., Art, T., & Hodgson, D. R. (2014). CHAPTER 9 - The respiratory system: Anatomy, physiology, and adaptations to exercise and training. In D. R. Hodgson, K. H. McKeever, & C. M. McGowan (Eds.), *The Athletic Horse (Second Edition)* (pp. 125–154). W.B. Saunders. https://doi.org/10.1016/B978-0-7216-0075-8.00018-6

León, B., & Ballesteros-Tato, A. (2021). Modulating Th2 Cell Immunity for the Treatment of Asthma. *Frontiers in Immunology*, *12*, 637948. https://doi.org/10.3389/fimmu.2021.637948

Li, F., Xu, X., Geng, J., Wan, X., & Dai, H. (2020). The autocrine CXCR4/CXCL12 axis contributes to lung fibrosis through modulation of lung fibroblast activity. *Experimental and Therapeutic Medicine*, *19*(3), 1844–1854. https://doi.org/10.3892/etm.2020.8433

Li, P., & Fan, H. (2023). Pericyte Loss in Diseases. *Cells*, *12*(15), 1931. https://doi.org/10.3390/cells12151931

Liekens, S., Schols, D., & Hatse, S. (2010). CXCL12-CXCR4 Axis in Angiogenesis, Metastasis and Stem Cell Mobilization. *Current Pharmaceutical Design*, *16*(35), 3903–3920. https://doi.org/10.2174/138161210794455003

Lin, C.-H., Shih, C.-H., Tseng, C.-C., Yu, C.-C., Tsai, Y.-J., Bien, M.-Y., & Chen, B.-C. (2014). CXCL12 Induces Connective Tissue Growth Factor Expression in Human Lung Fibroblasts through the Rac1/ERK, JNK, and AP-1 Pathways. *PLOS ONE*, *9*(8), e104746. https://doi.org/10.1371/journal.pone.0104746

Lin, S. L. (2008). Pericytes and perivascular fibroblasts are the primary source of collagen-producing cells in obstructive fibrosis of the kidney. *Am J Pathol*, *173*. https://doi.org/10.2353/ajpath.2008.080433

Lloyd, C. M., & Robinson, D. S. (2007). Allergen-induced airway remodelling. *European Respiratory Journal*, *29*(5), 1020–1032. https://doi.org/10.1183/09031936.00150305

Longden, T. A., Zhao, G., Hariharan, A., & Lederer, W. J. (2023). Pericytes and the Control of Blood Flow in Brain and Heart. *Annual Review of Physiology*, *85*, 137. https://doi.org/10.1146/annurev-physiol-031522-034807

Lu, N., & Malemud, C. J. (2019). Extracellular Signal-Regulated Kinase: A Regulator of Cell Growth, Inflammation, Chondrocyte and Bone Cell Receptor-Mediated Gene Expression. *International Journal of Molecular Sciences*, *20*(15), 3792. https://doi.org/10.3390/ijms20153792

Luker, K. E., Lewin, S. A., Mihalko, L. A., Schmidt, B. T., Winkler, J. S., Coggins, N. L., Thomas, D. G., & Luker, G. D. (2012). Scavenging of CXCL12 by CXCR7 Promotes Tumor Growth and Metastasis of CXCR4-positive Breast Cancer Cells. *Oncogene*, *31*(45), 4750–4758. https://doi.org/10.1038/onc.2011.633

Makino, H., Aono, Y., Azuma, M., Kishi, M., Yokota, Y., Kinoshita, K., Takezaki, A., Kishi, J., Kawano, H., Ogawa, H., Uehara, H., Izumi, K., Sone, S., & Nishioka, Y. (2013). Antifibrotic effects of CXCR4 antagonist in bleomycin-induced pulmonary fibrosis in

mice. *The Journal of Medical Investigation: JMI*, *60*(1–2), 127–137. https://doi.org/10.2152/jmi.60.127

Mederacke, I., Hsu, C. C., Troeger, J. S., Huebener, P., Mu, X., Dapito, D. H., Pradere, J.-P., & Schwabe, R. F. (2013). Fate tracing reveals hepatic stellate cells as dominant contributors to liver fibrosis independent of its aetiology. *Nature Communications*, *4*(1), 2823. https://doi.org/10.1038/ncomms3823

Menzies-Gow, A., Corren, J., Bourdin, A., Chupp, G., Israel, E., Wechsler, M. E., Brightling, C. E., Griffiths, J. M., Hellqvist, Å., Bowen, K., Kaur, P., Almqvist, G., Ponnarambil, S., & Colice, G. (2021). Tezepelumab in Adults and Adolescents with Severe, Uncontrolled Asthma. *The New England Journal of Medicine*, *384*(19), 1800–1809. https://doi.org/10.1056/NEJMoa2034975

Meyers, D. A., Bleecker, E. R., Holloway, J. W., & Holgate, S. T. (2014). The Genetics of Asthma: Towards a Personalised Approach to Diagnosis and Treatment. *The Lancet. Respiratory Medicine*, *2*(5), 405–415. https://doi.org/10.1016/S2213-2600(14)70012-8

Miligkos, M., Bannuru, R. R., Alkofide, H., Kher, S. R., Schmid, C. H., & Balk, E. M. (2015). Leukotriene receptor antagonists versus placebo in the treatment of asthma in adults and adolescents: A systematic review and meta-analysis. *Annals of Internal Medicine*, *163*(10), 756–767. https://doi.org/10.7326/M15-1059

Mongiat, M., Andreuzzi, E., Tarticchio, G., & Paulitti, A. (2016). Extracellular Matrix, a Hard Player in Angiogenesis. *International Journal of Molecular Sciences*, *17*(11), 1822. https://doi.org/10.3390/ijms17111822

Morales, D. R. (2013). LABA monotherapy in asthma: An avoidable problem. *The British Journal of General Practice*, *63*(617), 627–628. https://doi.org/10.3399/bjgp13X675250

Morikawa, S., Mabuchi, Y., Kubota, Y., Nagai, Y., Niibe, K., Hiratsu, E., Suzuki, S., Miyauchi-Hara, C., Nagoshi, N., Sunabori, T., Shimmura, S., Miyawaki, A., Nakagawa, T., Suda, T., Okano, H., & Matsuzaki, Y. (2009). Prospective identification, isolation, and systemic

transplantation of multipotent mesenchymal stem cells in murine bone marrow. *Journal of Experimental Medicine*, *206*(11), 2483–2496. https://doi.org/10.1084/jem.20091046

Mousavi, A. (2020). CXCL12/CXCR4 signal transduction in diseases and its molecular approaches in targeted-therapy. *Immunology Letters*, *217*, 91–115. https://doi.org/10.1016/j.imlet.2019.11.007

Moyer, R. A., Wendt, M. K., Johanesen, P. A., Turner, J. R., & Dwinell, M. B. (2007). Rho activation regulates CXCL12 chemokine stimulated actin rearrangement and restitution in model intestinal epithelia. *Laboratory Investigation; a Journal of Technical Methods and Pathology*, *87*(8), 807–817. https://doi.org/10.1038/labinvest.3700595

Muz, B., de la Puente, P., Azab, F., & Azab, A. K. (2015). The role of hypoxia in cancer progression, angiogenesis, metastasis, and resistance to therapy. *Hypoxia*, *3*, 83–92. https://doi.org/10.2147/HP.S93413

Naeem, A., & Silveyra, P. (2019). Sex Differences in Paediatric and Adult Asthma. *European Medical Journal*, 27–35. https://doi.org/10.33590/emj/10312930

Nakagawa, S., Deli, M. A., Nakao, S., Honda, M., Hayashi, K., Nakaoke, R., Kataoka, Y., & Niwa, M. (2007). Pericytes from Brain Microvessels Strengthen the Barrier Integrity in Primary Cultures of Rat Brain Endothelial Cells. *Cellular and Molecular Neurobiology*, *27*(6), 687–694. https://doi.org/10.1007/s10571-007-9195-4

Nasim, F., & Iyer, V. N. (2018). Bronchial thermoplasty-an update. *Annals of Thoracic Medicine*, *13*(4), 205–211. https://doi.org/10.4103/atm.ATM_365_17

Navarro, R., Compte, M., Álvarez-Vallina, L., & Sanz, L. (2016). Immune Regulation by Pericytes: Modulating Innate and Adaptive Immunity. *Frontiers in Immunology*, *7*, 480. https://doi.org/10.3389/fimmu.2016.00480

Nayak, R. C., Chang, K.-H., Vaitinadin, N.-S., & Cancelas, J. A. (2013). Rho GTPases control specific cytoskeleton-dependent functions of hematopoietic stem cells. *Immunological Reviews*, *256*(1), 10.1111/imr.12119. https://doi.org/10.1111/imr.12119

Negrete-Garcia, M., Negrete-García, M. C., Popoca-Coyotl, A., Montes-Vizuet, A. R., & Terán, L. M. (2009). CXCL12 is Released in the Bronchoalveolar Lavage of Asthmatic Subjects. *Journal of Allergy and Clinical Immunology*, *123*(3), 731–732. https://doi.org/10.1016/j.jaci.2009.01.036

Ngaha, T. Y. S., Zhilenkova, A. V., Essogmo, F. E., Uchendu, I. K., Abah, M. O., Fossa, L. T., Sangadzhieva, Z. D., D. Sanikovich, V., S. Rusanov, A., N. Pirogova, Y., Boroda, A., Rozhkov, A., Kemfang Ngowa, J. D., N. Bagmet, L., & I. Sekacheva, M. (2023). Angiogenesis in Lung Cancer: Understanding the Roles of Growth Factors. *Cancers*, *15*(18), 4648. https://doi.org/10.3390/cancers15184648

Nguyen, H. T., Reyes-Alcaraz, A., Yong, H. J., Nguyen, L. P., Park, H.-K., Inoue, A., Lee, C. S., Seong, J. Y., & Hwang, J.-I. (2020). CXCR7: A β-arrestin-biased receptor that potentiates cell migration and recruits β-arrestin2 exclusively through Gβγ subunits and GRK2. *Cell & Bioscience*, *10*, 134. https://doi.org/10.1186/s13578-020-00497-x

Nishida, N., Yano, H., Nishida, T., Kamura, T., & Kojiro, M. (2006). Angiogenesis in Cancer. *Vascular Health and Risk Management*, *2*(3), 213–219.

Nwadozi, E., Rudnicki, M., & Haas, T. L. (2020). Metabolic Coordination of Pericyte Phenotypes: Therapeutic Implications. *Frontiers in Cell and Developmental Biology*, *8*, 77. https://doi.org/10.3389/fcell.2020.00077

Oh, I.-H. (2010). Mesenchymal stromal cells: New insight on their identity and potential role in cell therapy. *The Korean Journal of Hematology*, *45*(4), 219–221. https://doi.org/10.5045/kjh.2010.45.4.219

Ortega, H. G., Liu, M. C., Pavord, I. D., Brusselle, G. G., FitzGerald, J. M., Chetta, A., Humbert, M., Katz, L. E., Keene, O. N., Yancey, S. W., Chanez, P., & MENSA Investigators. (2014). Mepolizumab treatment in patients with severe eosinophilic asthma. *The New England Journal of Medicine*, *371*(13), 1198–1207. https://doi.org/10.1056/NEJMoa1403290

Paggiaro, P., & Bacci, E. (2011). Montelukast in Asthma: A Review of its Efficacy and Place in Therapy. *Therapeutic Advances in Chronic Disease*, *2*(1), 47–58. https://doi.org/10.1177/2040622310383343

Papi, A., Blasi, F., Canonica, G. W., Morandi, L., Richeldi, L., & Rossi, A. (2020). Treatment strategies for asthma: Reshaping the concept of asthma management. *Allergy, Asthma, and Clinical Immunology : Official Journal of the Canadian Society of Allergy and Clinical Immunology*, *16*, 75. https://doi.org/10.1186/s13223-020-00472-8

Payne, L. B., Zhao, H., James, C. C., Darden, J., McGuire, D., Taylor, S., Smyth, J. W., & Chappell, J. C. (2019). The Pericyte Microenvironment during Vascular Development. *Microcirculation (New York, N.Y. : 1994)*, *26*(8), e12554. https://doi.org/10.1111/micc.12554

Pembrey, L., Barreto, M. L., Douwes, J., Cooper, P., Henderson, J., Mpairwe, H., Ardura-Garcia, C., Chico, M., Brooks, C., Cruz, A. A., Elliott, A. M., Figueiredo, C. A., Langan, S. M., Nassanga, B., Ring, S., Rodrigues, L., & Pearce, N. (2018). Understanding asthma phenotypes: The World Asthma Phenotypes (WASP) international collaboration. *ERJ Open Research*, *4*(3). https://doi.org/10.1183/23120541.00013-2018

Peng, L., Zhu, N., Mao, J., Huang, L., Yang, Y., Zhou, Z., Wang, L., & Wu, B. (2020). Expression levels of CXCR4 and CXCL12 in patients with rheumatoid arthritis and its correlation with disease activity. *Experimental and Therapeutic Medicine*, *20*(3), 1925–1934. https://doi.org/10.3892/etm.2020.8950

Pfeiffer, M., Hartmann, T. N., Leick, M., Catusse, J., Schmitt-Graeff, A., & Burger, M. (2009). Alternative implication of CXCR4 in JAK2/STAT3 activation in small cell lung cancer. *British Journal of Cancer*, *100*(12), 1949–1956. https://doi.org/10.1038/sj.bjc.6605068

Phillips, R. J., Burdick, M. D., Hong, K., Lutz, M. A., Murray, L. A., Xue, Y. Y., Belperio, J. A., Keane, M. P., & Strieter, R. M. (2004). Circulating fibrocytes traffic to the lungs in

response to CXCL12 and mediate fibrosis. *Journal of Clinical Investigation*, *114*(3), 438–446. https://doi.org/10.1172/JCI200420997

Pinho, S. (2013). PDGFR alpha and CD51 mark human Nestin(+) sphere-forming mesenchymal stem cells capable of hematopoietic progenitor cell expansion. *J Exp Med*, *210*. https://doi.org/10.1084/jem.20122252

Ponieman, D., Wisnivesky, J. P., Leventhal, H., Musumeci-Szabó, T. J., & Halm, E. A. (2009). Impact of positive and negative beliefs about inhaled corticosteroids on adherence in inner-city asthmatic patients. *Annals of Allergy, Asthma & Immunology: Official Publication of the American College of Allergy, Asthma, & Immunology*, *103*(1), 38–42. https://doi.org/10.1016/S1081-1206(10)60141-X

Postma, D. S. (2007). Gender differences in asthma development and progression. *Gender Medicine*, *4 Suppl B*, S133-146. https://doi.org/10.1016/s1550-8579(07)80054-4

Quirt, J., Hildebrand, K. J., Mazza, J., Noya, F., & Kim, H. (2018). Asthma. *Allergy, Asthma, and Clinical Immunology : Official Journal of the Canadian Society of Allergy and Clinical Immunology*, *14*(Suppl 2), 50. https://doi.org/10.1186/s13223-018-0279-0

Radonjic-Hoesli, S., Valent, P., Klion, A. D., Wechsler, M. E., & Simon, H.-U. (2015). Novel targeted therapies for eosinophil-associated diseases and allergy. *Annual Review of Pharmacology and Toxicology*, *55*, 633–656. https://doi.org/10.1146/annurev-pharmtox-010814-124407

Ramos, L., Novo, J., Rouco, J., Romeo, S., Álvarez, M. D., & Ortega, M. (2018). Retinal vascular tortuosity assessment: Inter-intra expert analysis and correlation with computational measurements. *BMC Medical Research Methodology*, *18*, 144. https://doi.org/10.1186/s12874-018-0598-3

Ranjbar, M., Whetstone, C. E., Omer, H., Power, L., Cusack, R. P., & Gauvreau, G. M. (2022). The Genetic Factors of the Airway Epithelium Associated with the Pathology of Asthma. *Genes*, *13*(10), 1870. https://doi.org/10.3390/genes13101870

Reddel, H. K., Bateman, E. D., Becker, A., Boulet, L.-P., Cruz, A. A., Drazen, J. M., Haahtela, T., Hurd, S. S., Inoue, H., Jongste, J. C. de, Lemanske, R. F., Levy, M. L., O'Byrne, P. M., Paggiaro, P., Pedersen, S. E., Pizzichini, E., Soto-Quiroz, M., Szefler, S. J., Wong, G. W. K., & FitzGerald, J. M. (2015). A summary of the new GINA strategy: A roadmap to asthma control. *European Respiratory Journal*, *46*(3), 622–639. https://doi.org/10.1183/13993003.00853-2015

Regenass, P. (2018). Discovery of a locally and orally active CXCL12 Neutraligand (LIT-927) with anti-inflammatory effect in a murine model of allergic airway hypereosinophilia. *J Med Chem*, *61*. https://doi.org/10.1021/acs.jmedchem.8b00657

Rodriguez, A., Brickley, E., Rodrigues, L., Normansell, R. A., Barreto, M., & Cooper, P. J. (2019). Urbanisation and asthma in low-income and middle-income countries: A systematic review of the urban–rural differences in asthma prevalence. *Thorax*, *74*(11), 1020–1030. https://doi.org/10.1136/thoraxjnl-2018-211793

Rossi, R. C., Anonni, R., Ferreira, D. S., da Silva, L. F. F., & Mauad, T. (2019). Structural alterations and markers of endothelial activation in pulmonary and bronchial arteries in fatal asthma. *Allergy, Asthma, and Clinical Immunology : Official Journal of the Canadian Society of Allergy and Clinical Immunology*, *15*, 50. https://doi.org/10.1186/s13223-019-0363-0

Rostovskaya, M., & Anastassiadis, K. (2012). Differential expression of surface markers in mouse bone marrow mesenchymal stromal cell subpopulations with distinct lineage commitment. *PLoS ONE*, *7*. https://doi.org/10.1371/journal.pone.0051221

Rowley, J., Strong, K., & Johnson, J. (2015). Characterisation of lung-resident pericytes in a house dust mite-driven model of asthma. *European Respiratory Journal*, *46*(suppl 59). https://doi.org/10.1183/13993003.congress-2015.PA887

Samitas, K., Carter, A., Kariyawasam, H. H., & Xanthou, G. (2018). Upper and lower airway remodelling mechanisms in asthma, allergic rhinitis and chronic rhinosinusitis: The one airway concept revisited. *Allergy*, *73*(5), 993–1002. https://doi.org/10.1111/all.13373

Sandoo, A., van Zanten, J. J. C. S. V., Metsios, G. S., Carroll, D., & Kitas, G. D. (2010). The Endothelium and Its Role in Regulating Vascular Tone. *The Open Cardiovascular Medicine Journal*, *4*, 302–312. https://doi.org/10.2174/1874192401004010302

Santagata, S., Ieranò, C., Trotta, A. M., Capiluongo, A., Auletta, F., Guardascione, G., & Scala, S. (2021). CXCR4 and CXCR7 Signaling Pathways: A Focus on the Cross-Talk Between Cancer Cells and Tumor Microenvironment. *Frontiers in Oncology*, *11*, 591386. https://doi.org/10.3389/fonc.2021.591386

Schittny, J. C. (2017). Development of the lung. *Cell and Tissue Research*, *367*(3), 427–444. https://doi.org/10.1007/s00441-016-2545-0

Schmidt, D., & von Hochstetter, A. R. (1995). The use of CD31 and collagen IV as vascular markers. A study of 56 vascular lesions. *Pathology, Research and Practice*, *191*(5), 410–414. https://doi.org/10.1016/S0344-0338(11)80727-2

Shi, X., Young, C. D., Zhou, H., & Wang, X.-J. (2020). Transforming Growth Factor-β Signaling in Fibrotic Diseases and Cancer-Associated Fibroblasts. *Biomolecules*, *10*(12), 1666. https://doi.org/10.3390/biom10121666

Shi, Y., Riese, D. J., & Shen, J. (2020). The Role of the CXCL12/CXCR4/CXCR7 Chemokine Axis in Cancer. *Frontiers in Pharmacology*, *11*. https://www.frontiersin.org/articles/10.3389/fphar.2020.574667

Shibuya, M. (2011). Vascular Endothelial Growth Factor (VEGF) and Its Receptor (VEGFR) Signaling in Angiogenesis. *Genes & Cancer*, *2*(12), 1097–1105. https://doi.org/10.1177/1947601911423031

Shu, H.-K. G., Yoon, Y., Hong, S., Xu, K., Gao, H., Hao, C., Torres-Gonzalez, E., Nayra, C., Rojas, M., & Shim, H. (2013). Inhibition of the CXCL12/CXCR4-Axis as Preventive Therapy for

Radiation-Induced Pulmonary Fibrosis. *PLoS ONE*, *8*(11), e79768. https://doi.org/10.1371/journal.pone.0079768

Siafakas, N. M., Antoniou, K. M., & Tzortzaki, E. G. (2007). Role of angiogenesis and vascular remodeling in chronic obstructive pulmonary disease. *International Journal of Chronic Obstructive Pulmonary Disease*, *2*(4), 453–462.

Siddiqui, M. R., Mayanil, C. S., Kim, K. S., & Tomita, T. (2015). Angiopoietin-1 Regulates Brain Endothelial Permeability through PTPN-2 Mediated Tyrosine Dephosphorylation of Occludin. *PLoS ONE*, *10*(6), e0130857. https://doi.org/10.1371/journal.pone.0130857

Song, Y.-Y., Liang, D., Liu, D.-K., Lin, L., Zhang, L., & Yang, W.-Q. (2023). The role of the ERK signaling pathway in promoting angiogenesis for treating ischemic diseases. *Frontiers in Cell and Developmental Biology*, *11*, 1164166. https://doi.org/10.3389/fcell.2023.1164166

Spergel, J. M. (2010). From atopic dermatitis to asthma: The atopic march. *Annals of Allergy, Asthma & Immunology*, *105*(2), 99–106. https://doi.org/10.1016/j.anai.2009.10.002

Spiering, D., & Hodgson, L. (2011). Dynamics of the Rho-family small GTPases in actin regulation and motility. *Cell Adhesion & Migration*, *5*(2), 170–180. https://doi.org/10.4161/cam.5.2.14403

Stapor, P. C., Sweat, R. S., Dashti, D. C., Betancourt, A. M., & Murfee, W. L. (2014). Pericyte Dynamics during Angiogenesis: New Insights from New Identities. *Journal of Vascular Research*, *51*(3), 163–174. https://doi.org/10.1159/000362276

Stephens, B. S., Ngo, T., Kufareva, I., & Handel, T. M. (2020). Functional anatomy of the full-length CXCR4-CXCL12 complex systematically dissected by quantitative model-guided mutagenesis. *Science Signaling*, *13*(640), eaay5024. https://doi.org/10.1126/scisignal.aay5024

Stoodley, I., Williams, L., Thompson, C., Scott, H., & Wood, L. (2019). Evidence for lifestyle interventions in asthma. *Breathe*, *15*(2), e50–e61. https://doi.org/10.1183/20734735.0019-2019

Strachan, D. P. (2000). The role of environmental factors in asthma. *British Medical Bulletin*, *56*(4), 865–882. https://doi.org/10.1258/0007142001903562

Su, X., Huang, L., Qu, Y., Xiao, D., & Mu, D. (2019). Pericytes in Cerebrovascular Diseases: An Emerging Therapeutic Target. *Frontiers in Cellular Neuroscience*, *13*, 519. https://doi.org/10.3389/fncel.2019.00519

Sundberg, C., Kowanetz, M., Brown, L. F., Detmar, M., & Dvorak, H. F. (2002). Stable Expression of Angiopoietin-1 and Other Markers by Cultured Pericytes: Phenotypic Similarities to a Subpopulation of Cells in Maturing Vessels During Later Stages of Angiogenesis In Vivo. *Laboratory Investigation*, *82*(4), 387–401. https://doi.org/10.1038/labinvest.3780433

Suresh, K., & Shimoda, L. A. (2016). Lung Circulation. *Comprehensive Physiology*, *6*(2), 897–943. https://doi.org/10.1002/cphy.c140049

Sweeney, M. D., Ayyadurai, S., & Zlokovic, B. V. (2016). Pericytes of the neurovascular unit: Key functions and signaling pathways. *Nature Neuroscience*, *19*(6), 771. https://doi.org/10.1038/nn.4288

Sze, E., Bhalla, A., & Nair, P. (2020). Mechanisms and therapeutic strategies for non-T2 asthma. *Allergy*, *75*(2), 311–325. https://doi.org/10.1111/all.13985

Takahashi, Y., Maki, T., Liang, A. C., Itoh, K., Lok, J., Osumi, N., & Arai, K. (2014). P38 MAP kinase mediates transforming-growth factor-β1-induced upregulation of matrix metalloproteinase-9 but not -2 in human brain pericytes. *Brain Research*, *0*, 1–8. https://doi.org/10.1016/j.brainres.2014.10.029

Takala, J., Vähätalo, I., Tuomisto, L. E., Niemelä, O., Ilmarinen, P., & Kankaanranta, H. (2024). Documentation of comorbidities, lifestyle factors, and asthma management during

primary care scheduled asthma contacts. *Npj Primary Care Respiratory Medicine*, *34*(1), 1–10. https://doi.org/10.1038/s41533-024-00360-3

Tashkin, D. P., & Fabbri, L. M. (2010). Long-acting beta-agonists in the management of chronic obstructive pulmonary disease: Current and future agents. *Respiratory Research*, *11*(1), 149. https://doi.org/10.1186/1465-9921-11-149

Tefft, J. B., Bays, J. L., Lammers, A., Kim, S., Eyckmans, J., & Chen, C. S. (2022). Notch1 and Notch3 coordinate for pericyte-induced stabilization of vasculature. *American Journal of Physiology-Cell Physiology*, *322*(2), C185–C196. https://doi.org/10.1152/ajpcell.00320.2021

Thomsen, M. S., Routhe, L. J., & Moos, T. (2017). The vascular basement membrane in the healthy and pathological brain. *Journal of Cerebral Blood Flow & Metabolism*, *37*(10), 3300–3317. https://doi.org/10.1177/0271678X17722436

Thurston, G., & Daly, C. (2012). The Complex Role of Angiopoietin-2 in the Angiopoietin–Tie Signaling Pathway. *Cold Spring Harbor Perspectives in Medicine*, *2*(9), a006650. https://doi.org/10.1101/cshperspect.a006650

To, T., Stanojevic, S., Moores, G., Gershon, A. S., Bateman, E. D., Cruz, A. A., & Boulet, L.-P. (2012). Global asthma prevalence in adults: Findings from the cross-sectional world health survey. *BMC Public Health*, *12*, 204. https://doi.org/10.1186/1471-2458-12-204

Tobal, R., Potjewijd, J., van Empel, V. P. M., Ysermans, R., Schurgers, L. J., Reutelingsperger, C. P., Damoiseaux, J. G. M. C., & van Paassen, P. (2021). Vascular Remodeling in Pulmonary Arterial Hypertension: The Potential Involvement of Innate and Adaptive Immunity. *Frontiers in Medicine*, *8*, 806899. https://doi.org/10.3389/fmed.2021.806899

Turley, S. J., Cremasco, V., & Astarita, J. L. (2015). Immunological hallmarks of stromal cells in the tumour microenvironment. *Nat Rev Immunol*, *15*. https://doi.org/10.1038/nri3902

Vicenzi, E., Liò, P., & Poli, G. (2013). The Puzzling Role of CXCR4 in Human Immunodeficiency Virus Infection. *Theranostics*, *3*(1), 18–25. https://doi.org/10.7150/thno.5392

Voelkel, N. F., Douglas, I. S., & Nicolls, M. (2007). Angiogenesis in Chronic Lung Disease. *Chest*, *131*(3), 874–879. https://doi.org/10.1378/chest.06-2453

Wadhwa, R., Dua, K., Adcock, I. M., Horvat, J. C., Kim, R. Y., & Hansbro, P. M. (2019). Cellular mechanisms underlying steroid-resistant asthma. *European Respiratory Review*, *28*(153). https://doi.org/10.1183/16000617.0096-2019

Wang, G., Huang, Y., Ma, K., Duan, Z., Luo, Z., Xiao, P., & Yuan, J. (2023). Automatic vessel crossing and bifurcation detection based on multi-attention network vessel segmentation and directed graph search. *Computers in Biology and Medicine*, *155*, 106647. https://doi.org/10.1016/j.compbiomed.2023.106647

Wang, K., Wen, D., Xu, X., Zhao, R., Jiang, F., Yuan, S., Zhang, Y., Gao, Y., & Li, Q. (2023). Extracellular matrix stiffness—The central cue for skin fibrosis. *Frontiers in Molecular Biosciences*, *10*, 1132353. https://doi.org/10.3389/fmolb.2023.1132353

Wang, S., Cao, C., Chen, Z., Bankaitis, V., Tzima, E., Sheibani, N., & Burridge, K. (2012). Pericytes Regulate Vascular Basement Membrane Remodeling and Govern Neutrophil Extravasation during Inflammation. *PLoS ONE*, *7*(9), e45499. https://doi.org/10.1371/journal.pone.0045499

Wang, S., Gao, S., Li, Y., Qian, X., Luan, J., & Lv, X. (2021). Emerging Importance of Chemokine Receptor CXCR4 and Its Ligand in Liver Disease. *Frontiers in Cell and Developmental Biology*, *9*, 716842. https://doi.org/10.3389/fcell.2021.716842

Wang, Y., Chen, S., Bao, S., Yao, L., Wen, Z., Xu, L., Chen, X., Guo, S., Pang, H., Zhou, Y., & Zhou, P. (2024). Deciphering the fibrotic process: Mechanism of chronic radiation skin injury fibrosis. *Frontiers in Immunology*, *15*, 1338922. https://doi.org/10.3389/fimmu.2024.1338922

Wang, Y., Ding, L., Li, Z., Chen, G., Sun, M., & Oupicky, D. (2019). Treatment of acute lung injury and early- and late-stage pulmonary fibrosis with combination emulsion siRNA

polyplexes. *Journal of Controlled Release*, *314*, 12–24. https://doi.org/10.1016/j.jconrel.2019.10.030

Wang, Y., Pan, L., Moens, C. B., & Appel, B. (2014). Notch3 establishes brain vascular integrity by regulating pericyte number. *Development*, *141*(2), 307–317. https://doi.org/10.1242/dev.096107

Wang, Z., Li, Y., Gao, Y., Fu, Y., Lin, J., Lei, X., Zheng, J., & Jiang, M. (2023). Global, regional, and national burden of asthma and its attributable risk factors from 1990 to 2019: A systematic analysis for the Global Burden of Disease Study 2019. *Respiratory Research*, *24*(1), 169. https://doi.org/10.1186/s12931-023-02475-6

Watanabe, M., Matsuyama, W., Shirahama, Y., Mitsuyama, H., Oonakahara, K., Noma, S., Higashimoto, I., Osame, M., & Arimura, K. (2007). Dual effect of AMD3100, a CXCR4 antagonist, on bleomycin-induced lung inflammation. *Journal of Immunology (Baltimore, Md.: 1950)*, *178*(9), 5888–5898. https://doi.org/10.4049/jimmunol.178.9.5888

Wenzel, S. E. (2012). Asthma phenotypes: The evolution from clinical to molecular approaches. *Nature Medicine*, *18*(5), 716–725. https://doi.org/10.1038/nm.2678

Whetstone, C. E., Ranjbar, M., Omer, H., Cusack, R. P., & Gauvreau, G. M. (2022). The Role of Airway Epithelial Cell Alarmins in Asthma. *Cells*, *11*(7), 1105. https://doi.org/10.3390/cells11071105

Wight, T. N., & Potter-Perigo, S. (2011). The extracellular matrix: An active or passive player in fibrosis? *American Journal of Physiology - Gastrointestinal and Liver Physiology*, *301*(6), G950–G955. https://doi.org/10.1152/ajpgi.00132.2011

Wijesinghe, M., Perrin, K., Harwood, M., Weatherall, M., & Beasley, R. (2008). The risk of asthma mortality with inhaled long acting beta-agonists. *Postgraduate Medical Journal*, *84*(995), 467–472. https://doi.org/10.1136/pgmj.2007.067165

Wilson, J. W., & Kotsimbos, T. (2003). Airway vascular remodeling in asthma. *Current Allergy and Asthma Reports*, *3*(2), 153–158. https://doi.org/10.1007/s11882-003-0028-3

Wilson, M. S., & Wynn, T. A. (2009). Pulmonary fibrosis: Pathogenesis, etiology and regulation. *Mucosal Immunology*, *2*(2), 103–121. https://doi.org/10.1038/mi.2008.85

Woodfin, A., Voisin, M.-B., & Nourshargh, S. (2007). PECAM-1: A Multi-Functional Molecule in Inflammation and Vascular Biology. *Arteriosclerosis, Thrombosis, and Vascular Biology*, *27*(12), 2514–2523. https://doi.org/10.1161/ATVBAHA.107.151456

Wu, X., Qian, L., Zhao, H., Lei, W., Liu, Y., Xu, X., Li, J., Yang, Z., Wang, D., Zhang, Y., Zhang, Y., Tang, R., Yang, Y., & Tian, Y. (2023). CXCL12/CXCR4: An amazing challenge and opportunity in the fight against fibrosis. *Ageing Research Reviews*, *83*, 101809. https://doi.org/10.1016/j.arr.2022.101809

Xiang, D.-N., Feng, Y.-F., Wang, J., Zhang, X., Shen, J.-J., Zou, R., & Yuan, Y.-Z. (2019). Platelet-derived growth factor-BB promotes proliferation and migration of retinal microvascular pericytes by up-regulating the expression of C-X-C chemokine receptor types 4. *Experimental and Therapeutic Medicine*, *18*(5), 4022–4030. https://doi.org/10.3892/etm.2019.8016

Xiong, D. (Jun P., Martin, J. G., & Lauzon, A.-M. (2022). Airway smooth muscle function in asthma. *Frontiers in Physiology*, *13*, 993406. https://doi.org/10.3389/fphys.2022.993406

Yan, J., Wang, W.-B., Fan, Y.-J., Bao, H., Li, N., Yao, Q.-P., Huo, Y.-L., Jiang, Z.-L., Qi, Y.-X., & Han, Y. (2020). Cyclic Stretch Induces Vascular Smooth Muscle Cells to Secrete Connective Tissue Growth Factor and Promote Endothelial Progenitor Cell Differentiation and Angiogenesis. *Frontiers in Cell and Developmental Biology*, *8*, 606989. https://doi.org/10.3389/fcell.2020.606989

Zanini, A., Chetta, A., Imperatori, A. S., Spanevello, A., & Olivieri, D. (2010). The role of the bronchial microvasculature in the airway remodelling in asthma and COPD. *Respiratory Research*, *11*(1), 132. https://doi.org/10.1186/1465-9921-11-132

Zhang, W., Lin, C., Sampath, V., & Nadeau, K. (2018). Impact of allergen immunotherapy in allergic asthma. *Immunotherapy*, *10*(7), 579–593. https://doi.org/10.2217/imt-2017-0138

Zhang, Y., & Yang, X. (2020). The Roles of TGF-β Signaling in Cerebrovascular Diseases. *Frontiers in Cell and Developmental Biology*, *8*. https://doi.org/10.3389/fcell.2020.567682

Zhang, Z.-S., Zhou, H.-N., He, S.-S., Xue, M.-Y., Li, T., & Liu, L.-M. (2020). Research advances in pericyte function and their roles in diseases. *Chinese Journal of Traumatology*, *23*(2), 89–95. https://doi.org/10.1016/j.cjtee.2020.02.006

Zhao, R., Liu, J., Li, Z., Zhang, W., Wang, F., & Zhang, B. (2022). Recent Advances in CXCL12/CXCR4 Antagonists and Nano-Based Drug Delivery Systems for Cancer Therapy. *Pharmaceutics*, *14*(8), 1541. https://doi.org/10.3390/pharmaceutics14081541

Zhao, X., Chen, J., Sun, H., Zhang, Y., & Zou, D. (2022). New insights into fibrosis from the ECM degradation perspective: The macrophage-MMP-ECM interaction. *Cell & Bioscience*, *12*(1), 117. https://doi.org/10.1186/s13578-022-00856-w

Zhou, B., Lin, W., Long, Y., Yang, Y., Zhang, H., Wu, K., & Chu, Q. (2022). Notch signaling pathway: Architecture, disease, and therapeutics. *Signal Transduction and Targeted Therapy*, *7*, 95. https://doi.org/10.1038/s41392-022-00934-y

Zhou, S.-Y., Guo, Z.-N., Zhang, D.-H., Qu, Y., & Jin, H. (2022). The Role of Pericytes in Ischemic Stroke: Fom Cellular Functions to Therapeutic Targets. *Frontiers in Molecular Neuroscience*, *15*, 866700. https://doi.org/10.3389/fnmol.2022.866700

Zhou, W., Guo, S., Liu, M., Burow, M. E., & Wang, G. (2019). Targeting CXCL12/CXCR4 Axis in Tumor Immunotherapy. *Current Medicinal Chemistry*, *26*(17), 3026–3041. https://doi.org/10.2174/0929867324666170830111531